QUANTIFICATION OF MINERALIZATION AROUND THE MURINE KNEE IN
RESPONSE TO UBIQUITOUS INTEGRIN α1β1 AND CARTILAGE-SPECIFIC TβRII
KNOCK-OUT

QUANTIFICATION OF MINERALIZATION AROUND THE MURINE KNEE IN RESPONSE TO UBIQUITOUS INTEGRIN α1β1 AND CARTILAGE-SPECIFIC TβRII KNOCK-OUT

BY ROSHAN BASHAR, B.ENG

A Thesis submitted to the School of Graduate Studies in Partial Fulfillment of the Requirements for the Degree Master of Applied Science

Lay Abstract

Osteoarthritis is a common joint disorder, associated mainly with cartilage degradation. Some genes have been identified that cause or prevent osteoarthritis. A previous study used two of these genes in a genetic mouse model to explore how osteoarthritis may develop. Removing the integrin α1 subunit from mice caused osteoarthritic changes in the cartilage of the mouse knee. When the transforming growth factor beta gene was removed from the cartilage, these changes were less severe. This project continued the study by exploring changes in bone around the mouse knee. We quantified bone changes around the mouse knee using high-resolution micro-computed tomography scans. Contrary to common findings in post-traumatic osteoarthritis, we found that there were no significant changes in the bone around the knees even where severe cartilage changes had been identified. However, there were significant increases in calcifications of soft tissues including the meniscus and ligaments around the knee.

Abstract

Osteoarthritis is the most common form of arthritis. Genetic models have been developed to determine if and how a targeted gene may influence cartilage degenerative changes. The *itga1*-null mouse model has an inhibited integrin α1β1 through a ubiquitous integrin α1 subunit knockout, which leads to fibrosis in articular cartilage through excessive signalling from transforming growth factor beta (TGFβ). Depleting this TGFβ signalling is proposed to have a protective effect on cartilage. This project is part of a foregoing study where a cartilage-specific knockout of TGFβ receptor type II (TβRII) was used to deplete TGFβ signalling in articular cartilage of the *itga1*-null mice to reduce the severity of cartilage degradation. This project continues the analysis of the genetic model into bone architecture at the knee. Mouse hindlimbs were scanned at a 13µm resolution using micro-computed tomography and segmented into 3D datasets containing calcified tissues and bone of the knee and surroundings. Quantification methods for trabecular bone parameters (bone volume fraction, trabecular separation, and trabecular thickness) and ectopic calcification of soft tissues were developed. Loss of trabecular bone around the involved joint is a hallmark of post-traumatic osteoarthritis. However, the results from this study showed no significant changes in trabecular bone of *itga1*-null mouse knees despite observing severe osteoarthritic changes in the adjacent cartilage. There were no significant effects in peri-articular trabecular bone when the TβRII knockout in cartilage was activated, but there were significant increases in ectopic calcifications of the menisci and collateral ligaments. These ectopic calcifications were also seen in tamoxifen control

mice, suggesting that tamoxifen, along with TβRII depletion in cartilage, had a role in increased abnormal calcifications. Although integrin α1β1 inhibition appears to have an important role in cartilage degeneration, it does not appear to influence the bony changes that normally accompany post-traumatic arthritis.

Acknowledgements

I sincerely want to thank my supervisor, Dr. Gregory Wohl, for all the guidance, support, and expertise he has provided over the years that I have worked with him. I am very grateful for his patience and motivation, especially with the hurdles of the COVID-19 pandemic. I want to sincerely thank Dr. Andrea Clark for her guidance and input on these analyses and for collaborating with us on this work. I also want to thank Jennifer St. Amant for all her work on the histological analysis. I would not have been able to do this without the support of fellow Wohl lab member, Elyse Rier, who was a constant source of support, motivation, and guidance in this project. I want to thank the rest of my family and friends for their patience and support as I have been working on this project. I look forward, as I'm sure they do, to talking to them about things other than mice. My sincere thanks also go to my committee: Dr. Clark, Dr. Noseworthy, Dr. Quenneville and Dr. Wohl for all their input and help in the preparation of this thesis.

Table of Contents

List of Figures

List of Tables

Abbreviations and Symbols

Abbreviation	Definition
α	alpha
β	beta
μCT	micro-computed tomography
BV/TV*	bone volume fraction – bone volume/total volume
Col2	collagen II
Col2Cre	Collagen II Cre recombinase
CTAn	CT Analyzer
ECM	extracellular matrix
itga1	Integrin α1 subunit
IQR	interquartile range
LAP	latency associated peptide
LCL	lateral collateral ligament
MCL	medial collateral ligament
OA	osteoarthritis
PTOA	post-traumatic osteoarthritis
ROI	Region of interest
Tb.Sp*	trabecular separation
Tb.Th*	trabecular thickness
TβRII	transforming growth factor beta type II receptor
TCPTP	T cell protein tyrosine phosphatase
TGF-β / TGFβ	transforming growth factor beta
VOI	volume of interest
WT	wild-type

* Standard nomenclature in trabecular analysis (Bouxsein et al., 2010; Parfitt, 1988)

Declaration of Academic Achievement

I, Roshan Bashar, scanned, reconstructed, and transformed scan data to analyze the samples. I developed the method used for the quantification of bone and mineralized tissue. I used the data to perform statistical analyses and draw conclusions related to the study focus. My supervisor, Dr. Gregory Wohl, provided expertise in genetics, the mechanisms of osteoarthritis progression, and phenotypes in the knee. Dr. Wohl provided guidance, expertise, and appropriate error analysis to the method development.

Dr. Andrea Clark provided expertise in genetics and important osteoarthritis phenotypes. Jennifer St. Amant and Dr. Clark provided the histological analysis results that guided the hypotheses of this thesis.

1 Introduction and Background

1.1 Introduction

This project is part of a foregoing analysis by Dr. A Clark and Jennifer St. Amant from the University of Guelph. Their focus was to analyze a genetic mouse model involving ubiquitous integrin α1 subunit and cartilage-specific transforming growth factor beta receptor II (TβRII) knockouts as they relate to the pathology of osteoarthritis. This project studied the effects of genetic modifications in the form of a ubiquitous integrin α1 subunit knockout (*itga1*) and a cartilage-specific conditional TβRII knockout on bone changes in the knees of mice. This genetic model was developed by Dr. Andrea Clark at the University of Guelph to explore the mechanisms by which early and more severe spontaneous osteoarthritis (OA) is triggered in the *itga1*-null mouse. The project presented in this thesis aimed to determine whether bone in the *itga1*-null mouse knee exhibited OA-like phenotypes in response to targeted genetic knockouts.

Information about OA and its pathology in the knee, the genetic model, bone observations in post-traumatic osteoarthritis (PTOA) studies, and resulting hypotheses, are outlined in section 1.2. Determination of the methods for the scanning, reconstruction, preparation of datasets, quantification, and analysis of mice hindlimbs follows in section 2. The results of the study are outlined in section 1. Discussion of the findings and conclusions of the study are found in sections 4 and 5.

1.2 Background

1.2.1 The Murine Knee

The murine (mouse) knee (Figure 1) has a similar structure to the human knee. But,

unlike in humans, the tibia and fibula are connected as one bone structure. The fibula sits

lower on the tibia on the lateral side of the limb.

Patella **(A)**

Femoral condyles

Lateral Meniscus **(C)**

Medial Meniscus **(B)**

Medial Collateral Ligament **(D)**

Lateral Collateral Ligament **(E)**

Tibial Epiphysis
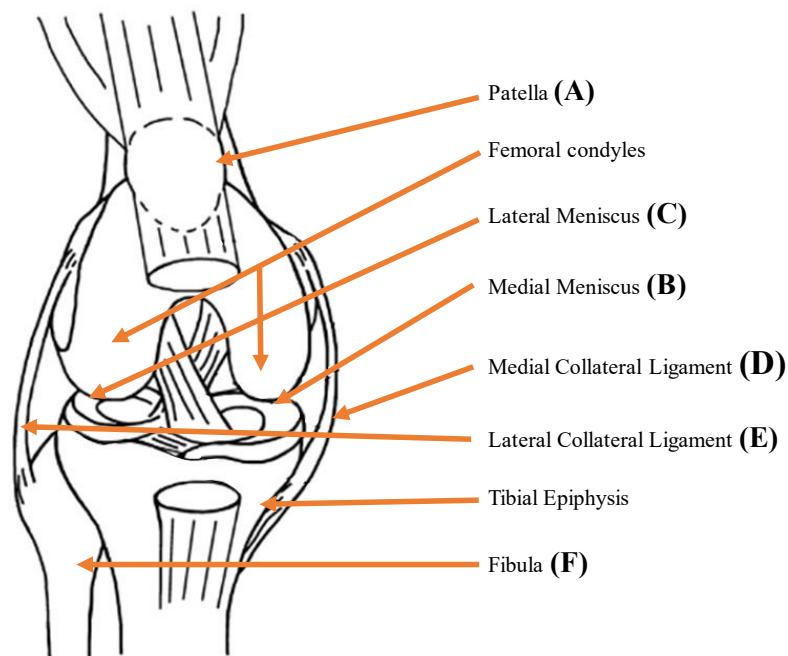
Fibula **(F)**

Figure 1: Schematic of the murine knee, adapted from (Kamekura et al., 2005)). The locations of the patella (A), medial meniscus (B), lateral meniscus (C), medial (D), and lateral (E) collateral ligaments are shown. The fibula (F) is located on the lateral side of the knee. The parts of bone directly involved in joint mechanics are the femoral condyles and tibial epiphysis. They are superior and inferior to the joint, respectively.

The patella is a body of bone that protects and facilitates movement of the knee, using the

quadriceps to pull the tibia forwards on the femur. The patella is attached to the patellar

ligament, which guides its movement along the patellofemoral joint on the surface of the

femur. (Christiansen et al., 2012; Kamekura et al., 2005) Patellar dislocation has been

observed in animal models of post-traumatic osteoarthritis (PTOA). (Kamekura et al.,

2005; Walton, 1979) The menisci (Figure 1B, C) are located between the tibial plateau

and femoral condyles. The medial and lateral menisci are anchored to the tibial plateau by

the medial and lateral meniscotibial ligament, respectively. (D. Chen et al., 2017) The

menisci act as shock absorbers in the knee. They are composed of cartilage (inner 2/3)

and ligament tissue (outer 1/3) which are made up mostly of type I and II collagen.

(Yoshioka et al., 2022) The medial and lateral collateral ligaments (Figure 1D, E) run

alongside the knee, aiding stability and movement in the knee. The medial collateral

ligament (MCL) connects the tibia and femur. The lateral collateral ligament (LCL)

connects the fibula and the femur. The extracellular matrix (ECM) of the ligaments is

made up mostly of type I collagen. (Hudson et al., 2021) Trabecular regions surrounding

the knee are located in the tibia and femur. The trabecular regions affected most by OA-

like phenotypes are in closest proximity to the joint line between the subchondral bone

and growth plate, encased by cortical bone. The trabecular region of the tibia is in the

tibial epiphysis. The trabecular region of the distal femur in closest proximity to the knee

lies within the femoral condyles.

1.2.2   Osteoarthritis Epidemiology

Osteoarthritis (OA), the most common form of arthritis, is considered a degenerative joint

disorder. (Loeser et al., 2012) OA develops at high-use, load-bearing joints, such as the

knee. OA is highly prevalent, with approximately 13.6% of Canadians aged 20 or older

having been diagnosed. (*Osteoarthritis in Canada*, 2020). A study on patients in Ontario, Canada found that the mean cost of medical services in 2012 was 2 times greater over a year for OA patients (CAD $2233) compared to a control group of non-OA patients (CAD $1033) (Tarride et al., 2012). Due to the complexity and lack of information on the underlying causes of OA, treatment thus far has focused on relieving painful symptoms, rather than preventative care. OA can develop spontaneously but there are also risk factors that increase the likelihood of developing OA. Such risk factors include injuries, genetics, age, and body weight. (Loeser et al., 2012) Genetic models that knock out/alter genes have been developed to isolate possible molecular or genetic causes of OA, especially in the case of spontaneous OA. Identifying the genes/disorders responsible for the progression and initiation of OA could provide information to aid in the development of future preventative and disease-altering treatments of OA.

1.2.3   Osteoarthritis Phenotypes and Tissue Adaptations

Characteristics of osteoarthritis include degraded articular cartilage, bone adaptation, osteophyte growth, fibrosis of the synovial lining, and ectopic mineralization. (Loeser et al., 2012) These characteristics irritate the joint region and can cause substantial pain and discomfort. Bone adaptations characteristic of OA include loss of trabecular bone, increased trabecular spacing, decrease in trabecular thickness, thickened subchondral bone, osteophytosis, and calcification of surrounding soft tissues. (Loeser et al., 2012) Studies of osteoarthritic-like bone adaptations have observed changes in the bone architecture within the femur and tibia, close to the knee (Botter et al., 2008; Christiansen

et al., 2012; Glasson et al., 2007) Overall, these studies have found that the bone volume fraction is less in the trabecular bone adjacent to joints that exhibit osteoarthritic characteristics. (Botter et al., 2008; Christiansen et al., 2012) Osteophytes are abnormal bone masses (bone spurs) that develop on and around joint tissues. Osteophyte formation around the knee in murine animal models has been reported in previous studies of OA. (Bakker et al., 2001; Blaney Davidson et al., 2006; Scharstuhl et al., 2003) Osteophytes found in these studies originated at the root of the medial collateral ligament (Blaney Davidson et al., 2006; Scharstuhl et al., 2003), the surface of the tibia near the articular cartilage (Botter et al., 2008; Scharstuhl et al., 2002) and at the joint margins (Christiansen et al., 2012; Scharstuhl et al., 2003). Dislocation of, and abnormal masses on, the patella have also been observed in previous models of OA. (Christiansen et al., 2012; Fang et al., 2018; Walton, 1979) However, dislocation of the patella could also be caused by handling of the specimens, rather than as a result of OA.

1.2.4   Bone and Cartilage Interactions

Joints are complex systems including bone, ligaments, articular cartilage, subchondral bone, the meniscus, the joint capsule, and the synovium. Changes to the articular cartilage are likely to affect the surrounding bone and soft tissues. Having frictionless movement for opposing surfaces is vital to normal joint function. When the soft tissues become damaged or calcified, the surrounding soft tissues and bone are exposed to greater loads and wear. (D. Chen et al., 2017; Glasson et al., 2007) Degrading cartilage and other phenomena linked to OA can cause malalignment, incorrect load distribution,

and a decreased range of motion, which can lead to more damage to the joint region (Fang et al., 2018; Glasson et al., 2007). Articular cartilage is especially vital for the biomechanical function of joints as it covers the joint surfaces and provides shock resistance to the joint and its surroundings. The collateral ligaments, meniscus, and synovial capsule are soft tissues that provide additional mechanical stability and guide joint motion. (Aigner et al., 2015) Previous studies in various animal subjects, including mice, have found that bone adaptations such as thinning of trabeculae, increased trabecular separation, and decreased bone volume fraction were observed in specimens exhibiting OA-like damage to cartilage at the knee. (Clark et al., 2010; Fang et al., 2018; Gupta et al., 2021; Shin et al., 2016; Wohl et al., 2001) These phenotypes were observed in studies of post-traumatic osteoarthritis, where a mechanical disturbance, typically altered loading or surgery, is induced at the joint, then analyzed in comparison to an undisturbed (sham) animal. (Christiansen et al., 2015)

1.2.5 Experimental Genetic Model

The genetic model used in this project was a double knockout of the integrin α1 subunit (ubiquitous) and transforming growth factor beta receptor type II (TβRII, cartilage-specific). The model was designed to inhibit excessive TGFβ signalling associated with fibrosis in the articular cartilage of *itga1*-null mice. Mice from this genetic model were bred from BALB/c mice with and without a ubiquitous integrin α1 subunit knockout activated (*itga1*-null and wild-type, respectively). The cartilage-specific TβRII knockout

was induced via a combination of a tamoxifen-inducible Cre, Col2CreER^T, and a TβRII

flox. (St. Amant, 2022)

1.2.5.1   Type II Collagen

Joint cartilage typically consists of 5% chondrocytes and 95% extracellular matrix. Type

II collagen is a protein present in the extracellular matrix of articular cartilage, providing

tensile strength. (Gupta et al., 2021) Upon binding by collagens, integrin α1β1 is

activated and thus able to regulate a profibrotic response by cells. Col2 provides

instructions to the chondrocyte for producing type II collagen. (Zemmyo et al., 2003)

Integrin α1β1, when bound to collagen and activated, sends a feedback signal to TβRII to

dampen TGFB signalling and downstream Smad activation. The feedback is sent via T

cell protein tyrosine phosphatase (TCPTP), an intracellular regulating protein. TCPTP

travels from the nucleus to bind with the integrin α1 subunit. Once bound, the TCPTP

leaves a residue on TβRII that obstructs the receptors ability to activate TGFB signalling

and downstream Smad 2/3 production. (M. Chen et al., 2007) A representation of the

negative feedback process in chondrocytes is shown in Figure 2. In mice with an integrin

α1 subunit knockout, TCPTP could not be recruited via integrin α1β1 and collagen

binding, to inhibit TβRII signalling (Figure 3). (M. Chen et al., 2007) Based on these

data, integrin α1β1 is likely vital in the regulation of Col2 protein production in

chondrocytes.
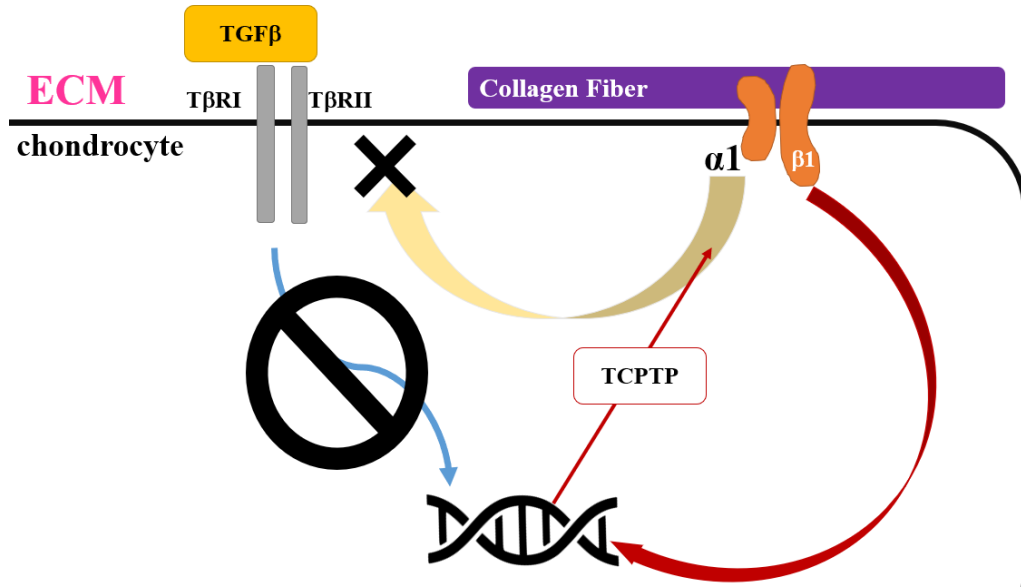
Figure 2: Integrin α1β1 regulates collagen production in the cell by commanding TβRII to stop signalling for production. When integrin α1β1 (orange kidney shapes) is bound to collagen in the extracellular matrix (ECM) (purple fibre), the regulating T cell protein tyrosine phosphatase (TCPTP) (red outlined rectangle) travels from the nucleus (red line to and from black DNA double helix) to bind with the integrin α1 subunit. Once bound, the TCPTP leaves a residue that inhibits TβRII (grey transmembrane rectangle) from facilitating signalling (blue wavy arrow) for collagen production.
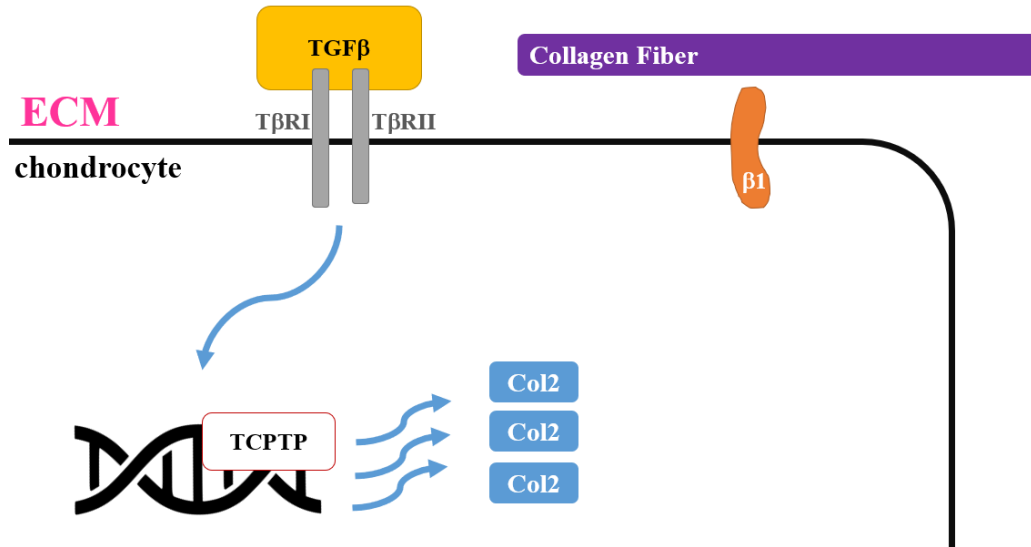
Figure 3: When the integrin α1 subunit is knocked out, the integrin α1β1 cannot form. In the ECM, collagen (purple) is present, but there is no integrin α1 subunit to bind with. Therefore, TCPTP (red-outlined rectangle) cannot be recruited via the integrin from the nucleus. TGFβ signalling continues, unregulated, facilitating the production of collagen. In the case of the chondrocyte this would be Col2 (blue).

1.2.5.2   Integrin α1β1 and the Integrin α1 subunit (*itga1*)

Integrins are transmembrane receptors, made with a pairing of α and β subunits, that perform vital functions in cells. Integrins facilitate interactions between cells, the extracellular matrix (ECM), growth factors, signalling components, and other important extracellular entities that are vital to cell development, adhesion, and maintenance. (Loeser, 2014; McEver & Luscinskas, 2017) Integrin α1β1 has an important role as a collagen-binding receptor, binding to collagen types I, II, IV and VI. (Loeser, 2014). The integrin α1 subunit (*itga1*) is expressed by fibroblasts, bone marrow mesenchymal stem cells, and chondrocytes. It is an important receptor for the facilitation of collagen and laminin production. (Gardner, 2014; Gardner et al., 1996) Zemmyo et al. found that wild-

type mice had an upregulated expression of the integrin α1 subunit in the superficial zone of articular cartilage before cartilage damage had occurred. (Zemmyo et al., 2003) Additionally, integrin α1β1 has been shown to reduce the severity of both spontaneous and post traumatic OA in the articular cartilage of wild-type mice. (Shin et al., 2016; St. Amant, 2022; Zemmyo et al., 2003) The integrin β1 subunit is required for the formation of several integrins, some of which are critical to fetal development. Knocking out the integrin β1 subunit therefore leads to embryonic death in mice. (Fässler & Meyer, 1995) The integrin α1 subunit, however, binds exclusively to the integrin β1 subunit. Therefore, knocking out the integrin α1 subunit prevents the formation of integrin α1β1 while leaving the β1 subunit to bind to its other alpha partners. In chondrocytes, the lack of integrin α1β1 inhibits the regulation of collagen production through the TGFβ signalling mechanism. (Gardner et al., 1996; Zemmyo et al., 2003)

1.2.5.3   The *itga1*-null Mouse Model

The *itga1*-null mouse, has the integrin α1 subunit knocked out ubiquitously. (Gardner et al., 1996) Initially, *itga1*-null mice were morphologically identical to wild type mice at 4 months. However, as the mice aged they were found to have more cartilage loss, exposure of subchondral bone, earlier onset of cartilage damage, and osteophyte formation than their wild-type counterparts. (Zemmyo et al., 2003). As a receptor for collagens, including type I collagen which is abundant in bone, knockout of integrin α1β1 was expected to influence bone architecture in *itga1*-null mice. (Gardner, 2014) Bone

calluses after fracture in *itga1*-null mice had decreased levels of type I collagen and smaller circumferences than in those of WT mice. (Ekholm et al., 2002) *Itga1*-null mice in studies of PTOA overall had lower bone volume fraction and greater trabecular separation than wild-type (WT) mice at 2 and 4 weeks. (Shin et al., 2016) The histological soft tissue study performed by St. Amant observed severe cartilage erosion in *itga1*-null mice, reaching full-thickness cartilage erosion at the tibia of 16-month male and female mice. Additionally, full-thickness cartilage erosion was observed at the femur in 16-month male mice.

1.2.5.4   Transforming Growth Factor Beta (β)

The transforming growth factor beta (TGFβ) family are anabolic growth factors important in the role of development, growth, and differentiation of cells. (Blaney Davidson et al., 2007; Gupta et al., 2021) TGFβ is an important anabolic factor in OA and benefits cartilage by facilitating proteoglycan and type II collagen protein production. (Blaney Davidson et al., 2005) In articular cartilage, TGFβ exists in the extracellular matrix, held inactive by latency associated peptide (LAP). (Plotkin et al., 2019) TGFβ can only bind to its receptors, TβRI and TβRII, when released from LAP via shear stress (Figure 4). (Li et al., 2022; Plotkin et al., 2019) Once released, TGFβ binds to TβRII, which then binds and activates TβRI, ultimately inducing SMAD signalling and Col2 protein production inside the cell (Figure 5). (Blaney Davidson et al., 2005; Scharstuhl et al., 2003) Inhibition of TGFβ has been implicated in reduced repair capacity of cartilage. (Blaney Davidson et al., 2005; Scharstuhl et al., 2002) In wild-type mice, normal cartilage typically expresses

TGFβ in high levels, while osteoarthritic cartilage has little or no TGFβ present. (Blaney Davidson et al., 2006; Gupta et al., 2021) Degenerative effects of TGFβ inhibition at the knee include degradation of articular cartilage, damage to the soft tissues, and degradation of bone in the femur and tibia. (Blaney Davidson et al., 2006) These results demonstrate that TGFβ is important for repair processes. However, excessive TGFβ can have detrimental effects relating to excessive calcified tissue formation. Abnormal calcification of soft tissues (ectopic calcification) and osteophyte (bone spur) formation is associated with the presence of excess TGFβ. (Bakker et al., 2001; Blaney Davidson et al., 2006; Scharstuhl et al., 2002, 2003) Therefore, TGFβ appears to have an important role in repair processes, but may have adverse effects when present in excess, leading to excessive tissue formation.
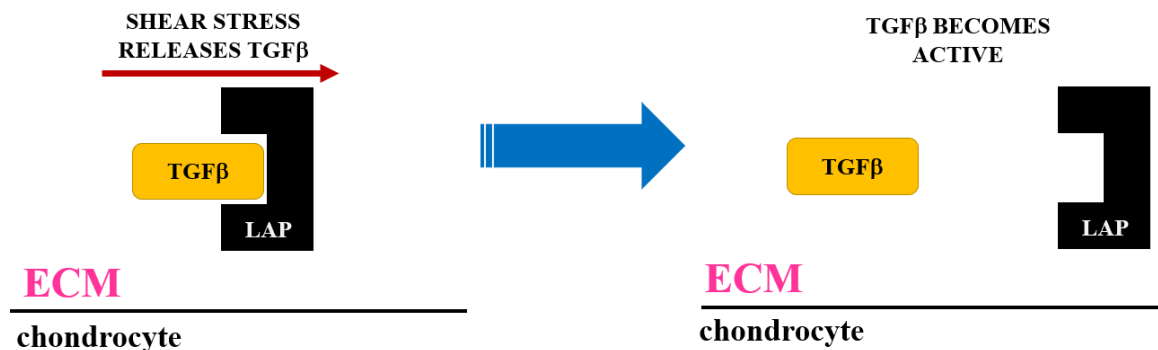
Figure 4: Activation of TGFβ. TGFβ (yellow) exists in the extracellular matrix (ECM). It is held inactive by latency associated peptide (LAP) (black). The TGFβ cannot bind with its receptors without being released from LAP. Shear stresses in the knee (red arrow) release TGFβ from LAP, leaving it in its active form.
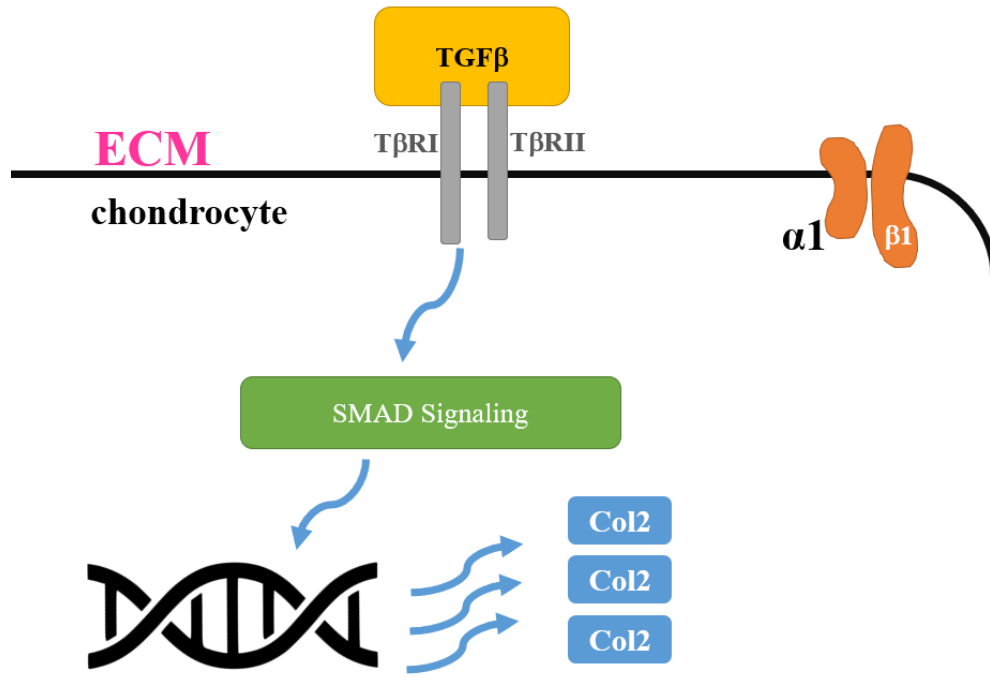
Figure 5: Activated TGFβ (yellow) in the ECM can bind with its type I and type II receptors, TβRI and TβRII (gray) respectively. Once bound, TβRI and TβRII induce SMAD signalling (green). Signals are sent to the nucleus (black double helix) to induce Col2 protein (blue) production.

1.2.5.5   Col2Cre – Cre-lox Combination

The term genetic knockout encompasses several techniques which target specific genes for removal or inactivation. A Cre-lox recombination technique targets genetic knockouts in specific tissues via breeding. Conditions can be introduced in breeding to allow controlled timing of the knockout. When conditions are met, the Cre-lox is activated and the specified gene is knocked out from the targeted region. (Lai et al., 2019) The Col2CreER^T and TβRII flox is a Cre-lox recombination which, when activated with tamoxifen, knocks out the TβRII in articular cartilage. Without TβRII present, the TGFβ

growth factor cannot trigger signalling inside the cell, and most important in our case, TGFβ cannot signal the production of type II collagen. It is important to note that the Col2CreER^T does not result in a complete knockout of TβRII. Conditional activation for the gene knockout is delayed so that the animal can develop normally. The success of the knockout depends on factors such as breeding, timing, and precision of the injection. (Lai et al., 2019; St. Amant, 2022) In St. Amant's study TβRII deletion in the articular cartilage was 70% effective, and other works have achieved ~85% effectiveness. (Shen et al., 2013; St. Amant, 2022) The protective effect of TβRII deletion in *itga1*-null mice may depend on the effectiveness of the knockout.

1.2.5.6   Tamoxifen

Tamoxifen was the chemical that was used to activate the Col2Cre in this study. Tamoxifen is a triarylethylene antioestrogen that is used in the treatment of breast cancer. (Creamer et al., 1994) Some patients treated for breast cancer with tamoxifen reported that they developed acute inflammatory arthritis. (Creamer et al., 1994) The patients were not on any other drug and their symptoms improved once treatment ceased. Since tamoxifen has noted musculoskeletal side effects, it was important to include tamoxifen controls in this study. The dosing method used in this study was different in concentration and administration, therefore these may not be comparable results. See section 2.2 for further information.

1.2.5.7   Previous Work with this Genetic Model

Dr. A. Clark and J. St. Amant from the University of Guelph. (St. Amant, 2022) assessed

the physical abilities of mice in the different cohorts at multiple stages of life and

assessed cartilage and joint degeneration using histological sections of the mouse knees at

4, 8, 12, and 16 months of age. The animal cohorts and the experimental models are

described in detail in section 2.1 of the Materials and Methods section. The study found

that relative to the wild-type mouse, 12-month male, and 16-month female, *itga1*-null

mice had severe erosion of cartilage in the medial compartment of the tibial plateau.

Additionally, 16-month male mice also had severe cartilage erosion in the medial femoral

condyle. Though almost all mice in all groups developed some degenerative changes by

16 months, *itga1*-null mice had more severe degenerative changes. These data suggest

that integrin α1β1 is important for cartilage maintenance and protection. In a similar

previous study using a post-traumatic osteoarthritis mouse model, *itga1*-null female mice

developed earlier and more severe post-traumatic OA than wild-type mice. (Shin et al.,

2016) Mice with the double knockout (ubiquitous integrin α1 subunit and cartilage-

specific TBRII knockout) had less severe OA, showing that the excessive TβRII

signalling in *itga1*-null mice is the main driver of OA in the *itga1*-null mouse. Therefore,

it is expected that integrin α1β1 protects articular cartilage from spontaneous OA by

regulating TβRII signalling.

1.2.6   Evaluation of Bone Architecture using Micro-Computed Tomography (µCT)

Imaging

Before the use of micro-computed tomography (µCT) images for the examination of bone

histomorphometry, methods were largely manual, labour-intensive, and lengthy. Previous

methods involved taking cross-sectional biopsies and using methods of direct

measurement on these samples to quantify the parameters (Parfitt, 1988). Different

parameters required different orientations of the cross-section and taking numerous

biopsies, thus limiting the accuracy of results. These 2D histomorphometry methods were

replaced by 3D methods such as the use of µCT images and reconstruction. µCT imaging

allows the analysis process to be semi-automated, with more accuracy and with limited

sample manipulation. With previous histological methods, histological sectioning was

destructive and once the sample was cut it could not be viewed in any other orientation.

The 3D datasets obtained with µCT allow the same regions to be analyzed from

numerous orientations. According to guidelines for trabecular bone analysis using µCT

imaging, several studies concluded that results from this method closely match those from

previous 2D methods. (Bouxsein et al., 2010) The µCT scanner creates 2D x-ray images,

taken at a chosen angular interval, as a specimen rotates about a central axis for a 360° or

180° revolution. The x-ray absorption at each pixel of the scanning area is taken to

recreate the specimen. Each image is consolidated into a 3D set of voxels with an

intensity assigned to each voxel. Micro-computed tomography has become a standard in

trabecular bone analysis, especially in murine and rodent specimens where trabeculae are

very small. Scans at lower resolutions can inaccurately represent the size of the

trabeculae, causing errors in trabecular parameter values. (Waarsing et al., 2004) Previous studies have found that trabecular thicknesses in mice are approximately 30 to 50µm. (Amblard et al., 2003) Previous studies have used isometric resolutions ranging from 6 to 16µm to successfully analyze trabeculae in mouse models of PTOA. (Anderson et al., 2016; Botter et al., 2008; Jia et al., 2018; Shin et al., 2016).

1.3 Study Aims and Hypotheses

Previous work in osteoarthritis pathologies found that integrin α1β1 has a protective effect in spontaneous osteoarthritis. TGFβ is also connected with osteoarthritic phenotypes with differing results. The foregoing study for this project by St. Amant, (2022) showed that *itga1*-null mice experienced earlier and more severe degenerative changes in the knee cartilage [and showed physical limitations associated with joint pain and stiffness that are consistent with osteoarthritis]. (St. Amant, 2022) This suggests that TGFβ signalling was unregulated and caused cartilage degeneration in the *itga1*-null mice. This was further supported by *itga1*-null mice with a cartilage-specific TβRII knockout, as they had less severe OA with the TβRII knockout than without - presumably because the TGFβ signalling was inhibited in the chondrocytes. Moreover, they observed that some of the soft tissues in and around the knees (medial and lateral menisci and medial and lateral collateral ligaments) experienced calcification in the groups with both the integrin α1 subunit and TβRII knocked out. The purpose of the work reported in this thesis was to extend the analysis from the cartilage and other joint soft tissues and to measure if there were changes to the trabecular bone architecture around the joint.

The specific aim of the study was to understand how bone responds to genetic knockouts (ubiquitous integrin α1 subunit, cartilage specific TβRII) that induce osteoarthritic elements in articular cartilage. To explore this, the project was designed to:

1. Quantify measures of trabecular bone architecture (trabecular thickness, trabecular separation, bone volume fraction) at the tibial epiphysis and femoral condyles.

2. To characterize and quantify ectopic (abnormally located) calcifications in soft tissues around the joint.

Based on the findings described in section 1.2, and especially from the findings of St. Amant, the hypotheses for the study were as follows:

1. Mice bred with a ubiquitous α1 knockout (*itga1*-null$^{-/-}$) will have OA-like bone adaptation compared to their 'wild type' counterparts.

2. The cartilage-specific inhibition of TβRII signalling will:

    a. Reduce previously reported OA-like phenotypes in trabecular bone found in the knees of *itga1*-null mice.

    b. increase ectopic calcification at and around the knee of *itga1*-null mice due to the heightened levels of TGFβ in the synovial fluid.

As previously stated, the behaviour of trabecular bone in *itga1*-null mice included decreased trabecular bone volume fraction and increased trabecular separation. (Shin et al., 2016) Ectopic calcifications noted in PTOA studies included bone spurs (osteophytes) at the collateral ligaments and patella, and calcification along soft tissue structures (collateral ligaments, menisci, quadriceps). (Bakker et al., 2001; Blaney Davidson et al., 2006; Scharstuhl et al., 2002, 2003)

2   Materials and Methods

2.1   Animal Model

All procedures have been approved by the institutional animal research ethics committee in compliance with the Canadian Council on Animal Care. For this investigation, 275 combined wild type (WT) and *itga1*-null samples were provided by Dr. Clark's lab from the University of Guelph. The genotypes of the mice we studied were combinations of a ubiquitous integrin α1 subunit knockout and cartilage-specific TGF-β receptor (TβRII) knockout. Of these samples, there were 139 female mice and 136 male mice. The mice were separated into six groups based on combinations of genetic knockouts of the integrin α1 subunit (ubiquitous) and TβRII (cartilage-specific). The genetics of these six groups are summarized in Table 1. All mice were bred with a single knockout (integrin α1 subunit or TβRII), double knockout (integrin α1 subunit and TβRII), or no knockouts. Within each of these cohorts, specimens were euthanized at four time points along their lifespan – 4, 8, 12, and 16 months. This was meant to track relative changes and degradation in tissue changes and potential development of osteoarthritis.

2.2   Cohort Groups

The mice in the study originated from an *itga1*-null colony which was cross-bred to create six genetic cohort groups using Col2CreER$^\text{T}$ and TβRII$^\text{flox/flox}$ mice. Cells in the *itga1*-null mice cannot produce integrin α1β1. Half of the mice were *itga1*-null (three groups with group names, "αTC*xx*"). The other half did not have the ubiquitous genetic knock-out of

the integrin α1 subunit (wild type; the other three groups with group names, "TC*xx*") and were able to produce integrin α1β1 normally. On days 14 and 16, mice with the Col2CreER^T and TβRII$^{flox/flox}$ were given either tamoxifen (2mg/0.1mL tamoxifen in corn oil vehicle) to trigger the conditional knock-out (αTC+t and TC+t, where "t" stands for tamoxifen) or corn oil vehicle control (10% ethanol in corn oil), which would not trigger the conditional knock-out (αTC+c and TC+c, where "c" stands for corn oil). Since the Cre targeted cells expressing the Col2 promotor, the administration of tamoxifen would induce deletion of TβRII only in tissues that make type II collagen (specifically, cartilage). Tamoxifen has also been reported to affect musculoskeletal tissues and so two additional control groups without the Col2CreER^T were created to control for the effects of tamoxifen (aTC**-t** and TC**-t**, where "-"means no Col2Cre, and "t" stands for tamoxifen). A summary of the genetic alterations and the function of the resulting cohorts in the study are compiled in Table 1 and Table 2. The breakdown of sample numbers by cohort, sex, and age is provided in Table 3. Figure 6-Figure 11 contain diagrams showing the results of their genetic alterations.

Table 1: Description of genetic alterations made for each cohort group and the breakdown of experimental interventions made for each cohort. The strain of *itga1*-null mouse, the presence of a tamoxifen-inducible Col2Cre, and the injection given to each cohort

Genetic Alterations or intervention		Ubiquitous Integrin α1 Subunit Knockout (α)	Col2Cre (+/-)	Injection (t/c)
Description		α – *itga1*-null mouse (integrin α1 subunit knockout)	+ bred with a conditional Col2Cre - bred without a conditional Col2Cre	t – subject received a tamoxifen injection c – the subject was injected with corn oil vehicle control
Intended Action		When the integrin α1 subunit is knocked out, the cartilage cells cannot make integrin α1β1 – loses the ability to dampen TβRII signalling	When Col2Cre is present and activated with tamoxifen, TβRII is knocked out. TβRII binds with TGFβ to activate downstream Smad signalling including collagen production.	Tamoxifen activates the conditional Col2Cre. Injection of corn oil, or, tamoxifen without a Cre, is used as a control for comparison to knockouts.
Cohort Groups	TC+c (+c)		+	c
	TC+t (+t)		+	t
	TC-t (-t)		-	t
	αTC+c (α+c)	α	+	c
	αTC+t (α+t)	α	+	t
	αTC-t (α-t)	α	-	t

Table 2: Description of the intention behind interventions in each cohort and the overall function of the cohort to the main focuses of the study.
* Gardner et al., 1996
** St. Amant, 2022

Cohort	Result in genetics	Function in Study
TC+c (+c)	No change – the 'wild type' mouse. *	'Wild-Type' (WT)
TC+t (+t)	TβRII is knocked out in cartilage by tamoxifen activation of Col2Cre. Without TβRII, TGFβ cannot bind to facilitate the production of collagen in cartilage.	To observe the effect of a TβRII knockout in articular cartilage by a tamoxifen activated Col2Cre.
TC-t (-t)	No genetic knockouts. Tamoxifen is injected but there is no Col2Cre to activate.	To observe if tamoxifen has an effect in WT mice. *
αTC+c (α+c)	Integrin α1 subunit is knocked out ubiquitously. No integrin α1β1 present to regulate TβRII signalling and collagen production. TβRII signalling is uninhibited. Excessive collagen production. *	The *itga1*-null mouse. Excessive signalling from TβRII leads to fibrosis and other OA-like phenotypes. *
αTC+t (α+t)	Double knockout of TβRII in cartilage and integrin α1 subunit ubiquitously.	Hypothesized to mitigate cartilage damage by inhibiting excessive TβRII signalling observed in *itga1*-null mice. *,**
αTC-t (α-t)	Integrin α1 subunit is knocked out ubiquitously. Integrin α1β1 cannot form to regulate the TβRII signalling and collagen production. Tamoxifen is injected but there is no Col2Cre to activate. TβRII signalling is uninhibited.	To observe whether tamoxifen affects *itga1*-null mice in the absence of a Col2Cre.
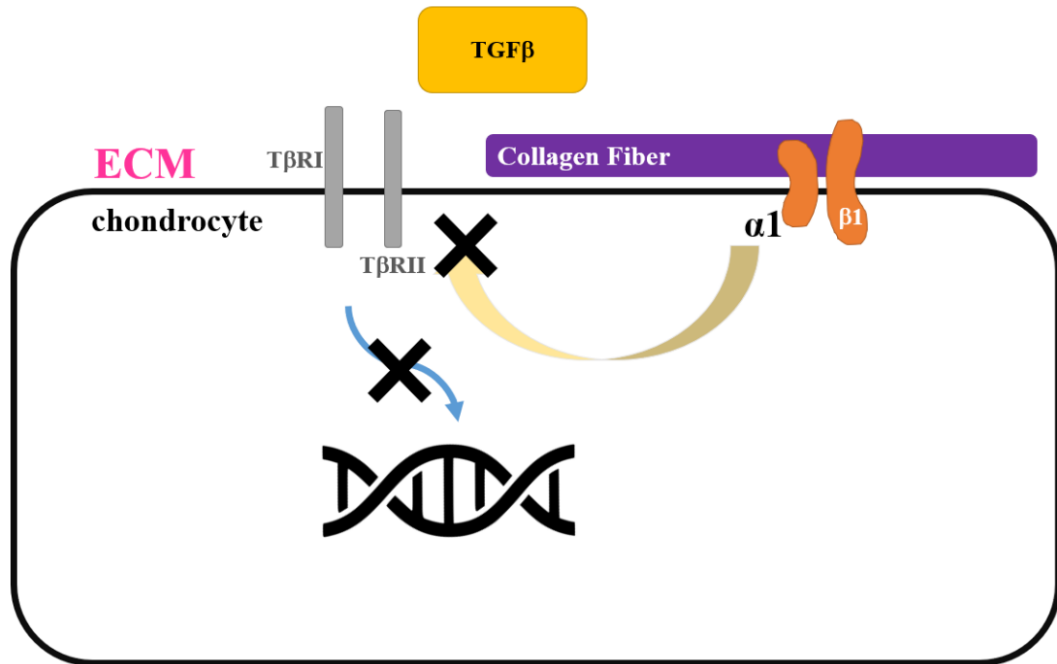
Figure 6: The wild-type (+c) mouse chondrocyte with collagen fiber in the ECM. The integrin α1β1 (orange) is activated by binding to collagen (purple) in the ECM. Once activated, it regulates TβRII (gray) via a negative feedback signal, which commands TβRII to cease signalling for collagen production. TβRII does not bind with TGFβ (yellow rectangle) in the extracellular matrix thus dampening collagen production.
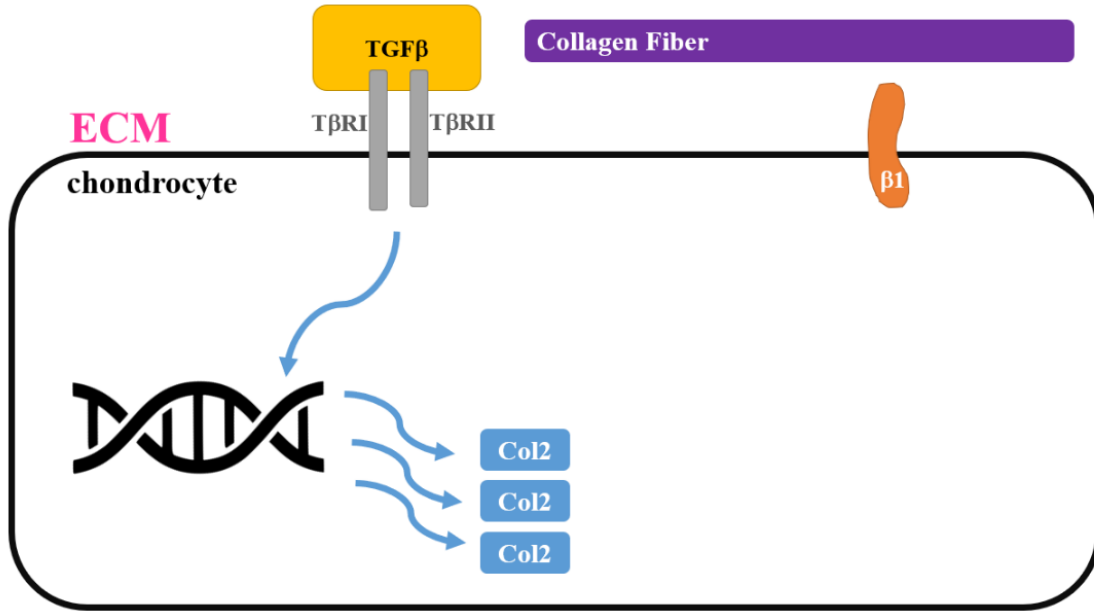
Figure 7: The intended behaviour of the *itga1*-null (α+c) mouse chondrocyte. The integrin α1 subunit is knocked out ubiquitously. The integrin β1 subunit (orange) cannot bind to form integrin α1β1. Collagen (purple fiber) is present in the ECM but collagen production cannot be regulated without integrin α1β1. Activated TGFβ binds to the uninhibited TβRII, facilitating signalling (blue arrows) to the nucleus (black double helix). The cell has excessive collagen production, leading to fibrosis. In the case of the chondrocyte, the excessive collagen would be Col2.
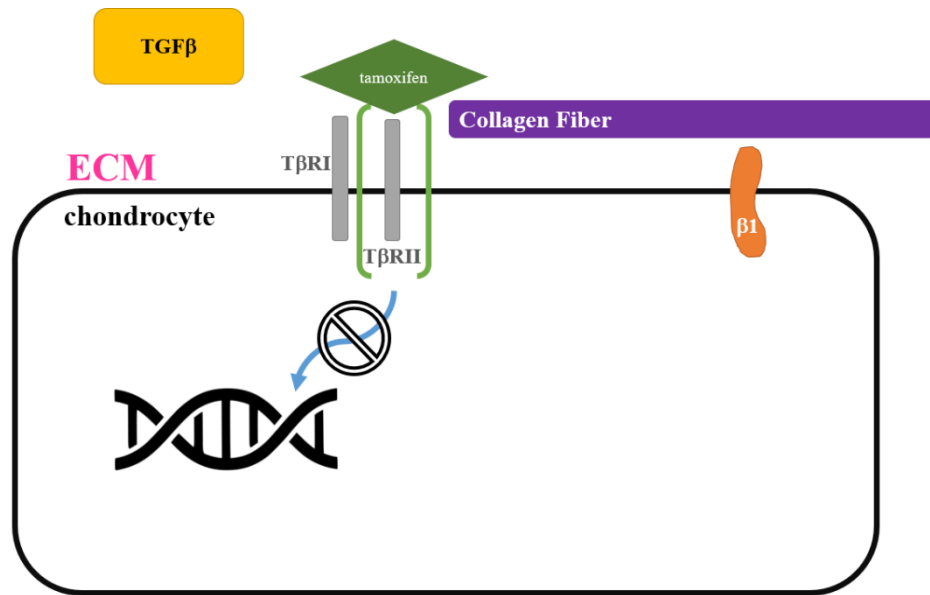
Figure 8: The intended behaviour of the *itga1*-null mouse chondrocyte with a cartilage-specific knockout of TβRII (α+t). The integrin α1 subunit is knocked out and integrin α1β1 is not formed. Tamoxifen (green diamond) injection activates the Col2Cre (green parentheses) and TβRII (gray rectangle) is knocked out. This knockout protects the *itga1*-null mouse from excessive collagen production and fibrosis.
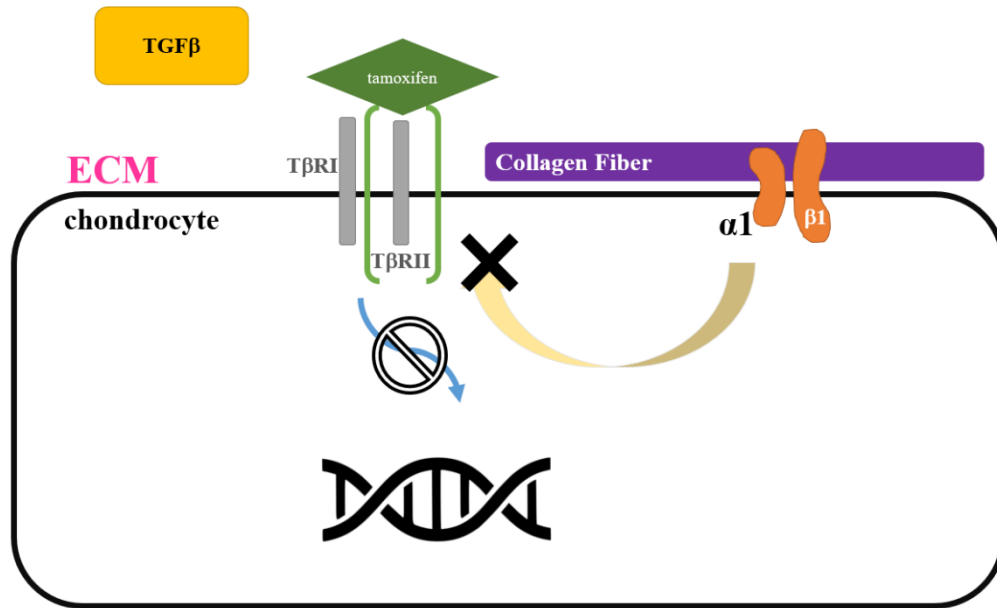
Figure 9: The intended behaviour of the wild-type mouse with a TβRII knockout (+t). Integrin α1β1 (orange) is bound to collagen (purple) and can regulate collagen production. The tamoxifen injection activates the Col2Cre (green diamond and parentheses), knocking out TβRII (gray rectangle in parentheses). Without TβRII, there is no signal to facilitate the production of collagens.
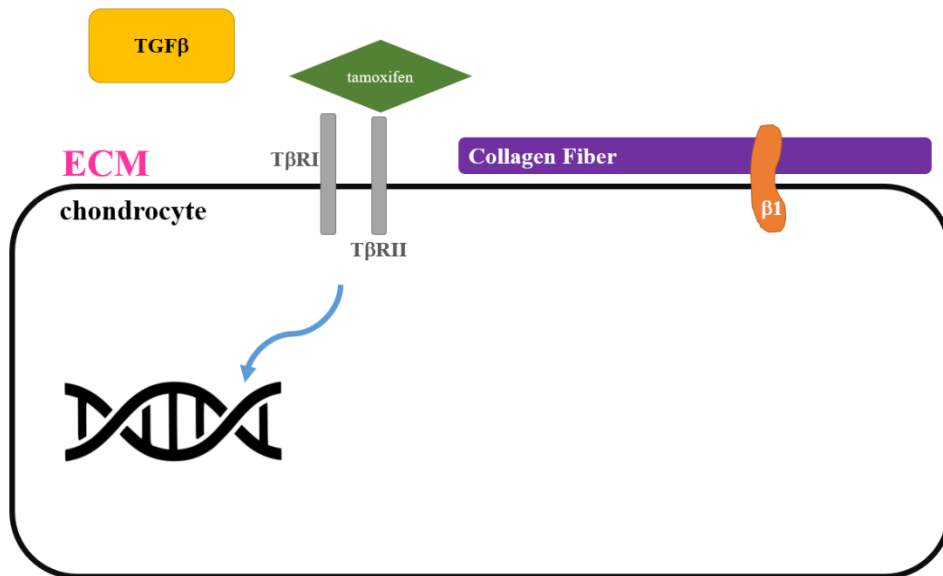
Figure 10: Tamoxifen control for the *itga1*-null mouse (α-t). Tamoxifen (green) is injected into a mouse with no Col2Cre. If tamoxifen does not have an effect, the cell should function like the corn oil injected *itga1*-null mouse (α+c).
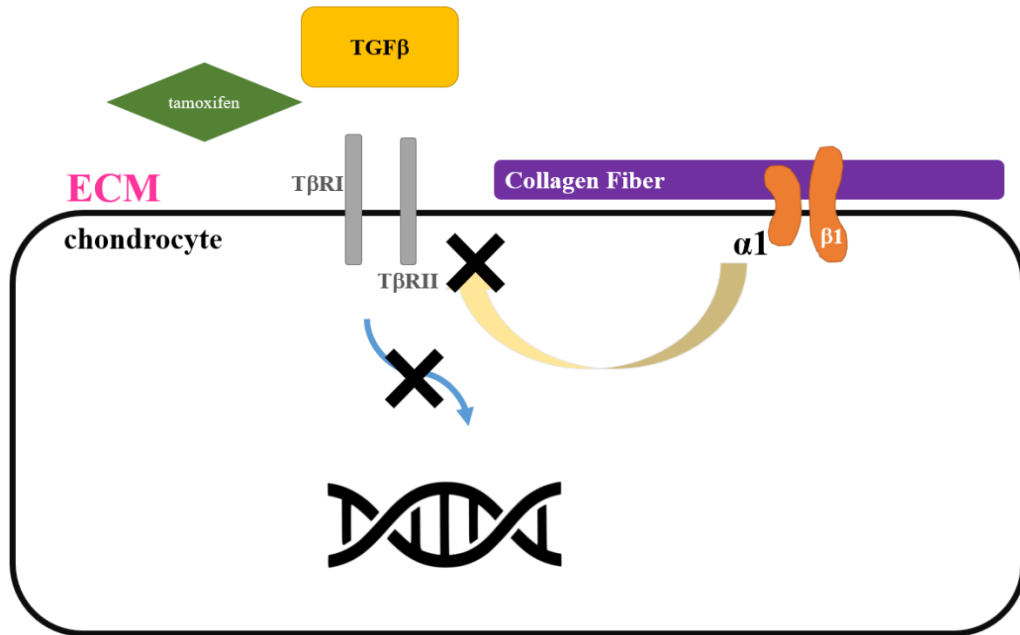
Figure 11: Tamoxifen control for the wild-type mouse(-t). Tamoxifen (green) is injected into a mouse with no Col2Cre. If tamoxifen does not have an effect, the cell should function like the corn oil injected wild-type mouse (+c).

Table 3: Breakdown of sample sizes for the 275 specimens provided by Dr. A Clark's lab. Groups are broken down by cohort, sex, and timepoint (age at death). Values in bold, males at 4 and 16-months, for a total of 71 specimens were analyzed in this study.

Timepoint (months)	**4**		8		12		**16**	
Subgroups /Sex	**M**	F	M	F	M	F	**M**	F
αTC+t (α+t)	**5**	5	5	5	6	5	**7**	8
αTC-t (α-t)	**5**	6	5	5	5	5	**7**	8
αTC+c (α+c)	**7**	5	5	5	7	5	**5**	8
TC+t (+t)	**5**	5	7	5	4	5	**5**	8
TC-t (-t)	**5**	6	5	5	6	5	**7**	8
TC+c (+c)	**5**	5	5	5	5	5	**8**	7
Total	**32**	32	32	30	33	30	**39**	47

The samples were fixed in formalin by our collaborators at the University of Guelph. The specimens were delivered in sealed plastic containers that had separated compartments by subgroup, age, and sex. Once obtained, the limbs were transferred, with their original labels, into individually labelled 15 mL tubes. For use in ongoing work, the entire length of the limb was scanned to capture the hip and ankle. The procedures for scanning, development, and validation of quantification procedure, and data analysis, detailed later in the chapter, were time-consuming. Therefore, the analysis was limited to groups of male mice at two time points, 4 and 16 months (12 groups at varying sample sizes, totalling 71 samples). Analysis performed by Jennifer St. Amant (Dr. Clark's previous Master's student) as well as previous work on this genetic model showed that the male mice had greater cartilage damage and earlier onset osteoarthritis than female mice. (Shin et al., 2016; St. Amant, 2022) Therefore, analyzing the male cohorts provides a more mature progression of OA-like changes to analyze.

2.3   Specimen Holder

A custom specimen holder was 3-D printed so that multiple limbs could be scanned at once. The holder provides stability and alignment to the samples as they rotate axially during scanning. The design was developed using Autodesk Inventor 2022 (Autodesk, San Rafael, California). The design went through several iterations to mitigate the effects of motion artifacts (limbs were moving within the holder spaces during scanning). The final design of the holder had a lid and base which would hold and stabilize 6 mouse hindlimbs within the scannable area (Figure 12). Indicators in the form of circular and

semi-circular cut-outs were added to confirm the orientation of the holder in the scan

images and to help identify the placement and correct identity of each sample when

analyzing the reconstructed datasets (Figure 13).
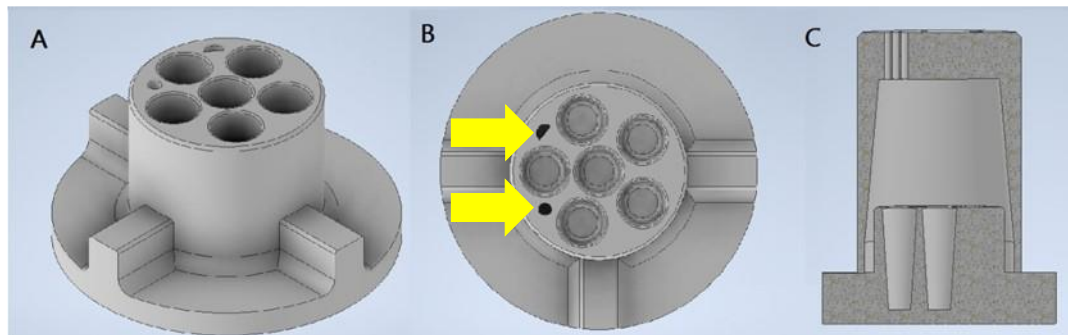
Figure 12: A - isometric view of the specimen holder base B- top view of the specimen holder base, indicator cutouts are shown (yellow arrows) C - section view of specimen holder with lid showing tapered inside and depth of limb cutouts.
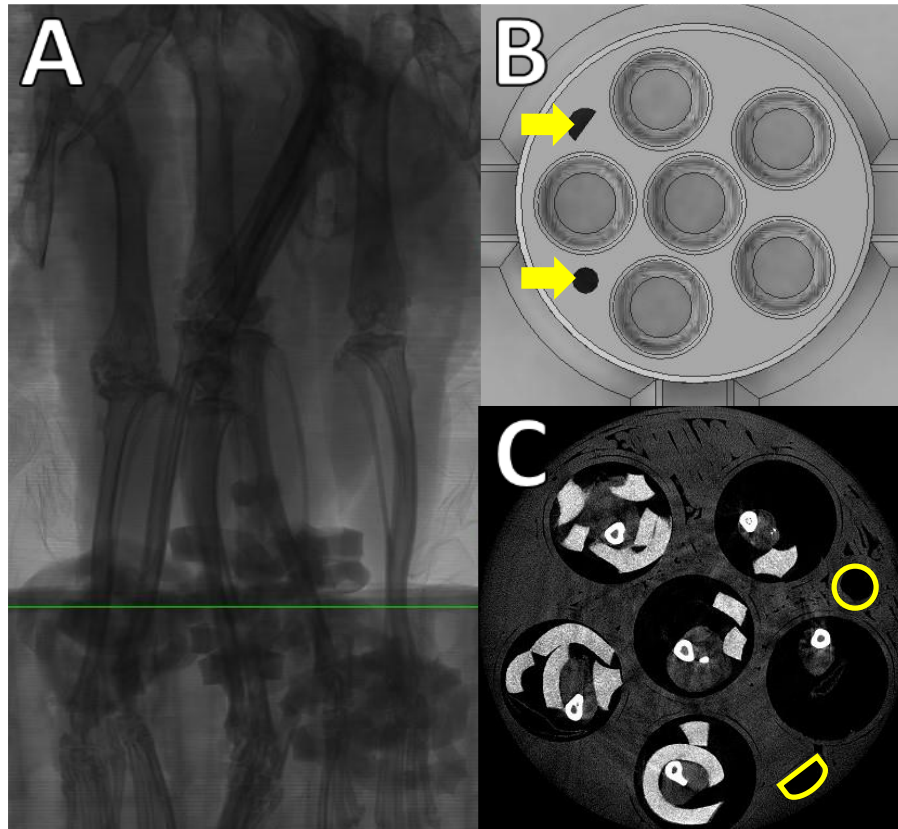
Figure 13: (A) Image of six hindlimbs in their holder from μCT images. The horizontal green preview line in (A) indicates the slice where the transverse view was taken (C). The top view of the holder CAD model (Autodesk Inventor, 2022), (B), shows the relative orientation of specimens and the circular and semi-circular locating features (yellow arrows). The transverse view from the preview line after reconstruction (C) where the corresponding locating features from the holder, outlined in yellow, were used to confirm the viewing plane and to verify specimen identity.

2.4   Sample Identification and Setup

For each scan, the limbs and their respective 15mL tubes were marked with differently coloured small elastic bands to ensure the samples could be identified after the scan. The specimens were placed vertically with feet downward into the slots of the specimen holder. The samples had been fixed in formalin, with the knee in various states of flexion.

Following fixation, the limbs were stiff and could not be adjusted. This limited the number of limbs that could fit in the scannable area, in this case, an ~26mm diameter. Additionally, analyzing calcification in tissues surrounding the joints (knee, hip, and ankle), was important for future study. Therefore, no dissection or alteration to the hindlimbs was done to fit more samples per scan. Gaps between the limbs exposed at the base and the holder lid were filled with paper towel to ensure a snug fit. For this reason, the lid was designed with a taper to hold the samples in place. Each elastic band colour, corresponding specimen ID, and slot number were recorded for each scan. The slot number was determined by its relative position to locating features (Figure 13).

2.5   µCT Scans

Micro-computed tomography (µCT) scans were performed using the Skyscan 1172 (Bruker/Skyscan) µCT scanner. A resolution of 13.16µm (isometric) was chosen to allow several specimens to be scanned at once while having a sufficient resolution to capture changes in the cortical and trabecular bone. (Bouxsein et al., 2010) Identical parameters were used for each scan, as summarized in Table 4. As described previously, each scan was able to hold six hindlimbs within the scanning area. Before each scan, six samples were prepared with a coloured elastic band around the limb as identifiers and placed into the custom holder. The specimens were secured in place with a lid that fit snugly around the muscle tissue. Due to variability in hindlimb height and orientation, the required height of the scan varied. Each sample was scanned as an "oversize" scan, typically taking around 16-19h to complete the scan. The oversize scan took the overall height of

the scan, which was outside the scannable area, split it into multiple scans, then aligned

them to create a contiguous dataset. The scan region spanned from above the hip joints to

just below the start of the metatarsal bones in the feet. The scanner was calibrated

frequently (daily or every other day) using a flat-field correction that compensated for

fluctuations in x-ray emissions and camera sensitivity. (Bruker Skyscan, 2005)

Table 4: Scanning Parameters for the Bruker SkyScan 1172 micro-computed tomography scanner. Parameters were identical for each scan.

Scanning Parameter	Value	Units
Reconstruction Resolution	13.16	µm
Camera	Medium	2000x2000 pixels
Filter	n/a	-
Current	193	µA
Voltage	52	kV
Exposure time	2500	ms
Power	10	W
Rotation Step Size	0.4 (900 views)	Degrees
Scanning Rotation	360	Degrees
Field of View	26.3(W) x 17.6(H)	mm^2
Averaging	8	Frames

2.5.1   Motion Artifact from Early Holder Design.

Before the specimen holder design and dimensions were corrected, specimens during the

scan had significant motion within the holder, resulting in motion artifacts and poor

image quality (Figure 14). The motion could not be corrected in post-processing in either

180° or 360° reconstructions. The holder design was adjusted to secure the limbs and remove motion artifact.
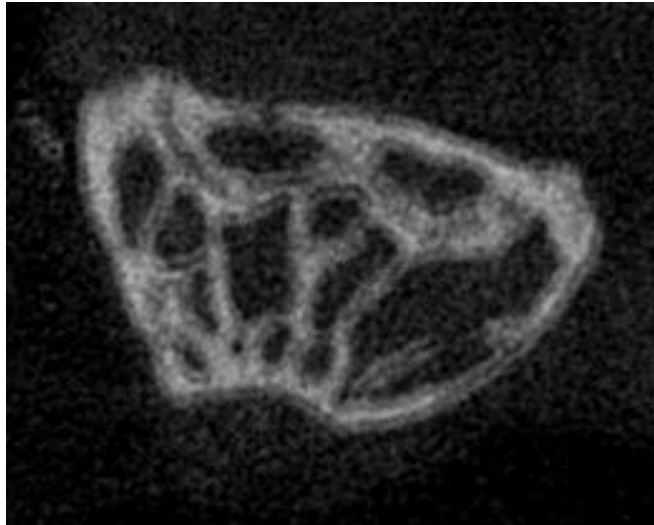
Figure 14: Transverse view (slice) of a mouse femur displaying significant motion artifact. The corresponding holder at the time left some clearance for the limbs to move during scanning. The design was modified to eliminate this error.

2.6 Reconstruction of μCT scans

Program: NRecon (Version 1.7.4.6, Bruker μCT 2011-present, Skyscan 2005-11)

Each dataset was reconstructed in the μCT reconstruction software NRecon. This was a custom program from Bruker, the manufacturer of the Skyscan 1172 μCT scanner. This instrument has three scanning/camera modes – large (4000x4000 pixels), medium (2000x2000 pixels), and small (1000x1000 pixels). The medium and small camera modes achieved higher resolutions by using a 2x2 and 4x4 pixel area, respectively, as one pixel. Therefore, as the resolution magnitude decreases, so do the scannable area dimensions.

Due to the large number of specimens in this project, a 13.16µm resolution was chosen, allowing six hindlimbs to be scanned simultaneously. The resolution was achieved at the medium camera mode and was sufficient to provide reliable results for trabecular analyses. This follows recommendations for murine trabecular analysis, as these measures lie within the 20-70µm range in mouse and rat models. (Bouxsein et al., 2010)

Imaging errors and artifacts were present in the µCT scans including ring-artifacts at the center of the scan (due to broken pixels), beam hardening, and misalignment errors. These errors are related to some combination of sample or scanner movement, x-ray absorption, and scanner defects. They were corrected with post-processing adjustments within reconstruction software. The NRecon software provides four adjustments. Our scans required the use of three of these adjustments, defined in Table 5, to address ring artifacts, beam hardening, and misalignment errors. A trial-and-error approach is required in the application of these adjustments, which was streamlined using the fine-tuning function in NRecon. This function allows the user to iterate through different values of each adjustment (one at a time) and displays the result of each value for the user to evaluate and compare.

Table 5: Description of reconstruction adjustments in NRecon v.1.7.4.6 (Bruker), adapted from the manual provided by Bruker. (Bruker MicroCT, 2016) Adjustments were used with caution in reconstructing datasets to preserve image quality and accuracy.

Adjustment	Definition from Bruker Definition / Purpose of Adjustment
Misalignment Compensation	- Corrects possible misalignment during scanning - Responsible for blurring and motion artifacts in images - Affects thresholding, quantifications, segmentation, etc. - Displays x-ray energy absorption at each pixel in the image at the chosen preview slice - First half (180°) of values from the scan laid over the second half (180°) (Figure 15) - Value is adjusted to synchronize the two datasets and provide a clearer/more accurate image - Automatically calculated by software then fine-tuning runs through several values and their visual result to choose the best alignment
Beam Hardening	- Compensates for beam hardening effects - Requires manual adjustment - Adjust value (0,1…100) and visibly determine the correct value - May require fine-tuning to adjust
Ring-Artifact Reduction	- Reduces ring artifacts present from malfunctioning pixels propagated through the image - Applied before all other post-processing adjustments - Requires manual adjustment - Select values (1,2…20) and visually determine from the preview image - Fine-tuning is recommended for the adjustment - generally not recommended to use an unnecessarily high value as blurring may occur - has nearly no effect if one camera pixel has varied sensitivity during the same scan (e.g., due to beam hardening), or is completely dead (0 sensitivity)

2.6.1   Misalignment Compensation

Misalignment compensation corrects the alignment of the images from the first 180° to

the next 180° of the full 360° rotation. It is used to compensate for any misalignment that

may have occurred during scanning or reconstruction. Typically, the value of the

correction was consistent for all six limbs. However, as the height of the knee varied

between specimens, the magnitude of the misalignment compensation was adjusted for

each reconstructed limb. Although each scan required 3 individual scans to capture the

entire limb, the position of each joint (ankle, knee, or hip) lay within the same scanning

area. Therefore, misalignment from scan to scan in trabecular bone was not an issue

within the reconstructions. Only calcified tissues where the total bone volume was

calculated extended between two scans. If misalignment occurred, only a small

translation was seen. This was not a concern because bone volume quantification used a

sum of voxels representing bone. Therefore, a slight misalignment between scans did not

change the voxel count. The misalignment compensation was adjusted using the fine-

tuning application within NRecon, which allows the user to preview a slice at different

post-alignment values. Misalignment compensation intends to ensure the bone

architecture is properly represented if there is any discrepancy between the first and last

half of the 360° rotation (Figure 15). NRecon first calculated the value automatically, and

the profiles and previews of scan data were used to confirm the value. The optimal value

was determined by applying an appropriate phase shift, determined from the given

profiles (Figure 15 A, B), then observing the preview of the trabecular region of the

specimen (Figure 15 C). Using the fine-tuning feature, multiple misalignment

compensation values (corresponding to the phase shift of the scan profile) could be cycled through at once. The value with the most defined trabecular alignment was used for the reconstruction. Areas with large trabecular regions such as the tibial and femoral epiphysis were best for these observations. In the case shown in Figure 15, the best value for the misalignment compensation was -2.5 as it had the best alignment, although the program calculated it to be -1.5. This demonstrated that fine-tuning was a vital process to achieve accuracy. Using the profiles determined from the program removed subjectivity, ensuring the repeatability of the process.
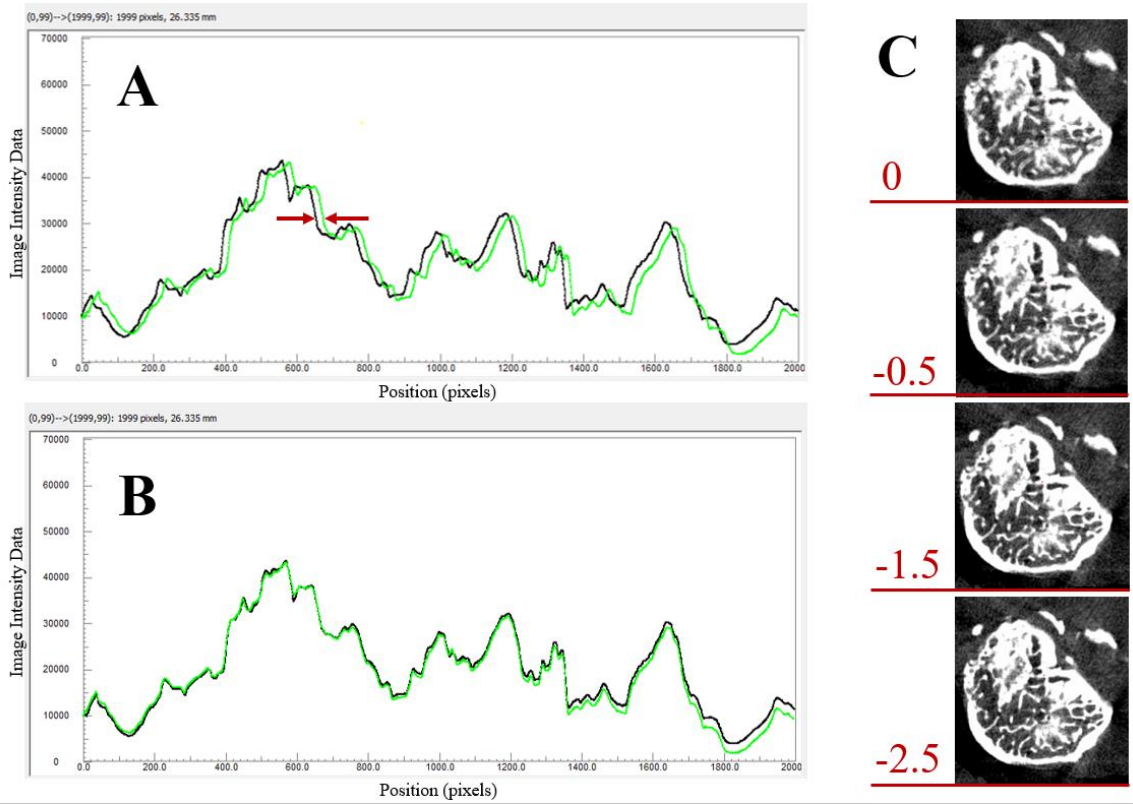
Figure 15: Figures A and B show the profile of an unaligned (A) and aligned (B) image dataset. The black line represents image data from the first 180° of rotation, and the green line represents the next 180° flipped horizontally. The curves are used to determine the phase shift required to align the data. Without adjustment, the top view in (C) shows the transverse view of the slice with no phase shift (0) that corresponds with the chart in A. The phase shift required to align the profiles (red arrows) is the misalignment compensation adjustment value. Images in (C) show the resulting transverse image when each phase shift is applied. In this case, when the profiles in (A) are aligned (B), a misalignment compensation of -2.5 has been applied. These profiles were used to determine that the correct adjustment was made in the reconstruction.

2.6.2   Ring Artifact Reduction

Ring artifacts were present in each scan. The ring artifact reduction was added at the

highest level (20) for each reconstruction. Generally, this is not recommended but, due to

the severe nature of the artifacts in our scans, we determined that the resulting image did

not have visible blurring (Figure 16) and was an acceptable value. Ring artifacts are often

caused by faulty or misaligned detectors that over- or underestimate the true pixel value.

(Anas et al., 2011; Orhan, 2020) As the scanner takes images around the full 360°, the

error is propagated around, forming the rings which are seen in the reconstructed image.
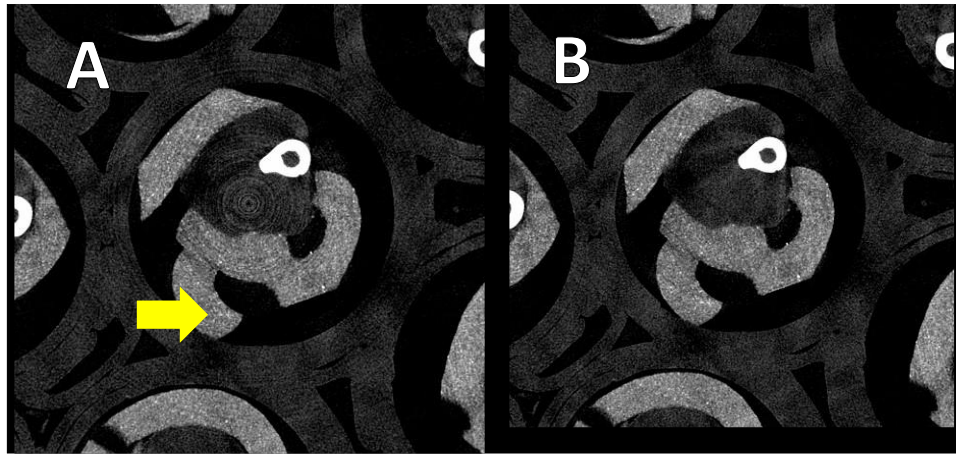
Figure 16: A reconstructed image of the hindlimb showing the difference between an image without (A) and with (B) a ring artifact reduction of 20. The image shows the reconstructed transverse view focused on the center cutout of the holder. The bright white pixels in the image are bone, specifically a cross-section at the distal tibia. Concentric light and dark circles originating at the center of the scan (A) are caused by pixel defects propagated around the scan. When the ring artifact reduction adjustment was implemented, the concentric rings were not visible (B)
Note, the bright spots surrounding the hindlimbs (yellow arrow in A), come from the coloured elastics that were used to identify samples after scanning. The elastics had a surprising amount of mineralized content that was prominent in the scan. Following discovery, the elastics were placed around the ankles where they could not interfere with knee images.

2.6.3   Beam Hardening

In the interest of time, multiple specimens were placed in one scan. It is worth noting that having multiple samples in a scan increases the likelihood of beam-hardening artifacts. When there are multiple subjects within a scan, the samples closest to the camera absorb the lower energy photons and affect the intensity readings of the subjects behind them. The closer samples appear to have greater mineralization. The hindlimbs in this study were scanned through a full 360° rotation around a central axis, which mitigates the effects of beam hardening as specimens are scanned at all angles. Beam hardening was present in all scans, but artifacts (visible as white 'beams' extending from the high-intensity bone) did not have visible effects (Figure 17C) unless the pixel intensity distribution was decreased excessively (Figure 17A). Beam hardening artifacts had values of intensity similar to soft tissues in the hindlimb. Since the study was focused on the behaviour of bone, the effects of beam hardening are negligible. Bone was segmented and values were used for comparisons within the study. Therefore, any beam hardening effects that may have been present in the data were negligible because the error would be approximately equal for every analysis and therefore could be considered negligible.
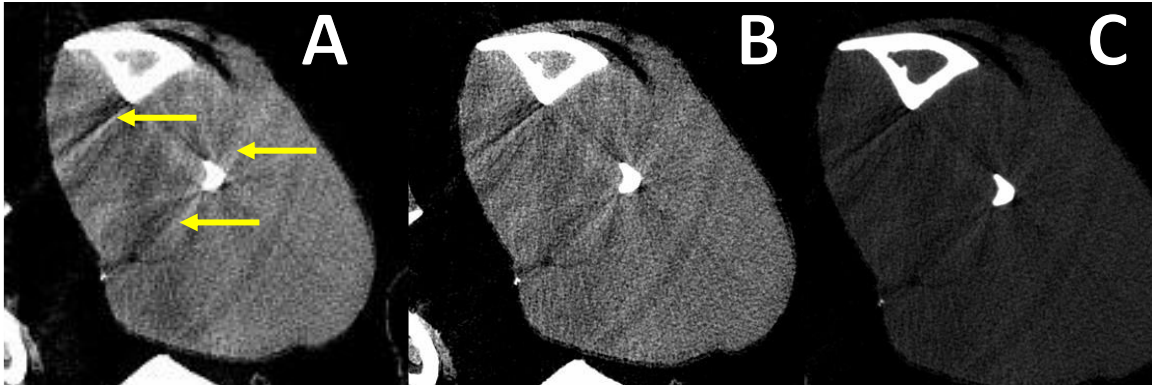
Figure 17: The presence of beam hardening can be seen in highly exposed images (A). The artifacts, indicated by the yellow arrows, are visibly corrected by applying a 20% beam hardening correction (B). Note images (A) and (B) have the distribution of pixel intensity dramatically reduced to emphasize the artifacts. The rightmost image (C) is the same region at the normal pixel intensity distribution used for the analysis.
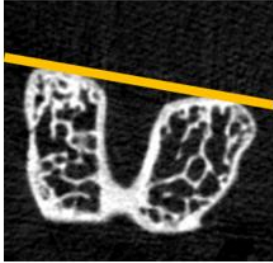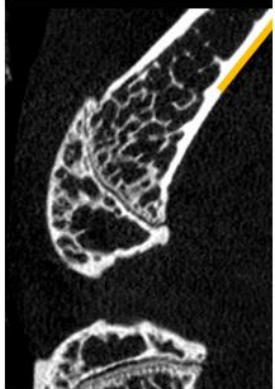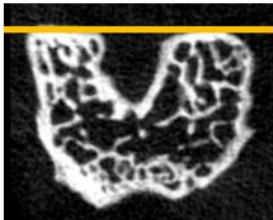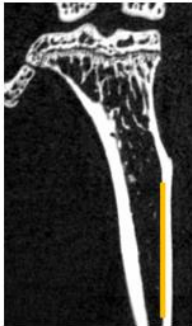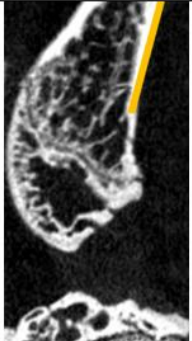
2.7   Preparation of Datasets

2.7.1   Orientation of the Tibia and Femur Datasets

The specimen holder was designed so that the long axis of the tibia was held as aligned with the vertical axis as possible. Samples arrived fixed in formalin in different states of flexion and could not be manipulated without damaging the sample. Thus, there was no way to ensure identical orientation for each sample. As such, we chose to rotate each dataset so that all datasets had the required bone (the tibia or femur) in the same orientation relative to the major axes. This was done to reduce variability in datasets and to ensure that, especially in trabecular analysis, the bone had the same orientation for every analysis. Once reconstructed, each hindlimb was separated into a unique dataset. The top, frontal, and sagittal views were analyzed, and the femur and tibia were rotated

according to specific angles as described below in Table 6. A threshold of ±5° was chosen

for rotating in each plane to minimize the amount of manipulation of the data.

Table 6:   Required orientation of the femur and tibia for analysis. These are the standards by which the datasets were prepared so that alignment with the major axes of the dataset was consistent. The yellow lines show the reference lines/angles used to orient the bone in each view.

Plane	Transverse	Frontal or Rear	Sagittal	
Line of rotation marker(s)	2 'lowest' points from each femoral condyle	Posterior aspect of the tibia at the slice that bisects the tibia	Posterior Cortex at the slice between femoral condyles	
Line of Rotation (Yellow)				
Dataset	Both	Both	Femur	Tibia
Desired Angle*	0° or 90° (Condyles lined up horizontally or vertically)	90°	70°	Fixed Angle (no rotation)
Desired Result				-

*(±5°, relative to the horizontal axis)

2.7.2   Orientation of the Femur for an Optimized Volume of Interest

To ensure repeatable, comparable measurements for the trabecular regions of the femoral

condyles, the femur datasets were rotated so that the long axis of the femur was 20° from

the scanning axis ("vertical"). At this orientation, the region between the growth plate and

the end of the femoral condyles was optimal to capture the most volume in the trabecular

region without losing data from the rotation of the dataset. The trabecular regions were

limited by the number of slices along the major vertical axis. The lowest point of the

femoral growth plate is the bottom of the valley-like geometries in the distal to the patella

near the femoral condyles (Figure 19). The number of slices from the subchondral bone

of the femoral condyles and the lowest point of the femoral growth plate was observed at

three angles in three different specimens. Ultimately, a 20° angle from the long axis of the

femur to the long axis of the tibia aligned the tangent of the lowest point of the femoral

growth plate and gave the greatest number of slices and therefore volume of trabecular

bone. (Figure 18, Table **7**) To assess if the trabecular measures were sensitive to re-

orientation, trabecular bone analysis in the medial femoral condyle was completed on the

three samples at each orientation. (Table **7**) Measures were sensitive to the 90° orientation

because the area and volume of the local region that was able to be captured were not

representative of the whole trabecular region. The other orientations captured a much

greater volume which was representative of the trabecular region. At these orientations,

the trabecular measures had similar results.

Slice range for trabecular analysis in the medial femoral condyle based on relative rotation of femur
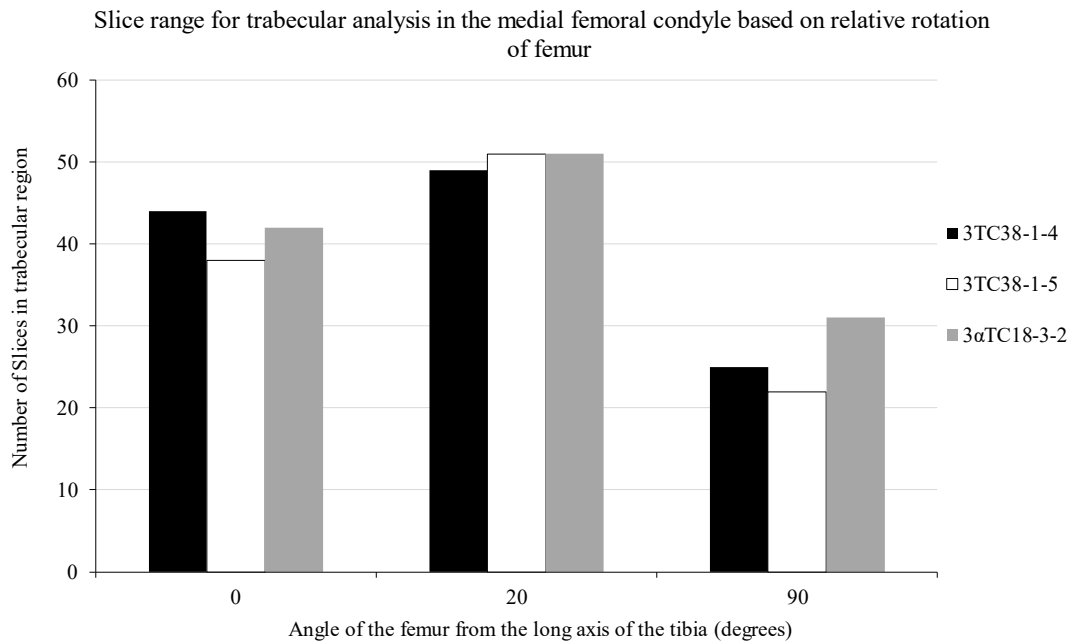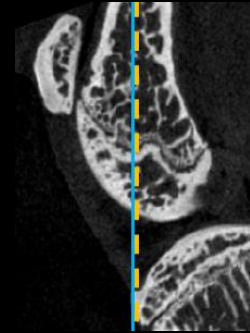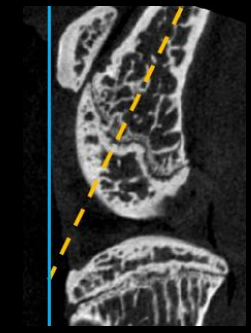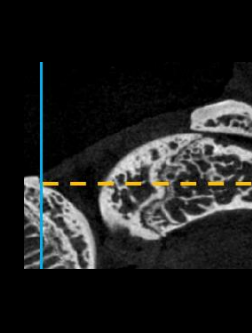
Figure 18: Chart showing the number of slices that make up the distance between the lowest point of the growth plate to the lowest point of the subchondral bone in the medial femoral condyle when rotating the long axis of the femur to 0°, 20° and 90° relative to the un-rotated long axis of the tibia. Three random 4-month specimens were chosen and rotated to three angles 0°, 20°, and 90°. The slices that make up the height of the trabecular region of the medial femoral condyle as defined in Table 7 and Table 8. The 20° orientation has the most slices for each sample in the region.

Table 7: Orientation of the femoral long axis (yellow dotted line) relative to the long axis of the scan ("vertical" axis - blue line) and the associated mean trabecular measures for each orientation in the trabecular region of the medial femoral condyle. In some cases, measurements from the 90° orientation differ – this is because the trabecular region there have a small volume and area that were not representative of the entire region.

		The angle of the long axis of the femur relative to the long axis of the tibia		
		0°	**20°**	**90°**
Measure	Sample			
Trabecular Thickness (mm)	3TC38-1-4	3.34	3.72	1.90
	3TC38-1-5	2.89	3.88	1.67
(Tb.Th)	3αTC18-3-2	3.19	3.88	2.36
Trabecular Separation (mm)	3TC38-1-4	0.48	0.50	0.46
	3TC38-1-5	0.48	0.48	0.52
(Tb.Sp)	3αTC18-3-2	0.52	0.49	0.58
Bone Volume Fraction (%)	3TC38-1-4	44	44	50
	3TC38-1-5	37	37	47
(BV/TV)	3αTC18-3-2	46	51	61

2.7.3   Mitigating Data Loss due to Dataset Rotation

Measurements such as trabecular thickness in mice are typically in the range of 70-80 mm

(6-7 pixels). If even one pixel representing bone is lost, the results could change

significantly. For this reason, it was important to analyze as large of a volume as possible

and keep manipulations of the dataset to a minimum. To minimize the error as much as

possible, bicubic rotation was chosen instead of the default bilinear rotation. Bicubic

rotation uses the average values of a volume, rather than an area to adjust the image.

(Pérez-Ramos & Figueirido, 2020)
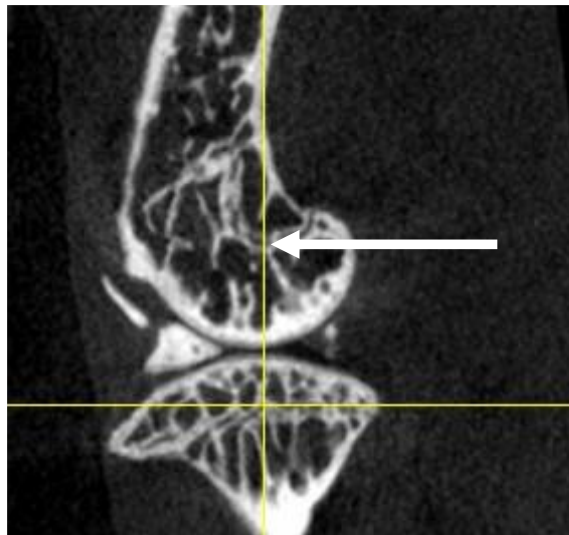
Figure 19: Sagittal view of mouse hindlimb showing a cross-section of the femur and tibia. The white arrow points to the lowest point of the femoral growth plate. This point was used to define the trabecular region of interest.

2.7.4   Definitions of Volumes of Interest used for Quantification.

The definitions of the regions used for quantification from the tibia and femur datasets are

described in Table 8 and Table 9 respectively. Each stack was defined before applying a

threshold to the image.

Table 8: Definitions of regions taken from the tibia dataset used to quantify bone architecture in and around the knee. The images are slices taken from the reconstructed μCT scans. A threshold has not been applied to the images to show finer details of the structure. Yellow lines in the frontal and sagittal views represent the plane of the transverse view.
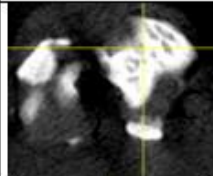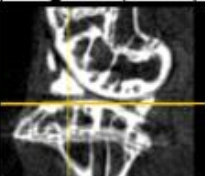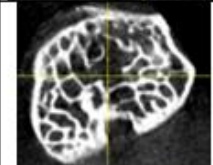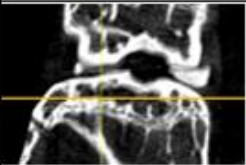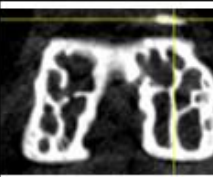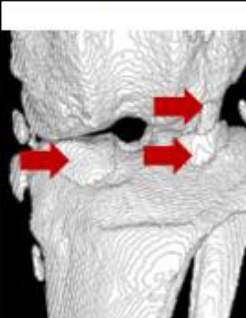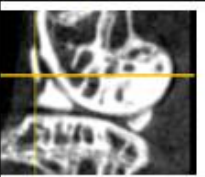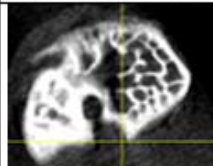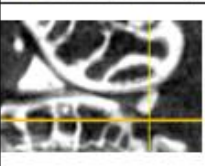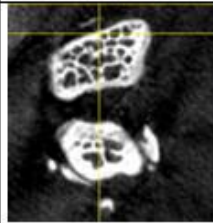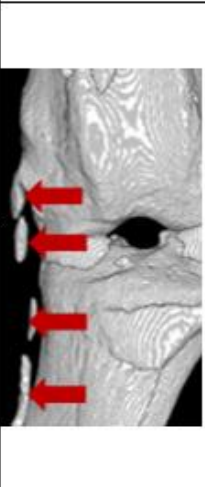
Region Name	Definition		View		
			Transverse	Frontal (or 3D)	Sagittal (or 3D)
Tibial Epiphysis	Top Slice	First sign of trabecular region (bone marrow cavity)			
Separate Stacks for medial and lateral	Bottom Slice	~1 slice above start of tibial growth plate			
Meniscus	Top Slice	Just above tip of the meniscal calcifications on femoral side			
	Bottom Slice	Just below bottom of meniscal calcifications on tibial side			
Collateral Ligaments	Top Slice	Just above top slice containing calcified collateral ligament			
Separate Stacks for medial and lateral	Bottom Slice	Just below bottom slice containing calcified collateral ligament			

Table 9: Definitions of regions taken from the femur dataset used to quantify bone architecture in and around the knee. The images are slices taken from the reconstructed µCT scans. A threshold has not been applied to the images to show finer details of the structure. Yellow lines in the frontal and sagittal views represent the plane of the transverse view.
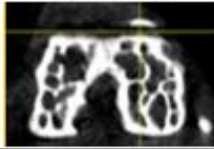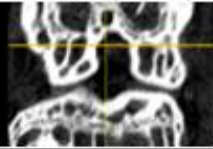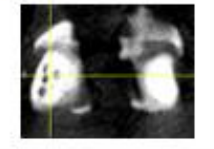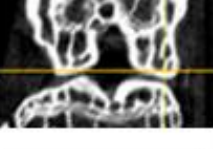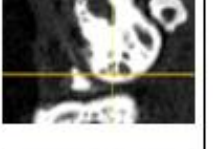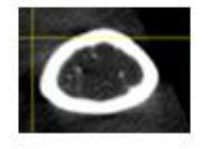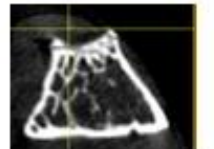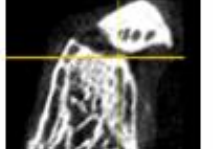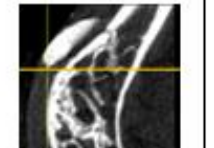
Region Name	Definition		View		
			Transverse	Frontal (or 3D)	Sagittal
Femoral Condyles Used separate stacks for medial and lateral	Top Slice	Just below the valleys of the femoral growth plate			
	Bottom Slice	The first sign of trabecular region (bone marrow cavity) in the femoral condyle			
Patella	Top Slice	Just above the last slice containing the patella			
	Bottom Slice	Just below the slice containing the bottom of the patella			

Table 10: Summary of the quantifications made in the analysis. Shows the region datasets that the quantifications were completed. Boxes with an X indicate the measurements taken in the associated region.

Analysis Type	Trabecular Bone				Ectopic calcifications					
Region	Femoral condyles		Tibial epiphysis		Patella	Meniscus		Collateral Ligaments	
Measure ↓	Lateral	Medial	Lateral	Medial		Lateral	Medial	Lateral	Medial
Trabecular Thickness (Tb.Th)	x	x	x	x					
Trabecular Spacing (Tb.Sp)	x	x	x	x					
Bone Volume Fraction* (BV/TV)	x	x	x	x					
Bone Volume (BV)					x	x	x	x	x

2.8 Quantification Methods

2.8.1   Trabecular Analysis Method

Programs: CT Analyzer (CTAn), version 1.20.3.0, 64bit, 2003-11 SkyScan, 2012-20, Bruker microCT

Fiji, version 1.53t, open source, National Institutes of Health

Fiji, formerly ImageJ is a peer-reviewed (Abràmoff et al., 2004) image analysis software widely used for CT image processing. Bone J is a plugin for Fiji that has been peer-reviewed (Doube et al., 2010) to provide an analysis of several bone characteristics. Initially, we used the built-in functions to calculate trabecular spacing (Tb.Sp), trabecular thickness (Tb.Th), bone volume (BV) total bone volume (TV), and bone volume fraction (BV/TV). However, after trying to validate the outcomes, it was found that the analysis

tools within BoneJ did not differentiate cortical bone from trabecular bone within the dataset. Therefore, it gave unreliable values unless a purely trabecular volume was extracted. Instead, CT Analyzer (CTAn) is proprietary software from Bruker that can be used to calculate several trabecular bone architectural measures based in part on published standardized histological methods (Parfitt, 1988) and 3D quantification tools (proprietary). Although proprietary, several studies have used CTAnalyzer for quantifying trabecular parameters. (Ketola et al., 2018; Roberts et al., 2017; Schrenker et al., 2022)

2.8.2   Separation of Medial and Lateral Regions

Development of OA in mouse knees triggered by TGFβ-driven fibrosis was shown to have more severe changes on the medial side than the lateral (Blaney Davidson et al., 2006). In St. Amant and Clark's study, when *itga1*-null mice were removed from the analysis, mice had more severe OA on the lateral side than the medial. Therefore, the calculations were performed on each side separately. This also simplifies the complexity of isolating the volume of calcification in the meniscus and the analysis of trabecular parameters. The lateral and medial regions were divided by selecting a rectangular region which split the medial and lateral regions at the point where the femoral condyles connect as seen in Figure 20.
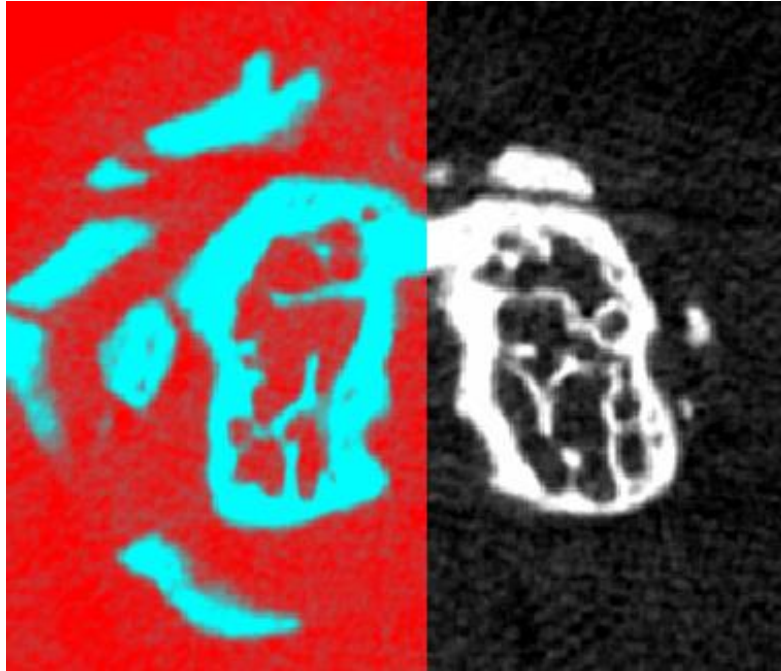
Figure 20: Separation of the medial and lateral regions in CTAn. The medial region (red background) is separated from the lateral region (black background) at the midpoint of the intercondylar notch. In this cross-section of the femur, the red rectangle represents the area that will make up the volume of interest extracted for analysis of the medial femoral condyle.

2.8.3   Automatic Threshold

Before any quantifications can be made, a threshold must be applied to the dataset to segment the bone tissue from the surrounding soft tissues. To maintain consistency, the threshold was set using the automatic threshold feature in CTAn, using the histogram of intensity values of the entire dataset. The automatic threshold feature used the Otsu method to find the appropriate threshold value. (Otsu & N., 1996) This method separates every pixel into the foreground class or background class. Thresholding is a vital part of the process of bone analysis from μCT images as it determines which voxels are bone and otherwise. As there were no control samples available for a specific determination of the

bone threshold value, there was no reliable way to determine exact intensity thresholds. To determine whether the use of the feature did not introduce error, an undergraduate research assistant (Haotian Xue) repeated a quantification to the same original dataset but applied different threshold values. These included threshold intensities above, below, and at the automatically calculated value. They determined that the automatic threshold value calculated was a good estimate and would not introduce errors in the analysis. The elastics used for specimen identification contained particles that had pixel intensities comparable to bone, as seen in Figure 16. In some scans, these elastics were adjacent to the knee and could have skewed the intensity histogram and therefore the threshold. To counter this potential error, the dataset was manipulated using the region of interest (ROI) feature in CTAn to remove the regions with the elastics from the region of interest before the threshold was found.

2.8.4   Extracting the Trabecular Region

For the 3D analysis functions in CTAn to work, the volume of interest (VOI) must contain only trabecular bone from the bone marrow cavity region. Using the custom processing tool and the procedure provided by Bruker in Method Note 8 (Bruker MicroCT, 2015), the trabecular bone can be segmented from the cortical bone and made into a purely trabecular dataset. Unlike the analysis performed in BoneJ, CTAN considers the boundaries of the cropped trabecular region to be the "total volume". The analysis process found the different features of the bone volume (including cortical bone, bone marrow cavity – i.e., the trabecular region, surrounding non-bony tissue, and any other

calcifications or noise) and removed all except the trabecular region from the ROI. Due to calcification at the meniscus, the calcified tissues around the cortical bone would affect the selection of the bone border, therefore additional manual selection of the tibia or femur was required before the analysis could be performed. The process for manual selection is described in the following section.

2.8.5   Volume of calcification at the meniscus

The calcifications that form on the meniscus were quantified using a bone volume analysis. The medial and lateral volumes were found separately to observe how the two regions differed in the amount of calcification, if at all. In CTAn, the volume of interest (VOI) was selected by choosing just above the top and just below the bottom of the calcified meniscus using the transverse view of each hindlimb. A volume of interest (VOI) region for each knee was selected manually, by identifying the slice at which the meniscus began and ended. The dataset was further separated into the medial and lateral VOIs. The femur and tibia were selected in an ROI throughout the stack from a combination of manual selection and interpolation (Figure 21). Using the subtractive ROI function (Figure 22) in CTAn, the femur and/or tibia were removed, isolating the calcified meniscus. Calcified collateral ligaments, osteophytes, and other calcified tissues were adjacent to the calcified meniscus in the scans (Figure 23). These volumes needed to be removed from the analysis for a true quantification of meniscus calcification volume. To ensure that the region of interest (ROI) for the meniscus contained only calcified meniscus, a slice within the middle of the meniscus region was first selected and then the

dataset was adjusted up and down (proximally and distally) to see which calcifications were connected. The regions of interest were then manually selected in several slices while CTAn automatically interpolated the ROIs between these slices. In each case, the dataset was visually checked again through all slices to confirm that only the meniscus was selected (Figure 23).
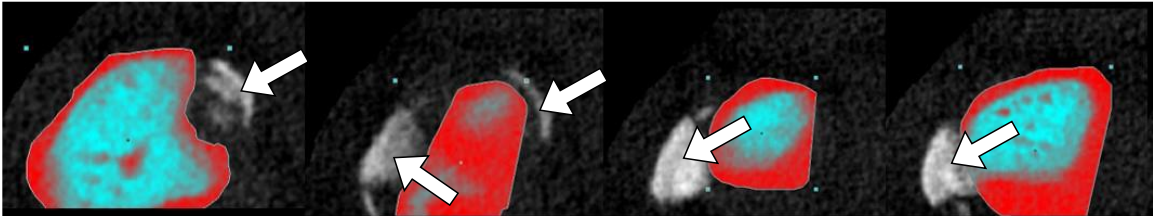
Figure 21: Progressive selection of the femur and tibia in CTAn to isolate the calcified meniscal volumes into a dataset. The region of interest, highlighted in red, is progressively selected so that calcified tissues (white arrows) are not included. Once the subtractive ROI function was used, only calcified tissue volumes remained for quantification.

Following ROI selection, a threshold was applied to the stack to segment the bone tissue. The dataset was analyzed for bone volume automatically in CTAn using their 3D analysis function. The bone volume, determined by the voxel count of bone in the dataset, was recorded as the calcified volume.
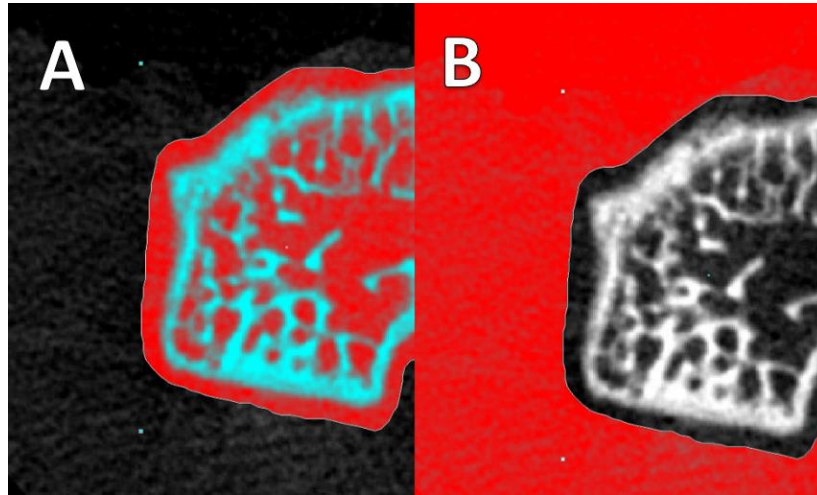
Figure 22: Example of subtractive selection in CTAn for analyzing calcified regions of the meniscus. The ROI is shown in red. The region in (A) has the body of the tibia selected throughout the dataset, when the subtractive ROI is applied, this results in an inverted selection (B) which captures any calcified tissue surrounding the tibia for analysis.
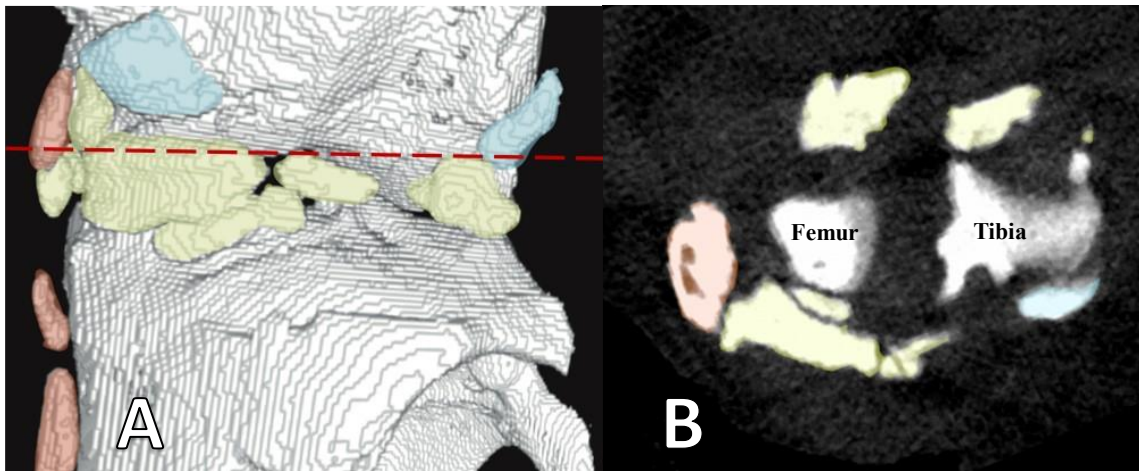
Figure 23: A 3D dataset of mouse knee with ectopic calcifications (A) and the transverse view of the data (B) at the designated slice (red dashed line in A). As seen in (B), one slice of the data may show multiple entities. Parts of the femur and tibia, calcifications at the menisci (green) and the medial collateral ligament (orange), and calcified tissues extending from the femur (blue) can be seen in the transverse view at the designated slice. Mineralized tissue had to be categorized for defining the region of interest. Both views were referenced when determining which mineralized tissues belonged in which quantifications.

2.8.6   Patellar Volume

The purpose of analyzing the total patellar volume was to determine if osteophytes had

developed around the patella. An alternative to total patellar volume would be selecting

regions that appeared to be osteophytes and only counting the volume of those in each

dataset. However, this latter method requires more user judgement and is prone to user

error. As a first pass, we chose to analyze the total patellar volume. The patellar volume

captures the bone volume of the continuous body of the patella and any osteophytes on

the surface of the patella. To select the patellar volume, the top and bottom of the stack

were selected, just above (superior) and just below (inferior) the patella, respectively.

Within this substack, The ROI was created by making several manual ROIs and

interpolating slice-by-slice ROI between these to select the region that contained only the

patella. Each slice of the substack was then visually checked to ensure that only the

patella was selected. A threshold was then applied to the stack to show only bone. The

CTAn 3D analysis tool was used to perform a voxel count to find the volume of the

patella (bone volume within the VOI). In addition to patellar osteophytes, some samples

were found to have calcification in the quadricep tissues.

2.8.7   Collateral Ligaments

We quantified the volume of calcifications seen along the medial collateral ligament

(MCL) and lateral collateral ligament (LCL). Several samples had calcification at the root

of the ligament originating from the tibia. Because there is typically a seamless transition

from the tibia body, it is difficult to accurately differentiate between the tibia and the

additional bone mass that might or might not have been part of the normal tibial insertion.

Therefore, only calcifications that were separated from the tibia were used to quantify the

calcifications of the MCL and LCL. These calcifications were excluded from the

quantification of bone volume but are an important step in the binary behaviour analysis

of the samples.
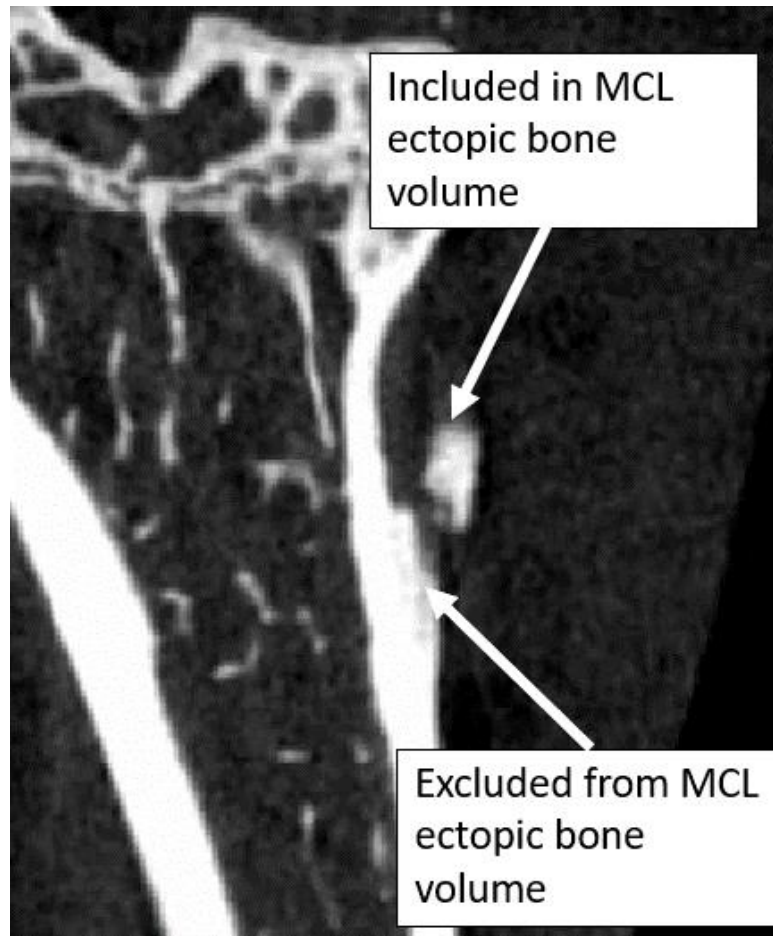
Figure 24: Definition of the volume of calcifications (ectopic bone volume) at the collateral ligaments. Bone formations that were attached to the tibial insertion were excluded from the quantification and addressed at the binary analysis stage.

2.9   Binary Analysis of Abnormal Calcifications

Due to the complexity of identification, binary checks were used for studying ectopic

bone formation away from the patella and joint region. Defining regions and segmenting

the tibia and femur into independent datasets was a complex task due to the identification

of the calcified bone and orientation of the femur and tibia. In one slice of CT data, it was

possible to have regions of the calcified meniscus and collateral ligaments, femoral

condyles, and the tibial plateau within proximity. Additionally, in cases like those seen in

Figure 24, calcified tissues rooting from bone cannot be reliably split off from the core

into a volume of interest. To characterize the different areas of abnormal calcification in

the areas around the joint, a binarized 3D model of each sample was created. The model

was visually inspected for abnormal calcifications. The binary analysis was used to

analyze ectopic bone formation that could not be easily quantified. Three main patterns of

ectopic bone formation emerged, osteophytes around the patella, calcification at the root

of the medial collateral ligament, and calcification of the quadriceps tendon/muscle. As

discussed in section 2.8.7, abnormal bone masses around the root of the medial collateral

ligament could not be reliably segmented for quantification and instead are assessed as

described in Table 11. Signs of osteophytosis were not present in every case where the

root was calcified and were assessed in another qualitative analysis described in Table 12.

In addition, the alignment of the patella in each limb was assessed by identifying if the

patella was subluxed outside of the femoral groove. The subluxation of the patella was

noted by observation of the 3D reconstruction as described in Table 13, as a quantitative

approach was too complex to determine in addition to the other measurements for this

project.

Table 11: Criteria for designation of abnormal calcified tissue at the root of the medial collateral ligament. The score is binary – 0 for insignificant or missing ectopic calcification at the MCL root. 1 for when the calcified root is clearly visible. The affected region is circled in yellow.
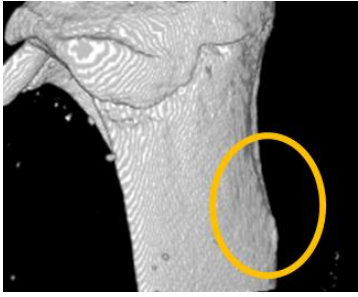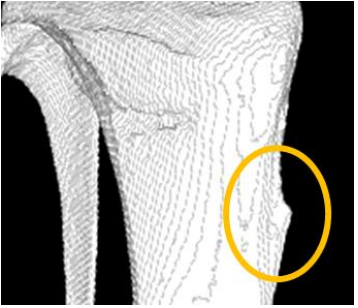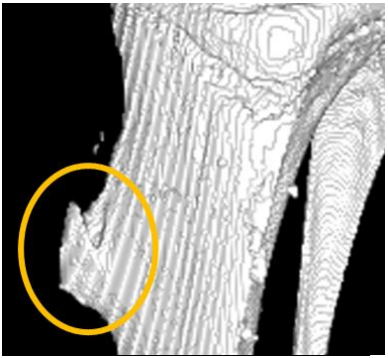
Score	0	0
Criteria	MCL root not clearly distinguishable from the tibia	MCL root is distinguishable from tibia but is not prominent
Example		
Score	1	1
Criteria	MCL root is small but prominent	MCL root has clear calcification
Example		

Table 12: Criteria for qualification of osteophytosis at the root of the medial collateral ligament. The samples are visually inspected and scored with a binary 0 or 1. Samples with a large ectopic mass at the medial collateral ligament are considered osteophytic and given a score of 1. The affected region is circled in yellow.
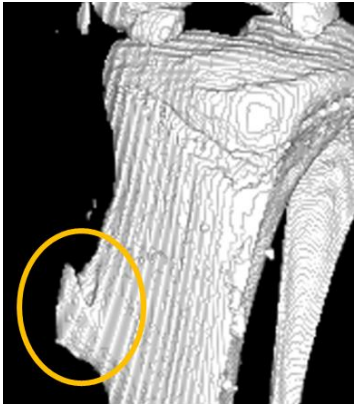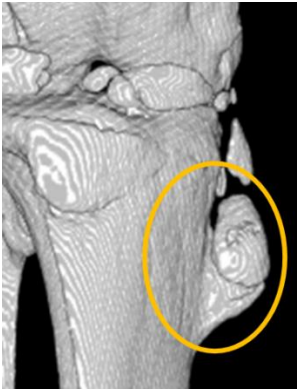
Score	0	0
Criteria	Root of the MCL is not calcified	Root of the MCL is calcified along its curvature with no abnormal masses
Example		
Score	1	1
Criteria	Root of the MCL is calcified along its curvature with some abnormal protrusion	Root of the MCL has abnormal bone masses that do not follow the curvature of the ligament
Example		

Table 13: Criteria for qualification of a subluxated patella. The line of symmetry of the patella-femoral groove is represented by the dashed red line for a clearer visual. A patella with a "centre" that was shifted beyond the ridges of the groove was considered subluxed (Score = 1). Each sample was graded by a binary 0 or 1.
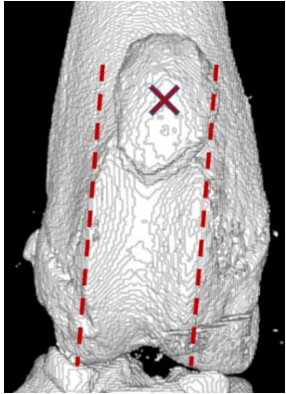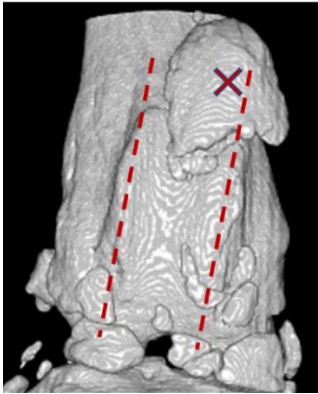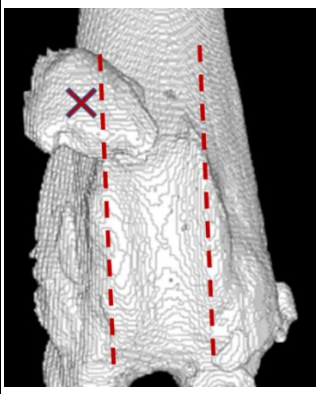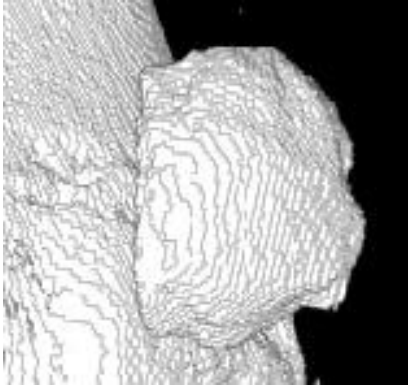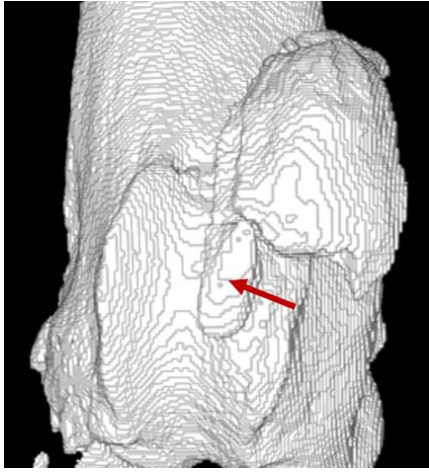
Score	0	0	1
Criteria	Patella lies in patellofemoral groove	Patella has shifted but still lies within the patellofemoral groove	Patella has shifted outside of the patellofemoral groove
Example			

Table 14: Criteria for qualification of an osteophytic patella. A patella that was a contiguous body with no clear protruding bone masses were scored as 0. If clear bone masses were protruding or detached from the patella, it was considered osteophytic and was scored with a 1.

Score	0	0
Criteria	Patella is one homogenous mass	Patella has an irregular, bumpy surface but no clearly defined osteophytes
Example		
Score	1	1
Criteria	Patella is one contiguous mass but has protruding bone masses	Patella has clear protruding bone masses that are both attached and detached from the patella
Example		
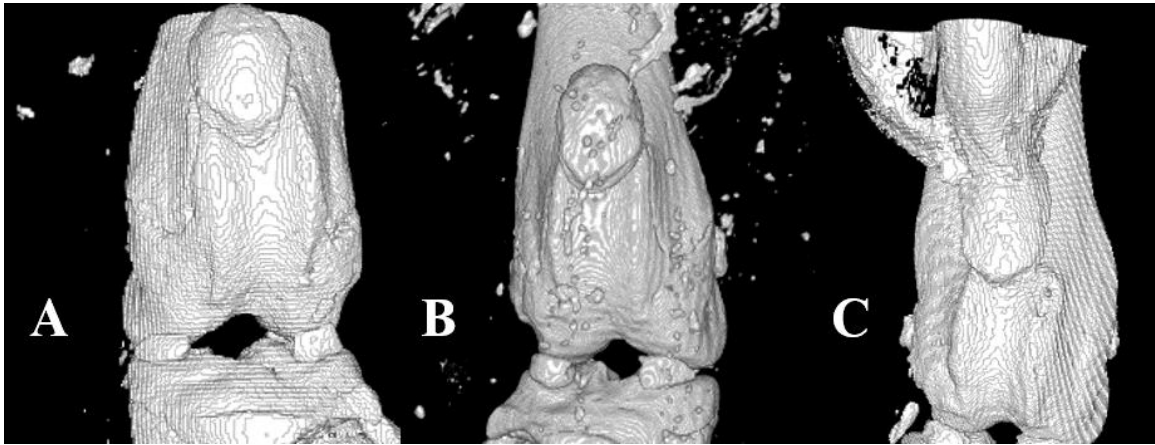
Figure 25: Samples with mineralized tissue in the quadricep region. The mineralized tissue typically appeared as small clusters (A), as groups of mineralized tissue in multiple areas (B), or as a large body of calcification connected to the patella (C)

2.10 Statistical Analyses

Programs: R, Version 4.2.2 (2022-10-31 ucrt))

RStudio, Version 2022.12.0+353, "Elsbeth Geranium" Release

Initially, the plan to determine any statistical differences among groups was to use a test for one-way analysis of variance (ANOVA), but this required that data were normally distributed. To determine whether the results were reliable, normality was determined using the Shapiro-Wilks test. This test of normality assigns a value to how closely the data follows a normal distribution (the p value). If the p value is less than the chosen significance level (typically, $\alpha=0.05$), the data were not normally distributed. The datasets that did not follow the normal distribution were volume quantifications. It made sense that these distributions were not normal because, by their nature, the range of values was large with most measurements near the extremes. For example, in the case of calcification

along the MCL, some specimens did not have any calcification, and others had large

amounts, which can be seen in Table 12. These datasets could not be viably transformed,

so instead the non-parametric Kruskal-Wallis test was used. Both an ANOVA and

Kruskal-Wallis test were run for each dataset and confirmed that no significant

relationships were lost using a non-parametric test on normally distributed data. Once

confirmed, all statistical analyses were performed using the Kruskal-Wallis method and

its associated post hoc Dunn Test. The analyses were completed for each characteristic,

using 4 and 16-month data separately and with cohort as the independent variable. To

correct errors from multiple comparisons in Dunn's test, a corrected p value was

determined using the Holm-Bonferroni method to give an accurate summary of

significant cohort differences. (Abdi, 2010)

2.10.1 Special Cases

2.10.1.1 Difference within Cohorts from 4 to 16 months

Separate analyses were run within a cohort using age (timepoint) as the independent

variable to observe progression in OA-like phenotypes, if any. Each characteristic was

run separately with the timepoints. A Kruskal-Wallis and Mann-Whitney U test were

performed for each characteristic (Table 15). Kruskal-Wallis tests work best when there

are more than two groups, while Mann-Whitney U works well with pairwise

comparisons. Performing both tests confirmed that the Kruskal-Wallis test captured all

significant measures. For consistency, the reported p values are results from the Kruskal-

Wallis analysis. The volume of calcification along the LCL could not be analyzed using

the Mann-Whitney U test. This test finds significance using ranks. In cases where there

are small sample numbers and several ties, the test cannot provide an analysis. This result

made sense because during quantification, calcifications along the lateral collateral

ligament were not often present or very small (See section 3.3.2).

Table 15: Results from the Kruskal-Wallis and Mann U Whitney tests for the difference in calcified tissue volumes between 4- and 16-month specimens.

		p value				
		Volume (mm^3)				
		Meniscus		Collateral Ligament		Patella
Test	Cohort	Medial	Lateral	Medial	Lateral	
Kruskal Wallis	+c	**0.03**	**0.00**	**0.01**	0.07	**0.02**
	α+c	**0.01**	**0.01**	**0.01**	0.15	0.17
	+t	**0.01**	**0.03**	0.68	0.22	**0.03**
	α+t	**0.00**	**0.00**	0.81	**0.02**	**0.00**
	-t	**0.00**	**0.01**	**0.00**	0.11	**0.02**
	α-t	**0.00**	**0.00**	**0.00**	0.59	**0.00**
Mann-Whitney U	+c	**0.03**	**0.00**	**0.01**	N/A	**0.02**
	α+c	**0.01**	**0.01**	**0.01**		0.20
	+t	**0.01**	**0.03**	0.75		**0.03**
	α+t	**0.00**	**0.00**	0.88		**0.00**
	-t	**0.00**	**0.01**	**0.00**		**0.02**
	α-t	**0.00**	**0.00**	**0.00**		**0.00**

2.10.1.2 Trabecular Bone Fraction

Results of the Shapiro Wilks showed that bone volume fraction data were normally

distributed. For the volume fractions, values were output as percentages. Because

percentages are limited from 0 to 100, they cannot be considered normal data. To

determine the agreement of ANOVA and Kruskal Wallis tests, the percentages had to be

transformed. The datasets were transformed using a square root and arcsine function. After confirming the agreement between tests, results from the non-parametric Kruskal-Wallis and post hoc Dunn's test, using the original percentage data, were reported.

2.10.1.3 Binary Analysis

Binary analyses, as described in section 2.9, are considered a count. Using a Kruskal-Wallis test on these data was not appropriate as there were only 2 possible values. To analyze these, the data was considered categorical with yes (1) and no (0) data as categories. A Chi-Square analysis was performed with all cohorts considered. Analyses were performed on the 4- and 16-month data separately. The post hoc analyses were completed as individual Chi-Square tests between cohorts which were vital to the study focus. Other cohort comparison results were not included in the results because they are scientifically irrelevant to the study. Binary analyses were not run using time as an independent variable, as these analyses were used to further investigate areas of ectopic calcifications.

2.10.2 Removal of Outliers for Error Analysis

Due to large magnitudes of standard deviations, the data was analyzed after removing outliers of data determined from the upper and lower quartile limits of each cohort dataset. Statistical tests were redone with outlier data removed. Repeating the analysis without outliers did not reveal significance differences in the data (Table 16). There were

four outliers in total, three from the 4-month timepoint, one from the 16-month timepoint, all were in different cohorts.

Table 16: Values of mean volume of calcified tissue at the medial meniscus of the knee. Values and significance levels shown with and without outliers removed for cohorts at four and 16-months. Removing outliers did not show significance.

age group	cohort	all data mean ± SD	p value	# of outliers	outliers removed mean ± SD	p value
4	+c	0.057 + 0.006	0.155	1/5	0.054 ± 0.003	0.265
	α+c	0.061 + 0.011		0/7	0.061 ± 0.011	
	+t	0.048 + 0.006		1/5	0.05 ± 0.004	
	α+t	0.055 + 0.007		0/5	0.055 ± 0.007	
	-t	0.054 + 0.012		0/5	0.054 ± 0.012	
	α-t	0.045 + 0.005		1/5	0.048 ± 0.003	
16	+c	0.116 + 0.068	0.437	0/8	0.116 ± 0.068	0.354
	α+c	0.251 + 0.23		0/5	0.251 ± 0.23	
	+t	0.092 + 0.018		1/5	0.098 ± 0.012	
	α+t	0.616 + 0.955		1/7	0.269 ± 0.28	
	-t	0.124 + 0.051		0/7	0.124 ± 0.051	
	α-t	0.221 + 0.197		0/7	0.221 ± 0.197	

2.10.3 Effect Size

Due to the large number of subgroups in the study, a power analysis (significance level = $\alpha = 0.05$, k = number of cohort groups = 6) was performed to determine an appropriate sample size for future work. The results are summarized in Table 17, showing the number of samples per cohort required for an estimated effect size (small, medium and large as defined by Jacob Cohen (Cohen, 1988)), determined using the recommended Cohen's d-test. (Fritz et al., 2012).

Table 17: Power analysis results for the required number of samples for a significant result at $\alpha=0.05$ for 6 cohorts. The 'small', 'medium' and 'large' effect sizes are guidelines* for use in power analyses to determine study parameters. *(Cohen, 1988; Fritz et al., 2012)

Cohen's d – effect size of results	Power (1-beta)	Effect size (f)	Required sample size (rounded up)
Small		0.2	55
Medium	0.8	0.5	10
Large		0.8	5
Small		0.2	70
Medium	0.9	0.5	12
Large		0.8	6

3 Results

All statistical tests were performed with the use of R (version 4.2.2) and RStudio (version 2022.12.0+353). Unless otherwise stated, all statistical tests were performed with a significance level of $\alpha=0.05$.

3.1 Distribution of Data in Each Characteristic and Dataset

Shapiro Wilks tests were run separately for every characteristic at each timepoint. The distributions for each characteristic are shown in Table 18.

Table 18: Normally distributed datasets based on the Shapiro Wilks test with a significance level of $\alpha = 0.05$. Shapiro Wilks test outputs a p value to compare to α Datasets where $p > \alpha$ are indicated with a "Y" for yes, having a normal distribution. Datasets where $p < \alpha$ are indicated with "N" for no, not following a normal distribution.

Analysis Type	Region		Characteristic	4-months	16-months
bone adaptation	tibial epiphysis	medial	trabecular thickness (Tb.Th)	Y	Y
			trabecular separation (Tb.Sp)	N	N
			bone volume fraction (BV/TV)	Y	N
		lateral	trabecular thickness (Tb.Th)	Y	Y
			trabecular separation (Tb.Sp)	Y	Y
			bone volume fraction (BV/TV)	Y	Y
	femoral condyles	medial	trabecular thickness (Tb.Th)	Y	N
			trabecular separation (Tb.Sp)	Y	Y
			bone volume fraction (BV/TV)	Y	N
		lateral	trabecular thickness (Tb.Th)	Y	N
			trabecular separation (Tb.Sp)	Y	N
			bone volume fraction (BV/TV)	Y	N
ectopic bone formation	patella		bone volume	N	Y
	collateral ligaments	medial	bone volume	N	N
		lateral	bone volume	N	N
	meniscus	medial	bone volume	Y	N
		lateral	bone volume	Y	N

3.2 Trabecular Bone Adaptation

3.2.1   Analysis of the Tibial Epiphysis

Trabecular analyses conducted on the tibial epiphysis included trabecular thickness (Tb.Th.), trabecular separation (Tb.Sp.), and bone volume fraction (BV/TV). The short-hand nomenclature for these measures is based on published and universally accepted standards for trabecular bone histological measures (Parfitt et al. 1987; Bouxsein et al. 2010). The data for the 4- and 16-month samples were analyzed separately for statistical significance by cohort using the non-parametric Kruskal-Wallis test. No significant difference between cohorts was found for any trabecular measure in the tibial epiphysis in the 4- or 16-month specimens (Figure 26, Figure 27, Figure 28). A post hoc analysis was completed using the non-parametric Dunn's test, results are shown in Table 19.
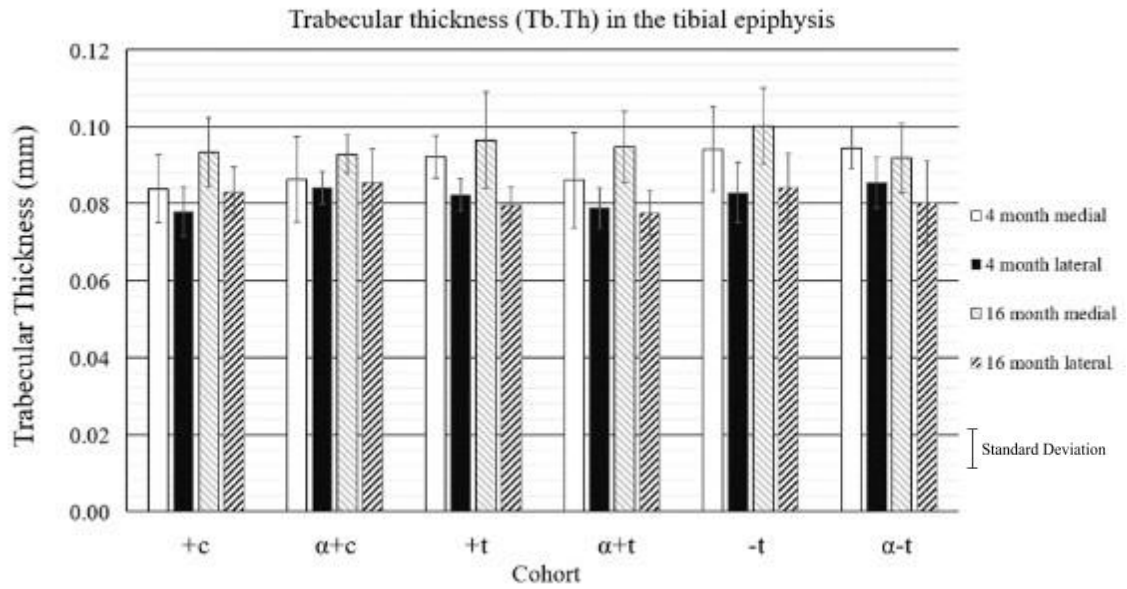
Figure 26: Trabecular thickness data in the tibial epiphysis by cohort. The 4-month medial (white), 16-month medial (gray hatched), 4-month lateral (black), and 16-month lateral (black hatched) mean values are shown by cohort. No significant differences were found between cohorts in any dataset.
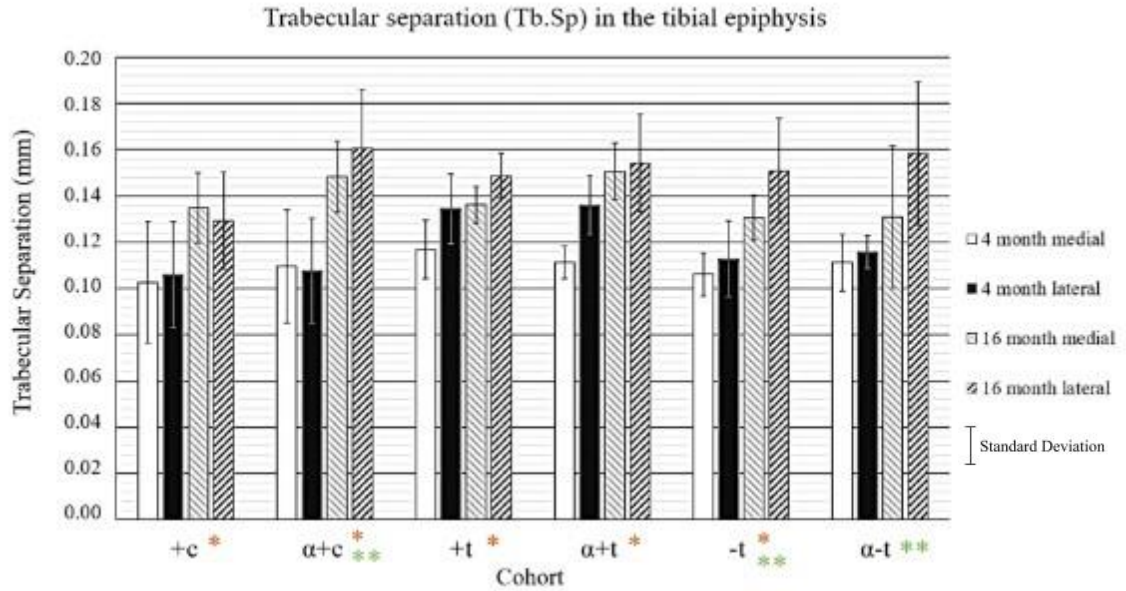
Figure 27: Trabecular separation data in the tibial epiphysis by cohort. The 4-month medial (white), 16-month medial (gray hatched), 4-month lateral (black), and 16-month lateral (black hatched) mean values are shown by cohort. The initial Kruskal-Wallis test showed there were significant differences between cohorts ($p < 0.05$) in the 4-month lateral dataset, but the post hoc Dunn's test did not find any significant differences between cohorts.
* Significant difference on the medial side between 4- and 16-month timepoints within the cohort.
** Significant difference on the lateral side between 4- and 16-month timepoints within the cohort.
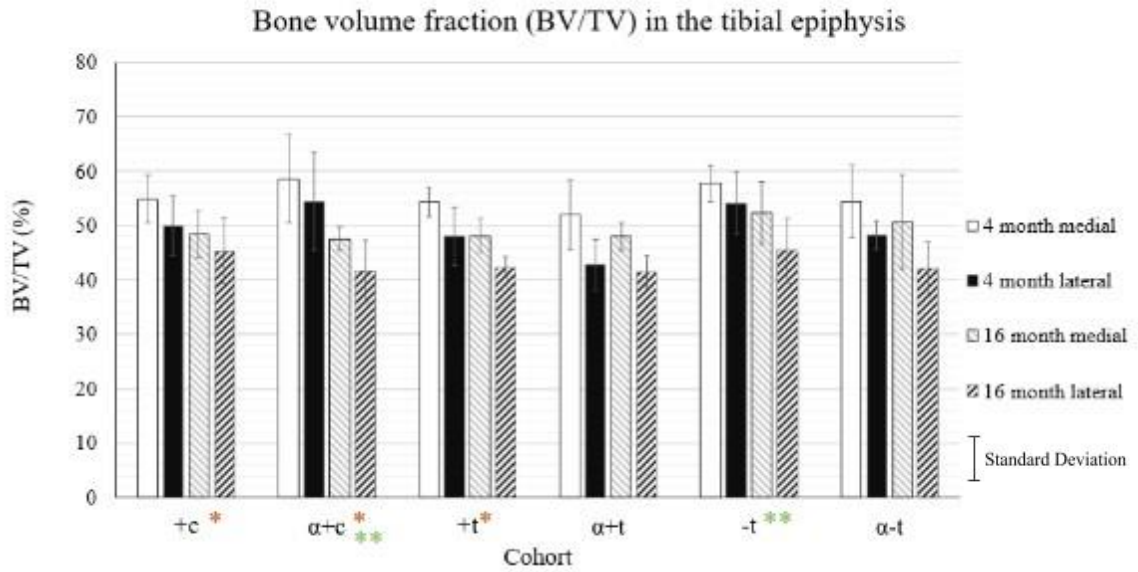
Figure 28: Bone volume fraction data in the tibial epiphysis by cohort. The 4-month medial (white), 16-month medial (gray hatched), 4-month lateral (black), and 16-month lateral (black hatched) mean values are shown by cohort. After a Kruskal-Wallis test, no subset of data was shown to have statistical significance with respect to cohort.
* Significant difference on the medial side between 4- and 16-month timepoints within the cohort.
** Significant difference on the lateral side between 4- and 16-month timepoints within the cohort.

Table 19: Post hoc results using non-parametric Dunn's test of trabecular bone adaptations in the tibial plateau for the 4-month cohort combinations. Cohort combinations highlighted in gray are the study focus comparisons. The *p* values for the initial Kruskal-Wallis test are shown above the post hoc *p* values. No dataset found significantly different differences between cohorts (*p*<0.05).

Timepoint		4 months					
		Tibial Epiphysis					
		Medial			Lateral		
Dataset		Trabecular Thickness	Trabecular Separation	Bone Volume Fraction	Trabecular Thickness	Trabecular Separation	Bone Volume Fraction
Abbreviation		Tb.Th	Tb.Sp	BV/TV	Tb.Th	Tb.Sp	BV/TV
p value for dataset (factor : cohort)		0.68	0.68	0.64	0.64	0.64	0.15
Cohort Comparison		Post Hoc *p* value					
+c	α+c	1.00	1.00	1.00	1.00	1.00	1.00
	+t	1.00	1.00	1.00	1.00	1.00	1.00
	-t	1.00	1.00	1.00	1.00	1.00	1.00
α+c	α+t	1.00	1.00	1.00	1.00	1.00	0.29
	α-t	1.00	1.00	1.00	1.00	1.00	1.00
+t	-t	1.00	1.00	1.00	0.97	1.00	1.00
α-t	α+t	1.00	1.00	1.00	1.00	1.00	1.00
	-t	1.00	1.00	1.00	1.00	1.00	1.00
+c	α+t	1.00	1.00	0.95	1.00	1.00	0.66
	α-t	1.00	1.00	1.00	1.00	1.00	1.00
α+c	+t	1.00	1.00	1.00	1.00	1.00	1.00
	-t	1.00	1.00	1.00	1.00	1.00	0.99
+t	α+t	1.00	1.00	1.00	1.00	1.00	1.00
	α-t	1.00	0.95	1.00	1.00	0.97	1.00
α+t	-t	1.00	1.00	1.00	1.00	1.00	0.43

Table 20: Post hoc results of trabecular bone adaptations in the tibial epiphysis for the 16-month cohort combinations. Cohort combinations highlighted in gray are the study focus comparisons. The p values for the initial Kruskal-Wallis test are shown above the post hoc p values No dataset found significantly different differences between cohorts ($p<0.05$).

Timepoint		16 months					
		Tibial Epiphysis					
		Medial			Lateral		
Dataset		Trabecular Thickness	Trabecular Separation	Bone Volume Fraction	Trabecular Thickness	Trabecular Separation	Bone Volume Fraction
Abbreviation		Tb.Th	Tb.Sp	BV/TV	Tb.Th	Tb.Sp	BV/TV
p value for dataset (factor : cohort)		0.57	0.06	0.80	0.48	0.18	0.39
Cohort Comparison		Post Hoc p value					
+c	α+c	1.00	1.00	1.00	1.00	0.70	1.00
	+t	1.00	0.99	0.91	1.00	1.00	1.00
	-t	1.00	1.00	1.00	1.00	0.67	1.00
α+c	α+t	1.00	1.00	1.00	1.00	0.98	1.00
	α-t	1.00	1.00	1.00	1.00	1.00	1.00
+t	-t	1.00	1.00	1.00	1.00	1.00	1.00
α-t	α+t	1.00	0.73	1.00	1.00	1.00	1.00
	-t	1.00	1.00	1.00	1.00	1.00	1.00
+c	α+t	1.00	0.76	1.00	1.00	0.48	1.00
	α-t	0.92	1.00	1.00	1.00	0.29	1.00
α+c	+t	1.00	1.00	1.00	1.00	1.00	1.00
	-t	1.00	0.34	1.00	1.00	1.00	1.00
+t	α+t	1.00	1.00	1.00	1.00	1.00	0.99
	α-t	1.00	1.00	1.00	0.99	1.00	1.00
α+t	-t	1.00	0.05	1.00	1.00	1.00	1.00

3.2.1.1   Difference Between 16-month and 4-month Specimens Within a Cohort

Kruskal-Wallis tests were used to determine whether there were significant differences in the trabecular bone characteristics between the 4- and 16-month samples within a cohort. The test results are shown in Table 21. Significant differences in the trabecular thickness occurred only on the lateral side. The *itga1*-null (α+c) and wild-type tamoxifen control (-t) mice had significantly greater trabecular thickness at 16 months than at 4 months. The tamoxifen control for *itga1*-null mice (α-t) had significantly reduced trabecular thickness at 16 months. In 16-month specimens, all cohorts, except for the *itga1*-null mouse tamoxifen control mice (α-t), had significantly increased trabecular separation on the medial side. On the lateral side, the *itga1*-null (α+c) mice and both tamoxifen control mice (α-t, -t) had significantly greater trabecular separation at 16 months. Bone volume fraction was reduced on the medial side at 16 months in wild-type mice with (+t) or without (+c) a cartilage-specific TβRII knockout compared to the respective 4-month animals. The *itga1*-null (α+c) mice had significantly reduced bone volume fractions at 16 months in both the medial and lateral compartment of the tibial epiphysis. The wild-type tamoxifen control mice (-t) also had significantly reduced bone volume fraction on the lateral side of the 16-month specimens.

Table 21: Results from the Kruskal-Wallis test between the 4- and 16-months within each cohort. Values which are bolded and highlighted in green, were found to have a statistically significant difference between the timepoints ($p<0.05$). ↓ 16-month specimens had an average value less than the 4-month specimens. ↑ 16-month specimens had an average value greater than the 4-month specimens.

		p value (Kruskal Wallis)					
		Tibial Epiphysis					
		Medial			Lateral		
Cohort	Measure	Trabecular Thickness	Trabecular Separation	Bone Volume Fraction	Trabecular Thickness	Trabecular Separation	Bone Volume Fraction
		Tb.Th	Tb.Sp	BV/TV	Tb.Th	Tb.Sp	BV/TV
+c		0.08	**0.02↑**	**0.04↓**	0.19	0.14	0.08
α+c		0.37	**0.00↑**	**0.02↓**	**0.00↑**	**0.00↑**	**0.03↓**
+t		0.75	**0.03↑**	**0.01↓**	0.12	0.12	0.08
α+t		0.22	**0.00↑**	0.29	0.12	0.12	0.17
-t		0.46	**0.00↑**	0.09	**0.03↑**	**0.03↑**	**0.04↓**
α-t		0.94	0.12	0.17	**0.04↓**	**0.04↑**	0.12

3.2.2   Analysis of the Femoral Condyles

Trabecular analyses conducted on the femoral condyles included the trabecular thickness, trabecular separation, and bone volume fraction. The data for the 4 and 16-month samples were analyzed separately using the non-parametric Kruskal-Wallis test. No groups from the 4-month timepoint (Table 22) were found to have any statistical significance. Results in the 16-month medial femoral condyles were statistically significant in all three measures (Table 23). The lateral femoral condyles had a statistically significant difference in the cohorts for the trabecular thickness and separation, but not for bone volume

fraction. The comparisons of trabecular characteristics for each dataset are in Figure 29, Figure 30 and Figure 31. A post hoc analysis, using Dunn's test, for 4 and 16-month data are shown in Table 22 and Table 23, respectively. The Kruskal-Wallis test detected a significant difference among the overall combined cohorts for bone volume fraction in the medial femoral condyles, but no significant differences were detected between cohorts in the post hoc results. In both the medial and lateral femoral condyles of 16-month specimens, the *itga1*-null (α+c) mice had significantly greater trabecular thickness than the wild-type mice (+c). Also, in 16-month specimens, trabecular separation in the medial femoral condyles was significantly greater in wild-type mice with the cartilage-specific TβRII knockout (+t) than without (+c). In 16-month *itga1*-null mice, the tamoxifen control mice (α-t) had significantly greater values of trabecular separation in the lateral femoral condyle than those with a corn oil injection (α+c).
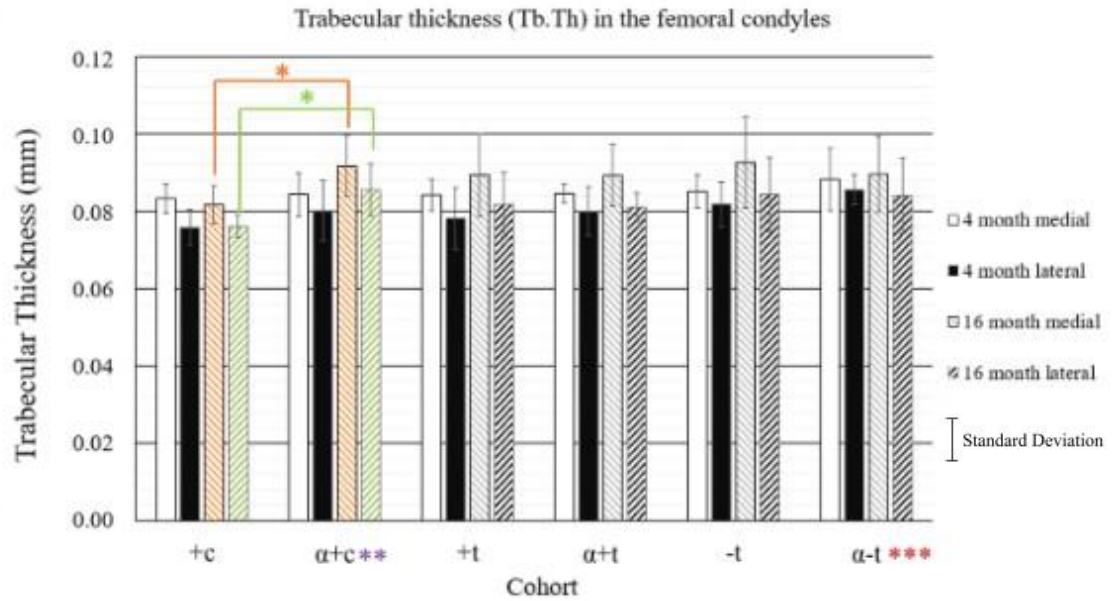
Figure 29: Trabecular thickness data in the femoral condyles by cohort. The 4-month medial (white), 16-month medial (gray hatched), 4-month lateral (black), and 16-month lateral (black hatched) mean values are shown by cohort.
* Statistically significant difference between study focus cohort combinations ($p < 0.05$) following Kruskal-Wallis and post hoc Dunn's test.
** Significant difference ($p < 0.05$) on the medial side between 4- and 16-month timepoints within the cohort (Kruskal-Wallis).
*** Significant difference ($p < 0.05$) on the lateral side between 4- and 16-month timepoints within the cohort (Kruskal-Wallis).
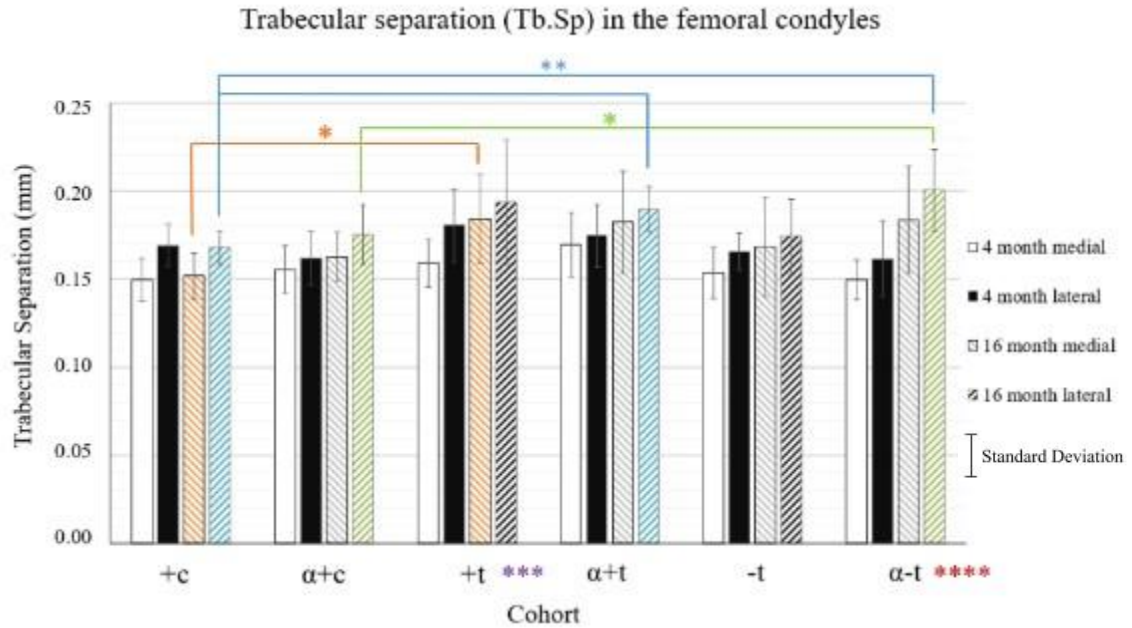
Figure 30: Trabecular separation data in the femoral condyles by cohort. The 4-month medial (white), 16-month medial (gray hatched), 4-month lateral (black), and 16-month lateral (black hatched) mean values are shown by cohort. At 4 and 16-months, the average trabecular separation in the double knockout (α+t) mice was greater than in the wild type mice.
* Statistically significant difference between study focus cohort combinations ($p < 0.05$) following Kruskal-Wallis and post hoc Dunn's test.
** Statistically significant difference between cohort combinations outside of study focus ($p < 0.05$) following a Kruskal-Wallis test and post hoc Dunn's test.
*** Significant difference ($p < 0.05$) on the medial side between 4- and 16-month timepoints within the cohort (Kruskal-Wallis).
**** Significant difference ($p < 0.05$) on the lateral side between 4- and 16-month timepoints within the cohort (Kruskal-Wallis).
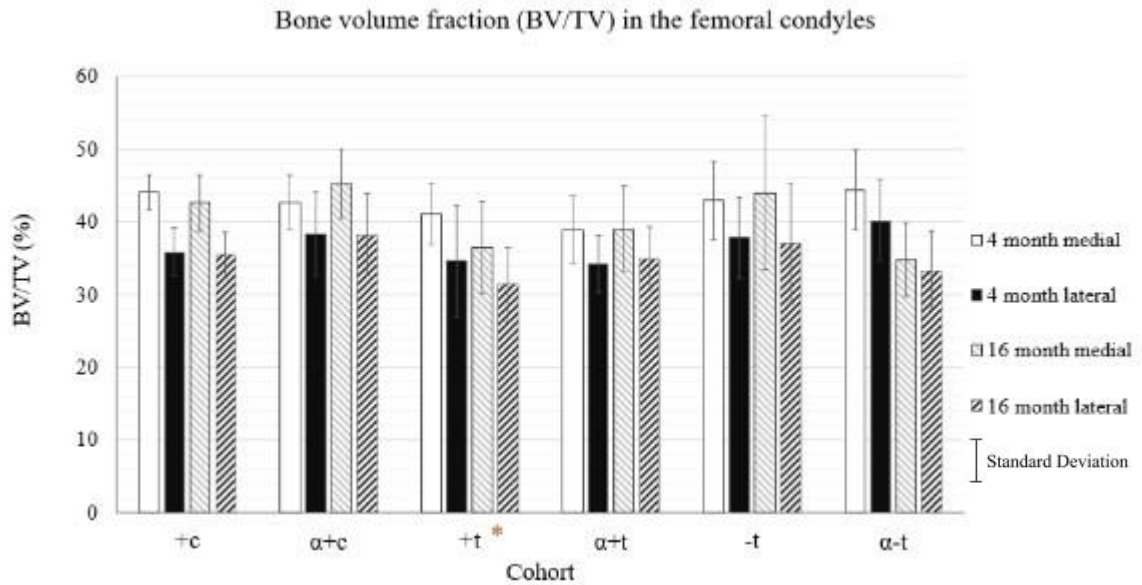
Figure 31: Bone volume fraction data in the femoral condyles by cohort. The 4-month medial (white), 16-month medial (gray hatched), 4-month lateral (black), and 16-month lateral (black hatched) mean values are shown by cohort. The initial Kruskal-Wallis test showed there were significant differences between cohorts ($p < 0.05$) for the bone volume fraction in the medial femoral condyle for 16-month specimens, but the post hoc Dunn's test did not find any significant differences between cohorts.

* Significant difference ($p < 0.05$) on the medial side between 4- and 16-month timepoints within the cohort (Kruskal-Wallis).

Table 22: Post hoc results of trabecular bone adaptations in the femoral condyles for the 4-month cohort combinations using Dunn's test. Cohort combinations highlighted in gray are the study focus comparisons. The p values for the initial Kruskal-Wallis test are shown above the post hoc p values No dataset found significantly different differences between cohorts ($p < 0.05$).

Timepoint		4 months					
		Femoral Condyles					
		Medial			Lateral		
Dataset		Trabecular Thickness	Trabecular Separation	Bone Volume Fraction	Trabecular Thickness	Trabecular Separation	Bone Volume Fraction
Abbreviation		Tb.Th	Tb.Sp	BV/TV	Tb.Th	Tb.Sp	BV/TV
p value for dataset (factor : cohort)		0.38	0.22	0.24	0.38	0.08	0.44
Cohort Comparison		Post Hoc p value					
+c	α+c	1.00	0.98	1.00	0.96	1.00	1.00
+c	+t	1.00	0.40	0.65	0.98	0.28	1.00
+c	-t	1.00	0.95	1.00	0.98	1.00	1.00
α+c	α+t	0.94	0.51	1.00	1.00	0.96	1.00
α+c	α-t	1.00	1.00	0.94	1.00	0.76	1.00
+t	-t	1.00	0.89	1.00	0.73	0.56	1.00
α-t	α+t	1.00	0.37	1.00	1.00	1.00	1.00
α-t	-t	1.00	0.99	1.00	1.00	1.00	0.95
+c	α+t	1.00	0.24	0.55	0.92	1.00	1.00
+c	α-t	1.00	1.00	1.00	0.95	0.96	1.00
α+c	+t	1.00	1.00	1.00	0.54	0.46	0.56
α+c	-t	1.00	1.00	1.00	1.00	0.91	1.00
+t	α+t	1.00	1.00	1.00	0.54	0.46	1.00
+t	α-t	0.36	0.56	1.00	0.62	0.75	1.00
α+t	-t	1.00	0.74	1.00	1.00	1.00	1.00

Table 23: Post hoc (Dunn's test) results of trabecular bone characteristics in the femoral condyles for the 16-month cohort combinations. Cohort combinations highlighted in gray are the study focus comparisons. The p values for the initial Kruskal-Wallis test are shown above the post hoc p values. Values that are bolded and highlighted in green showed a significant difference in means between the listed cohorts ($p < 0.05$). The initial Kruskal-Wallis test showed there were significant differences between cohorts ($p < 0.05$) in the bone volume fraction in the medial femoral condyles, but the post hoc Dunn's test did not find any significant differences between cohorts.
$\downarrow$ second cohort listed (second column from left) has average value less than that of the cohort from the first cohort (first column from the left)
$\uparrow$ second cohort listed (second column from left) has average value greater than that of the cohort from the first cohort (first column from the left)

Timepoint		16 months					
		Femoral Condyles					
		Medial			Lateral		
Dataset		Trabecular Thickness	Trabecular Separation	Bone Volume Fraction	Trabecular Thickness	Trabecular Separation	Bone Volume Fraction
Abbreviation		Tb.Th	Tb.Sp	BV/TV	Tb.Th	Tb.Sp	BV/TV
p value for dataset (factor : cohort)		**0.03**	**0.01**	**0.02**	**0.02**	**0.00**	0.22
Cohort Comparison		Post Hoc p value					
+c	α+c	**0.02**$\uparrow$	1.00	1.00	**0.01**$\uparrow$	0.88	1.00
	+t	1.00	**0.04**$\uparrow$	0.31	0.39	0.46	1.00
	-t	0.36	0.80	1.00	0.41	1.00	1.00
α+c	α+t	1.00	0.85	0.52	0.89	0.15	1.00
	α-t	1.00	1.00	0.08	1.00	**0.04**$\uparrow$	0.97
+t	-t	1.00	1.00	0.86	1.00	1.00	1.00
α-t	α+t	1.00	1.00	1.00	1.00	1.00	1.00
	-t	1.00	1.00	0.71	1.00	0.17	1.00
+c	α+t	0.30	0.05	1.00	0.60	**0.04**$\uparrow$	1.00
	α-t	0.74	0.15	0.19	0.26	**0.01**$\uparrow$	1.00
α+c	+t	1.00	0.67	0.13	1.00	0.77	1.00
	-t	1.00	1.00	1.00	1.00	1.00	1.00
+t	α+t	1.00	0.73	1.00	1.00	1.00	1.00
	α-t	0.98	1.00	0.99	0.98	1.00	0.14
α+t	-t	1.00	1.00	1.00	1.00	0.52	1.00

3.2.2.1   Difference Between 4-month and 16-month Specimens Within a Cohort

Kruskal-Wallis tests determined whether there were significant differences in the trabecular bone characteristics between the 4-month and 16-month animals within a cohort. The test results are summarized in Table 24. 16-month *itga1*-null mice had significantly increased trabecular thickness in the medial femoral condyles compared to the 4-month samples. 16-month wild-type mice with a cartilage-specific TβRII knockout (+t) had significantly greater values of trabecular separation and significantly reduced bone volume fraction in the medial femoral condyles compared to 4-month specimens. In the lateral femoral condyles of tamoxifen control *itga1*-null mice (α-t), older mice had significantly decreased measures of trabecular thickness and separation.

Table 24: Results from the Kruskal-Wallis test between the 4- and 16-month specimens within each cohort. Values which are bolded and highlighted in green were found to have a statistically significant difference between the timepoints ($p<0.05$).
↓ 16-month specimens had an average value less than the 4-month specimens.
↑ 16-month specimens had an average value greater than the 4-month specimens.

		P value (Kruskal Wallis)					
		Femoral Condyles					
		Medial			Lateral		
Cohort	Measure	Trabecular Thickness	Trabecular Separation	Bone Volume Fraction	Trabecular Thickness	Trabecular Separation	Bone Volume Fraction
		Tb.Th	Tb.Sp	BV/TV	Tb.Th	Tb.Sp	BV/TV
+c		0.38	0.56	0.56	0.24	0.24	0.11
α+c		**0.01↑**	0.17	0.17	0.37	0.06	0.68
+t		0.17	**0.03↑**	**0.03↓**	0.17	0.35	0.60
α+t		0.37	0.17	0.17	0.68	0.06	0.29
-t		0.57	0.37	0.37	0.46	0.46	0.94
α-t		0.68	0.06	0.06	**0.02↓**	**0.01↓**	0.57

3.3 Ectopic Bone Volume Quantifications

Ectopic bone volume quantification results were shown using box and whisker plots. The data were not normally distributed, and these plots provided more insight into the distribution of data. The quartiles were calculated with the median point included.

3.3.1 Patellar Volume

Datasets at each timepoint were tested for statistical significance between cohorts. No dataset was found to have statistical significance by cohort. The volumes of the patella for each cohort and timepoint are shown in Figure 32. Kruskal-Wallis tests within a cohort

determined whether there was a significant difference in volume between the 4- and 16-month samples within a cohort. The test results are summarized in Table 27. Older mice had significantly larger patellar volumes in all cohorts except for the *itga1*-null mice, which did not show significance.
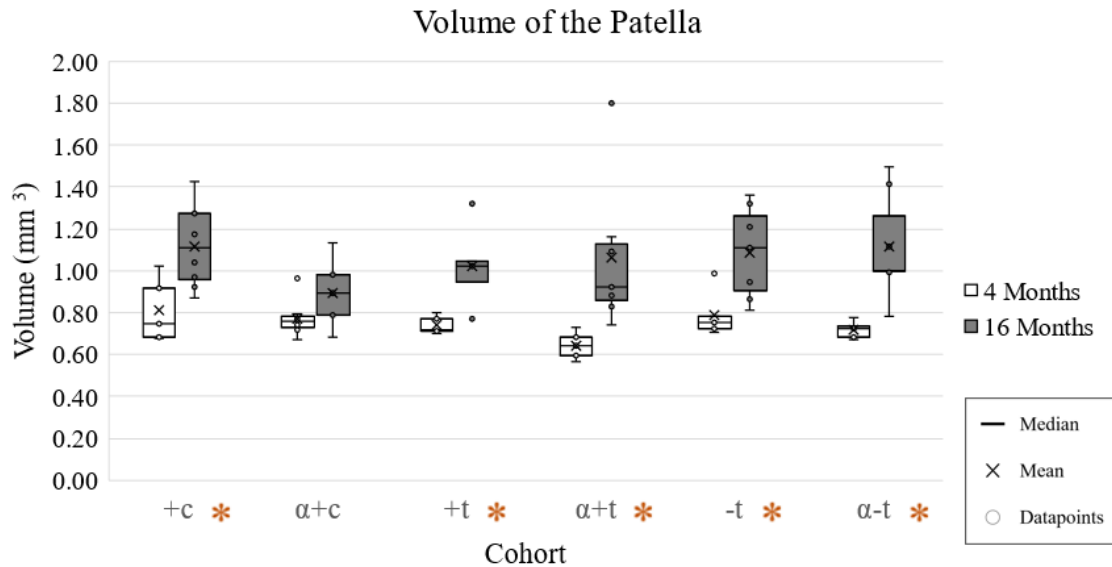
Figure 32: Volume of the patella by cohort for the 4-(white) and 16-month (dark gray) samples. There was no statistical significance found in any dataset by cohort. The data are shown using box and whisker plots. The box represents the interquartile range (IQR) of data which contain the datapoints within the first (bottom of range) to the third (top of range) quartile. When data is organized in ascending order, the first and third quartile represent the values encompassing the first 25% and 75% of the datapoints respectively. The median is represented by the solid horizontal line, the mean is represented by an 'X', and the black outlined points represent the datapoints. The 'whiskers' (capped lines) that extend from the box show the upper and lower limits of data, outside of these, data are considered outliers. The limits are determined by the IQR.
* Significant difference ($p < 0.05$) between 4- and 16-month timepoints within the cohort (Kruskal-Wallis).

3.3.2   Volume of Calcification at the Collateral Ligaments

The volume of calcified tissue along the collateral ligaments by cohort is shown in Figure 33. There was a significant difference between cohorts for calcification along the medial collateral ligament for the 4-month samples ( ). The post-hoc Dunn's test found that in *itga1*-null mice, those with a cartilage-specific TβRII knockout (α+t) had significantly greater volumes of calcified tissue along the medial collateral ligament than those without (α+c) (Figure 34). No other significant differences were detected in the collateral ligaments at any timepoint (Table 25 and Table 26). Kruskal-Wallis tests were run to detect any significant difference in volume between the 4- and 16-month samples within a cohort. The test results are summarized in Table 27. Older mice in the wild-type (+c) and *itga1*-null (α+c) and their respective tamoxifen controls (-t and α-t) had significantly greater volumes of calcified tissue along the medial collateral ligament (Table 25). The older *itga1*-null mice with a cartilage-specific TβRII knockout (α+t) had significantly increased volumes of calcified tissue along the lateral collateral ligament.
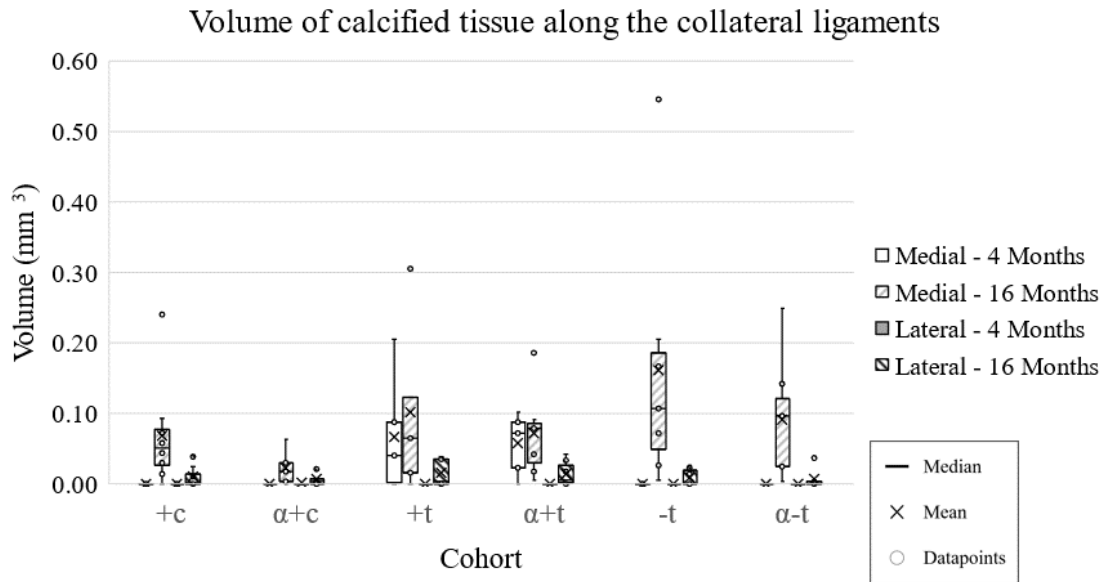
Figure 33: Volume of calcified tissue along the collateral ligaments by cohort. The 4-month medial (white), 16-month medial (gray hatched), 4-month lateral (dark gray), and 16-month lateral (black hatched) values are shown by cohort. Significant differences were found in the medial collateral ligament. The following figures show the medial and lateral collateral ligament volumes separately to explore these relationships. The data are shown using box and whisker plots. The box represents the interquartile range (IQR) of data which contain the datapoints within the first (bottom of range) to the third (top of range) quartile. When data is organized in ascending order, the first and third quartile represent the values encompassing the first 25% and 75% of the datapoints respectively. The median is represented by the solid horizontal line, the mean is represented by an 'X', and the black outlined points represent the datapoints. The 'whiskers' (capped lines) that extend from the box show the upper and lower limits of data, outside of these, data are considered outliers. The limits are determined by the IQR.

Figure 34: Volume of calcified tissue at the medial collateral ligament (MCL) by cohort for 4- (white) and 16-month (gray - hatched) samples. The data are shown using box and whisker plots. The box represents the interquartile range (IQR) of data which contain the datapoints within the first (bottom of range) to the third (top of range) quartile. When data is organized in ascending order, the first and third quartile represent the values encompassing the first 25% and 75% of the datapoints respectively. The median is represented by the solid horizontal line, the mean is represented by an 'X', and the black outlined points represent the datapoints. The 'whiskers' (capped lines) that extend from the box show the upper and lower limits of data, outside of these, data are considered outliers. The limits are determined by the IQR.
* Statistically significant difference ($p < 0.05$) between 4- and 16-month volumes within the cohort determined by Kruskal-Wallis test.
** Statistically significant difference ($p < 0.05$) based on post hoc Dunn's test between cohorts that have a relationship important to study focus.

Figure 35: Volume of calcified tissue at the lateral collateral ligament (LCL) for 4-month (dark gray) and 16-month (dark gray hatched) samples. Data was not significantly different between cohorts for either the 4 or 16-month groups. The data are shown using box and whisker plots. The box represents the interquartile range (IQR) of data which contain the datapoints within the first (bottom of range) to the third (top of range) quartile. When data is organized in ascending order, the first and third quartile represent the values encompassing the first 25% and 75% of the datapoints respectively. The median is represented by the solid horizontal line, the mean is represented by an 'X', and the black outlined points represent the datapoints. The 'whiskers' (capped lines) that extend from the box show the upper and lower limits of data, outside of these, data are considered outliers. The limits are determined by the IQR.
* Statistically significant difference ($p < 0.05$) between 4- and 16-month volumes within the cohort determined by Kruskal-Wallis test.

3.3.3 Volume of Calcified Tissue at the Menisci

The volume of calcified tissue at the medial and lateral meniscus were quantified separately. Results for all datasets that quantified the volume of calcified tissue at the medial and lateral meniscus are shown together in Figure 36, and then separately in Figure 37 and Figure 39, respectively. A Kruskal-Wallis test and post hoc Dunn's test were performed to look for statistical significance between calcified tissue volumes by cohort. In the medial meniscus of 4-month samples, *itga1*-null (α+c) mice had greater volumes of calcified tissue than in the tamoxifen control *itga1*-null mice (α-t) (Figure 38). No set of data had any significant difference among 16-month cohorts (Table 26). Kruskal-Wallis tests determined whether there was a significant difference in volume between the 4- and 16-month samples within a cohort. Every cohort had significantly increased volumes of calcified tissue along the medial and lateral meniscus in 16-month animals compared to the respective 4-month animals.
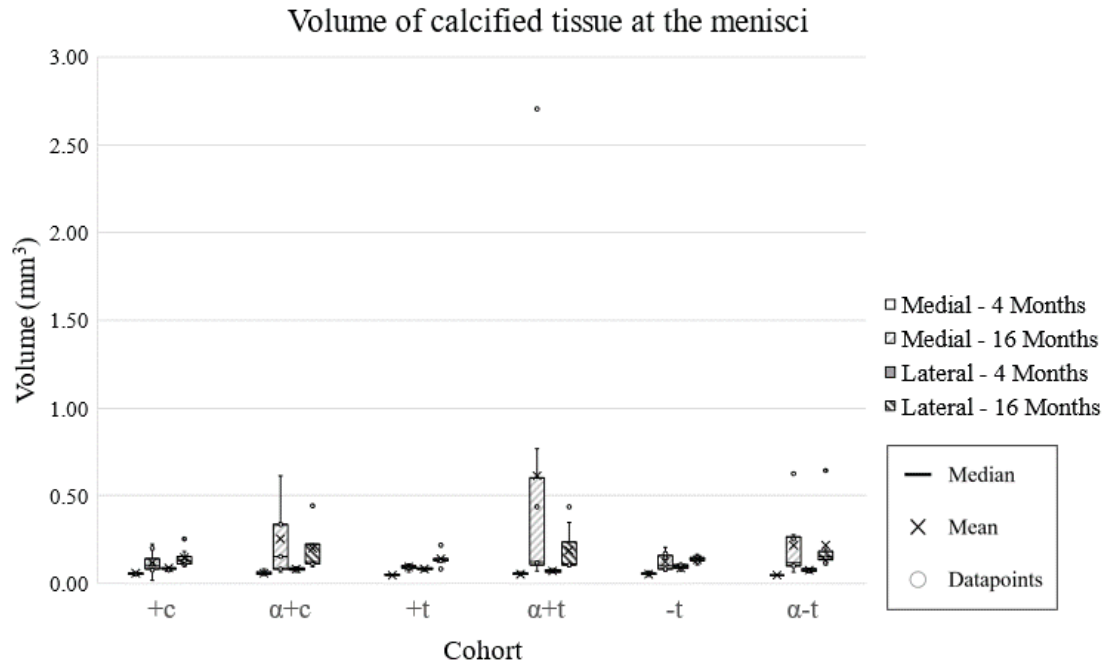
Figure 36: Volume of calcified tissue at the menisci. The 4-month medial (white), 16-month medial (gray hatched), 4-month lateral (black), and 16-month lateral (black hatched) values are shown by cohort. Significant differences with respect to cohort were found in the medial meniscus. The following figures show the calcified tissue volumes for the medial and lateral meniscus regions separately to explore these relationships. The data are shown using box and whisker plots. The box represents the interquartile range (IQR) of data which contain the datapoints within the first (bottom of range) to the third (top of range) quartile. When data is organized in ascending order, the first and third quartile represent the values encompassing the first 25% and 75% of the datapoints respectively. The median is represented by the solid horizontal line, the mean is represented by an 'X', and the black outlined points represent the datapoints. The 'whiskers' (capped lines) that extend from the box show the upper and lower limits of data, outside of these, data are considered outliers. The limits are determined by the IQR.

Figure 37: Volume of calcified tissue at the medial meniscus by cohort for 4- (white) and 16-month (gray hatched) samples. The 4-month results are shown alone in the next figure for a better representation of the significant difference between cohorts. The data are shown using box and whisker plots. The box represents the interquartile range (IQR) of data which contain the datapoints within the first (bottom of range) to the third (top of range) quartile. When data is organized in ascending order, the first and third quartile represent the values encompassing the first 25% and 75% of the datapoints respectively. The median is represented by the solid horizontal line, the mean is represented by an 'X', and the black outlined points represent the datapoints. The 'whiskers' (capped lines) that extend from the box show the upper and lower limits of data, outside of these, data are considered outliers. The limits are determined by the IQR.

* Statistically significant difference ($p < 0.05$) between 4- and 16-month volumes within the cohort determined by Kruskal-Wallis test.

** Statistically significant difference ($p < 0.05$) based on post hoc Dunn's test between cohorts that have a relationship important to study focus.

Figure 38: Volume of calcified tissue at the medial meniscus by cohort for 4-month specimens. The data are shown using box and whisker plots. The box represents the interquartile range (IQR) of data which contain the datapoints within the first (bottom of range) to the third (top of range) quartile. When data is organized in ascending order, the first and third quartile represent the values encompassing the first 25% and 75% of the datapoints respectively. The median is represented by the solid horizontal line, the mean is represented by an 'X', and the black outlined points represent the datapoints. The 'whiskers' (capped lines) that extend from the box show the upper and lower limits of data, outside of these, data are considered outliers. The limits are determined by the IQR.
* Statistically significant difference ($p < 0.05$) based on results from the post hoc Dunn's test between cohorts that have a relationship important to the study focus.
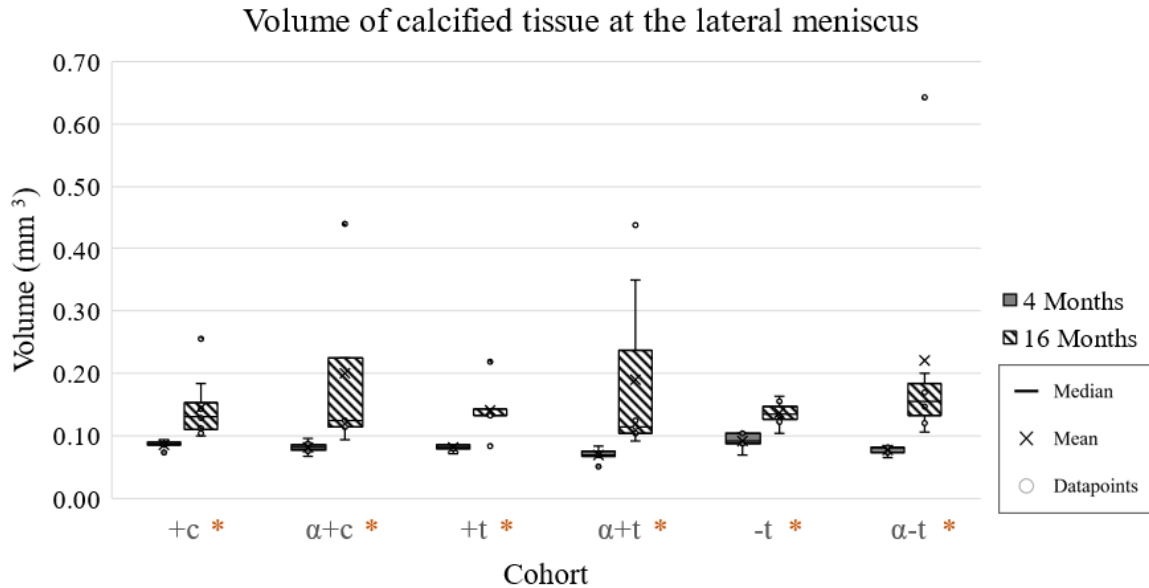
Figure 39: Volume of calcified tissue at the lateral meniscus in 4- (white) and 16-month (black) cohorts. The initial Kruskal-Wallis test showed there were significant differences in volume between cohorts ($p < 0.05$) in 4-month specimens, but the post hoc Dunn's test did not find any significant differences between cohorts. The data are shown using box and whisker plots. The box represents the interquartile range (IQR) of data which contain the datapoints within the first (bottom of range) to the third (top of range) quartile. When data is organized in ascending order, the first and third quartile represent the values encompassing the first 25% and 75% of the datapoints respectively. The median is represented by the solid horizontal line, the mean is represented by an 'X', and the black outlined points represent the datapoints. The 'whiskers' (capped lines) that extend from the box show the upper and lower limits of data, outside of these, data are considered outliers. The limits are determined by the IQR.
* Significant difference ($p < 0.05$) in volume between 4- and 16-month specimens within the cohort (Kruskal-Wallis).

Table 25: Post hoc results (Dunn's test) of volume quantifications in the 4-month cohort combinations. Cohort combinations highlighted in gray are the study focus comparisons. The *p* values for the initial Kruskal-Wallis test are shown above the post hoc *p* values. Values that are bolded and highlighted in green showed a significant difference in means between the listed cohorts ($p < 0.05$).
↓ second cohort listed (second column from left) has average value less than that of the cohort from the first cohort (first column from the left)
↑ second cohort listed (second column from left) has average value greater than that of the cohort from the first cohort (first column from the left)

Timepoint		4 months				
Region		Patella	Menisci		Collateral ligaments	
			Medial	Lateral	Medial	Lateral
Measurement		Bone Volume	Volume of calcified tissue			
p value for dataset (factor : cohort)		0.10	**0.05**	**0.05**	**0.01**	0.70
Cohort Comparison		Post Hoc *p* value				
+c	α+c	0.88	0.97	1.00	1.00	1.00
	+t	1.00	0.56	1.00	0.28	1.00
	-t	1.00	1.00	1.00	1.00	1.00
α+c	α+t	0.21	0.78	0.91	**0.03↑**	1.00
	α-t	1.00	**0.04↓**	1.00	1.00	1.00
+t	-t	1.00	0.84	1.00	0.09	1.00
α-t	α+t	1.00	0.53	1.00	0.23	1.00
	-t	1.00	0.55	0.44	1.00	1.00
+c	α+t	0.44	1.00	0.19	0.23	1.00
	α-t	1.00	0.28	0.94	1.00	1.00
α+c	+t	1.00	0.83	0.84	0.06	1.00
	-t	1.00	0.76	1.00	1.00	1.00
+t	α+t	0.76	0.83	1.00	1.00	1.00
	α-t	1.00	1.00	1.00	0.28	1.00
α+t	-t	0.21	1.00	0.06	0.06	1.00

Table 26: Post hoc results of volume quantifications in the 16-month cohort combinations. The volume of the patella, as well as ectopic calcifications of soft tissues at the menisci and collateral ligaments were analyzed for significance. No dataset found significantly different differences between cohorts ($p < 0.05$).

Timepoint		16 months				
Region		Patella	Menisci		Collateral ligaments	
			Medial	Lateral	Medial	Lateral
Measurement		Bone Volume	Volume of calcified tissue			
p value for dataset (factor : cohort)		0.66	0.23	0.69	0.36	0.82
Cohort Comparison		Post Hoc p value				
+c	α+c	0.61	1.00	1.00	1.00	1.00
	+t	0.98	1.00	1.00	1.00	1.00
	-t	1.00	0.81	1.00	1.00	1.00
α+c	α+t	0.85	1.00	1.00	1.00	1.00
	α-t	0.65	1.00	1.00	1.00	1.00
+t	-t	1.00	1.00	1.00	1.00	1.00
α-t	α+t	1.00	1.00	1.00	1.00	1.00
	-t	1.00	1.00	1.00	1.00	1.00
+c	α+t	1.00	1.00	1.00	1.00	1.00
	α-t	1.00	1.00	1.00	1.00	1.00
α+c	+t	1.00	1.00	1.00	1.00	1.00
	-t	0.76	1.00	1.00	0.35	0.93
+t	α+t	1.00	0.99	1.00	0.99	1.00
	α-t	0.99	1.00	1.00	1.00	1.00
α+t	-t	1.00	1.00	1.00	1.00	1.00

Table 27: Results from the Kruskal-Wallis test between the 4- and 16-month specimens within each cohort. Values which are bolded and highlighted in green were found to have a statistically significant difference between the timepoints ($p < 0.05$).
↓ 16-month specimens had an average value less than the 4-month specimens.
↑ 16-month specimens had an average value greater than the 4-month specimens.

Cohort	Volume (mm³)				
	Meniscus		Collateral Ligament		Patella
	Medial	Lateral	Medial	Lateral	
+c	**0.03↑**	**0.00↑**	**0.01↑**	0.07	**0.02↑**
α+c	**0.01↑**	**0.01↑**	**0.01↑**	0.15	0.17
+t	**0.01↑**	**0.03↑**	0.68	0.22	**0.03↑**
α+t	**0.00↑**	**0.00↑**	0.81	**0.02↑**	**0.00↑**
-t	**0.00↑**	**0.01↑**	**0.00↑**	0.11	**0.02↑**
α-t	**0.00↑**	**0.00↑**	**0.00↑**	0.59	**0.00↑**

3.4   Binary Analyses of Ectopic Calcifications

Results from the binary analyses, as described in section 2.9, are shown below in Table 28. The data were analyzed as categorical data using the Chi-Square test. Results of the statistical analysis for cohort comparisons important to the study focus are given in Table **29**.

Table 28:   Data from the binary analysis, showing the fraction of samples in each cohort that exhibited each behaviour. Criteria for these data are described in section 2.9.

Timepoint (months)	Cohort	Fraction of samples exhibiting the behaviour				
		Calcification at the root of the MCL	Osteophytosis at the root of the MCL	Defined osteophytes at the patella	Mineralized tissue in quadriceps	patella subluxed from patellofemoral groove
4	+c	2/5	1/5	4/5	3/5	0/5
	α+c	0/7	0/7	1/7	2/7	2/7
	+t	4/5	3/5	3/5	0/5	0/5
	α+t	5/5	4/5	0/5	0/5	0/5
	-t	5/5	0/5	3/5	1/5	1/5
	α-t	5/5	0/5	0/5	0/5	1/5
16	+t	3/8	2/8	7/8	1/8	3/8
	α+c	2/5	1/5	5/5	0/5	0/5
	+t	5/5	1/5	5/5	0/5	1/5
	α+t	7/7	5/7	7/7	1/7	2/7
	-t	6/7	4/7	7/7	1/7	1/7
	α-t	7/7	1/7	6/7	2/7	4/7

Table 29: Results from the Chi-Square test of the binary analysis of ectopic calcification at the root of the medial collateral ligament. The p values resulting from testing all cohorts together are shown above the p values for the study focus cohort comparisons. Values that are bolded and highlighted in green showed a significant difference ($p < 0.05$) in the frequency distribution of data from the theoretical between cohorts.

		Root of Medial Collateral Ligament			
		Calcified		Osteophytosis	
		4	16	4	16
p value for dataset		**0.00**	**0.00**	**0.00**	0.15
Cohort Comparison		p value between cohorts			
+c	α+c	0.07	0.93	0.22	0.84
+c	+t	0.20	**0.02↑**	0.20	0.84
+c	-t	**0.04↑**	0.06	0.29	0.20
α+c	α+t	**0.00↑**	**0.02↑**	**0.00↑**	0.08
α+c	α-t	**0.00↑**	**0.02↑**	1.00	0.79
+t	-t	0.29	0.38	**0.04↓**	0.20
α-t	α+t	1.00	1.00	**0.01↑**	**0.03↑**
α-t	-t	1.00	0.30	1.00	0.09

Table 30: Results from Chi-Square test of the binary analysis of ectopic calcification and phenomenon at the patella and tissue in the quadricep region. The *p* values resulting from testing all cohorts together are shown above the *p* values for the study focus cohort comparisons. Values that are bolded and highlighted in green showed a significant difference ($p < 0.05$). in means between the listed cohorts.

		Patella				Calcified Tissue in Quadricep Region	
		Osteophyte Presence		Subluxed from Patellofemoral groove			
		4	16	4	16	4	16
p value for dataset		**0.02**	0.64	0.51	0.30	0.09	0.69
Cohort Comparison		*p* value between cohorts					
+c	α+c	**0.02↓**	0.41	0.19	0.12	0.28	0.41
+c	+t	0.49	0.41	1.00	0.51	1.00	0.41
+c	-t	0.49	0.33	0.20	0.92	0.29	0.31
α+c	α+t	0.38	1.00	0.19	0.19	0.19	0.38
α+c	α-t	0.38	0.38	0.74	1.00	0.19	0.19
+t	-t	1.00	1.00	0.29	0.79	0.29	0.38
α-t	α+t	1.00	0.30	0.29	0.28	1.00	0.51
α-t	-t	**0.04↑**	0.30	1.00	0.09	0.29	0.51

3.4.1 Calcification and Osteophytosis at the Root of the Medial Collateral Ligament

Samples were designated as having calcified tissue at the root of the medial collateral ligament by the criteria outlined in Table 11. The results of the Chi-square analysis of these data are shown in Figure 40. There was a significant difference in the frequency of calcified MCL roots at both timepoints. In both 4- and 16-month samples, the *itga1*-null mice with tamoxifen injections (α+t, α-t), regardless of whether the tamoxifen activated a TβRII knockout, had more instances of calcified medial collateral ligament roots than the corn oil injected mice (α+c). In 4-month samples, the wild-type tamoxifen control mice (-

t) had more instances of a calcified medial collateral ligament root than in the corn oil injected wild type mice (+c). 16-month mice with a cartilage-specific TβRII knockout (+t) had a calcified medial collateral ligament root significantly more frequently than wild-type mice (+c). These relative frequencies can be seen in Figure 40. There were significant differences in the frequency of osteophytes originating at the root of the medial collateral ligament. In 4-month specimens, the mice with an activated cartilage-specific TβRII knockout, with (α+t) and without (+t) the integrin α1 subunit knockout have a significantly greater proportion of mice with osteophyte formation at the root of the medial collateral ligament than their respective tamoxifen controls (α-t and -t). This significant difference occurred in the same way in 16-month specimens for the *itga1*-null mice injected with tamoxifen (α+t and α-t). Additionally, 4-month *itga1*-null mice with a cartilage-specific TβRII knockout had a greater proportion of mice with osteophytes at the medial collateral ligament root than those with intact TβRII. These proportions can be seen in Figure 41.
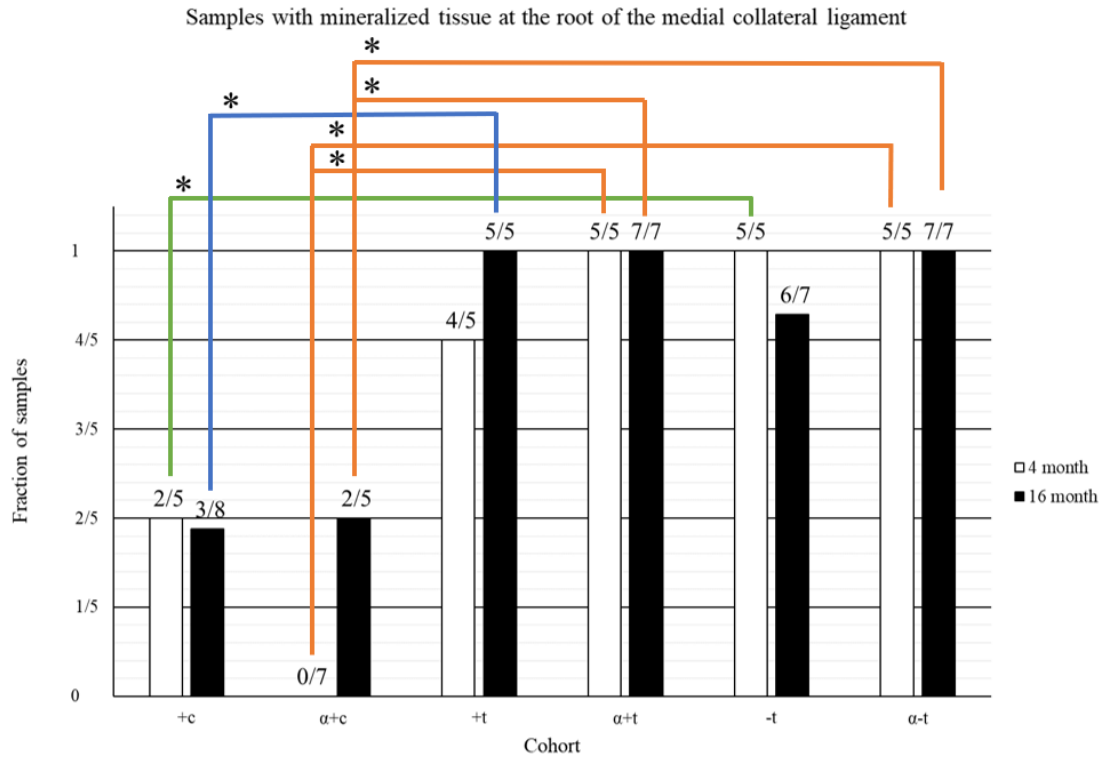
Figure 40: Fraction of samples from the 4 (white) and 16 (black) month timepoints in each cohort that have calcified tissue at the root of the medial collateral ligament.
* Statistically significant difference between cohorts ($p < 0.05$)
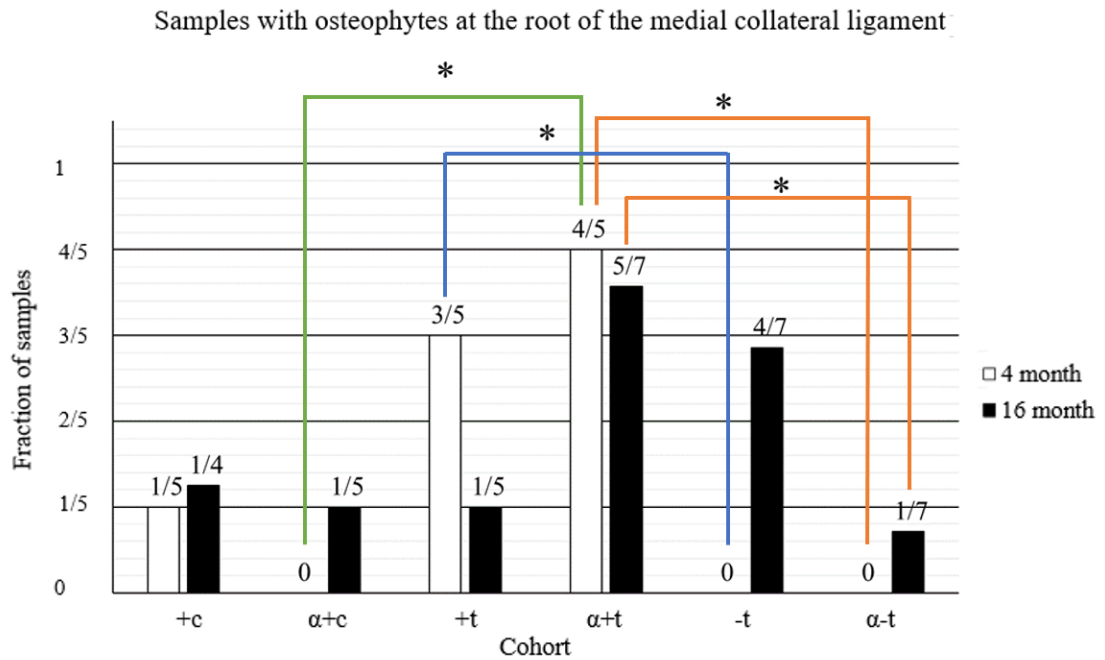
Figure 41: Fraction of samples from the 4 (white) and 16 (black) month timepoints in each cohort where osteophytosis was observed at the root of the medial collateral ligament.
* Statistically significant difference between cohorts ($p < 0.05$)

3.4.2 Osteophyte Presence and Subluxation of the Patella

Based on the criteria outlined in section 2.9, samples were analyzed for the presence of osteophytes or dislocation (subluxation) of the patella within the patellofemoral groove. The proportions of samples where the patella had osteophytes or was dislocated are shown in Figure 42 and Figure 43. The binary analysis was treated as categorical data, and the Chi-Square test was performed to analyze significant differences between cohorts. The results of this test are reported in Table 30. In 4-month specimens, the *itga1*-null (α+c) mice had significantly fewer mice with osteophytes at the patella than the wild-type

mice (+c). Additionally, the *itga1*-null tamoxifen control mice (α-t) had significantly

fewer samples with osteophytes at the patella than the wild-type tamoxifen control mice

(-t). There were no significant differences between cohorts at any timepoint in patellar

dislocation.
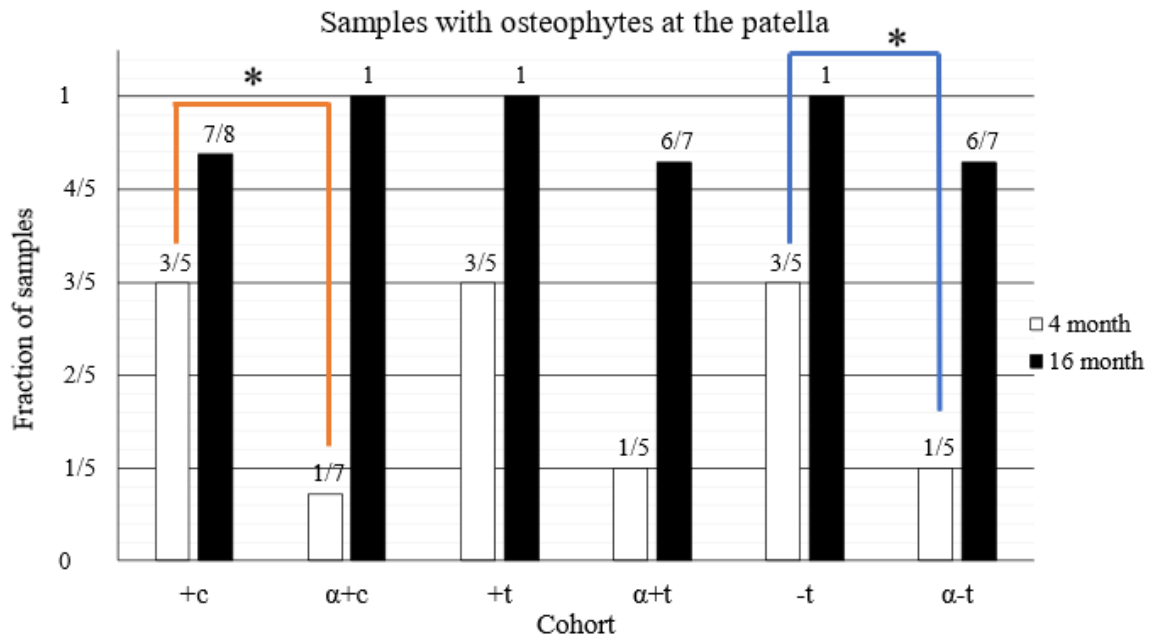
Figure 42: The number of samples from each cohort and timepoint in which osteophytes had formed at the patella. To represent differing sample sizes, the data labels represent the ratio of specimens with patellar osteophytes to the total number of samples in the group.
* Statistically significant difference between cohorts ($p < 0.05$)
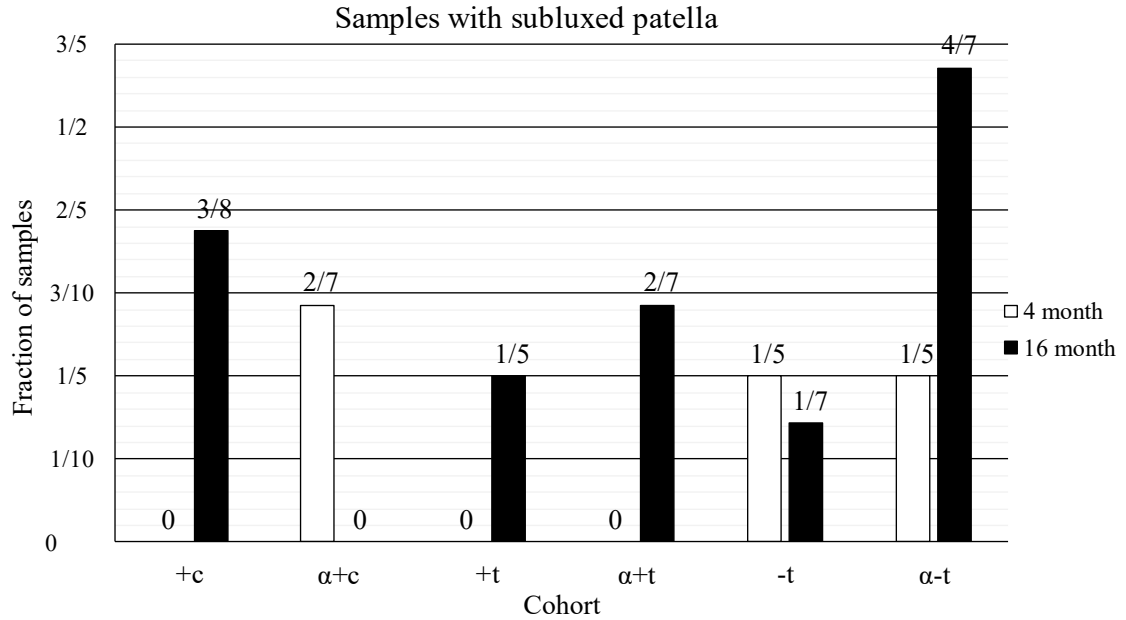
Figure 43: The number of samples from each cohort and timepoint where the patella was dislocated (subluxed) from the patellofemoral groove. To represent differing sample sizes, the data labels represent the ratio of specimens with a subluxed patella to the total number of samples in the group.

3.4.3 Mineralized Tissue in the Quadriceps

The proportion of samples per cohort with mineralized tissue present in the quadricep region, as described in section 2.9, was determined. A Chi-Square test was performed for the study focus cohorts, results are reported in Table 30. No significant differences were found in the relative proportions of samples per cohort with calcified tissue in this region. The proportion of samples per cohort with calcified tissue in the quadriceps is shown below in Figure 44.
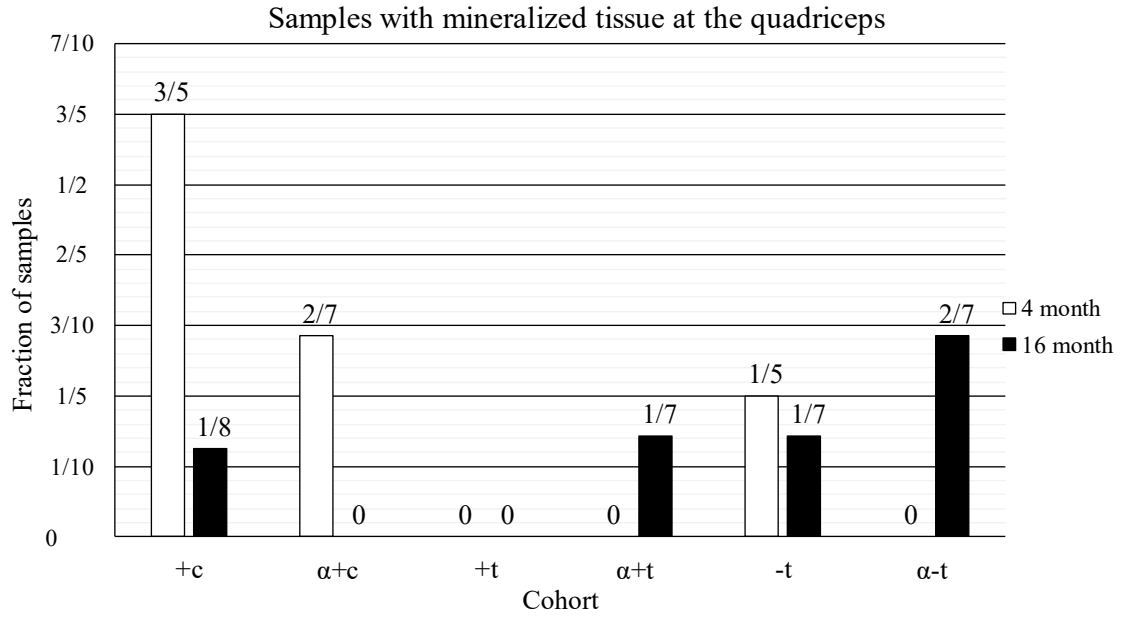
Figure 44: Fraction of samples that showed mineralized tissue in the quadricep region in each cohort at the 4-month (white) and 16-month (black) timepoints.

4   Discussion

The goal of the study was to quantify bone adaptation and abnormal tissue calcifications around the joint in a genetic mouse model of osteoarthritis (OA). Prior observation of fibrosis in the kidney of integrin α1 subunit knockout (*itga1*-null) mice was determined to be a result of excessive TGFβ signalling. (X. Chen et al., 2014) The mouse model in this project was used to observe whether a cartilage-specific knockout of TβRII had a protective effect on the cartilage of *itga1*-null mice. This study was meant to further the foregoing study by Dr. A Clark at the University of Guelph. St. Amant and Clark (St. Amant, 2022) determined there was OA-like damage to the articular cartilage in their histological analysis of the integrin α1 subunit knockout (*itga1*-null) mice. They also observed that the inhibition of TβRII protects articular cartilage from some of the OA-like damage associated with the *itga1*-null mice. Based on their results, we expected to see adaptations in the trabecular bone around the knees that are typical hallmarks of OA progression in the joint including lower volume fraction, decreased trabecular thickness, and increased trabecular separations. Because the ubiquitous integrin α1 subunit knockout in mice induced osteoarthritic phenotypes in the cartilage (St. Amant, 2022), we expected to see these trabecular bone adaptations in mice with an α1 knockout (αTC cohort). We also expected to see ectopic bone formation around the joint including osteophytes and soft tissue calcifications in the *itga1*-null mice, related to uninhibited TβRII signalling in all tissues. Additionally, the conditional knock-out of the TGFβ receptor, TβRII resulted in less severe OA degenerative changes to the cartilage in *itga1*-null mice (St. Amant,

2022), and so we hypothesized that the TβRII knockout would result in less change in the trabecular bone around the joints in *itga1*-null mice.

4.1   Trabecular Bone in *itga1*-null Mice Did Not Have Expected OA-like Changes

While there were significant effects in the trabecular thickness in the medial and lateral femoral condyles in the 16-month samples, in both cases, the mean trabecular thickness was greater for *itga1*-null mice (α+c) than in the wild-type (+c) mice. Osteoarthritis phenotypes typically include degradation of bone and loss of trabecular bone (Anderson et al., 2016; Christiansen et al., 2012; Wegner et al., 2019; Wohl et al., 2001); therefore, it was expected that trabecular thickness would be less in the *itga1*-null mice compared to wild-type. However, our results were contrary, with an overall greater trabecular thickness in the femoral condyles. While St. Amant concluded that *itga1*-null mice had more severe OA changes to the cartilage, we did not observe the typical OA-associated changes in the trabecular bone. The other OA animal models from which we observe bone changes related to cartilage changes during OA development are from studies of post-traumatic OA (Christiansen et al., 2012; Doschak et al., 2004; Radin et al., 1978; Shin et al., 2016; Wohl et al., 2001) or adjuvant arthritis – a response to inflammatory arthritis. (Zernicke et al., 1997) Both of these types of models tend to trigger bone changes around the joint. In post-traumatic OA, the bone will change in response to damage (Radin & Rose, 1986) or altered mechanics in the affected limb (Anderson et al.,

2016; Wohl et al., 2001). In the model of adjuvant arthritis, there is increased

inflammation around the joint that can trigger a loss of bone near the joint (Doschak et al.,

2004; Zernicke et al., 1997). In the mouse knock-out model, it appears that the cartilage

degradative changes occurred due to increased TGFβ signalling in the cartilage (St.

Amant, 2022). This supports that TGFβ signalling contributes to cartilage degeneration in

OA progression, but there appear to be other factors that affect bone.

4.2   TβRII Has No Clear Protective Role in Integrin α1 Subunit Knockout Mice

The double knockout "rescue" cohort (α+t) (ubiquitous integrin α1 subunit, cartilage-

specific TβRII knockout) is expected to mitigate osteoarthritic phenotypes caused by the

integrin α1 subunit knockout. The cartilage-specific knockout of TβRII was intended to

inhibit excessive TβRII signalling previously observed in *itga1*-null mice. The ubiquitous

integrin α1 subunit knockout leaves no integrin α1β1 present to mediate TGFβ signalling

in all cells. The uninhibited signalling results in a fibrotic response including excessive

production of collagens, leading to fibrosis in the cartilage. Inhibition of excessive TβRII

signalling is thought to cause this. Thus, we hypothesized that as in the cartilage, OA-like

effects would be mitigated in the peri-articular trabecular bone as well. Between the

itga1-null (α+c) and the double knockout mice (α+t), there were no significant differences

in any trabecular measures at any timepoint. There is no clear evidence from our results to

support or negate the hypothesis that cartilage-specific inhibition of TβRII signalling is

protective in the peri-articular trabecular bone, as it was in the cartilage of *itga1*-null mice.

4.3 Effect of TβRII Knockout in Trabecular Bone of Wild-Type Mice

In normal articular cartilage, TGFβ is highly expressed. Therefore, the wild-type mice with depleted levels of TβRII from the cartilage-specific knockout (+t) are expected to have OA-like phenotypes. In the cartilage, St. Amant did not observe a significant acceleration of OA-like phenotypes. (St. Amant, 2022) Our results showed that trabecular separation in the medial femoral condyles of 16-month mice was significantly greater in wild-type mice with the cartilage-specific TβRII knockout (+t) than those without (+c). Increased trabecular separation is indicative of the overall trabecular bone loss observed as a phenotype of bone in post-traumatic OA studies. (Christiansen et al., 2015; Shin et al., 2016) This result supports the hypothesis that the TβRII knockout in wild-type mice caused OA-like changes in bone, which was not the case in cartilage.

4.4 Presence of TGFβ Associated with Increased Ectopic Bone Calcification

Injection of TGFβ, the growth factor that binds to TβRII, into the knee has previously resulted in significant ectopic bone formation in the early stages of OA development. (Blaney Davidson et al., 2006) The knockout of TβRII in our study was targeted only at the articular cartilage, however it was important to see if the knockout influenced other

surrounding tissues as a consequence of increased levels of TGFβ in the synovial fluid. In 4-month *itga1*-null mice (α+c, α+t), the specimens with a cartilage-specific TβRII knockout (α+t) had significantly greater volumes of calcified tissue along the medial collateral ligament (Figure 34). Additionally, binary analyses showed that there were a greater proportion of samples with calcified tissue (in 4- and 16-month samples) and osteophytes (4-month samples) at the root of the MCL in the TβRII knockout *itga1*-null mice (α+t) compared to the samples with intact TβRII (α+c, α-t). Similar changes were seen in the binary analysis between the TBRII knockout (+t) and tamoxifen control (-t) wild-type mice. The double knockout mice also had greater proportions of specimens with osteophytes at the root of the MCL compared to the *itga1*-null tamoxifen control mice in 4-and 16-month specimens. These results show several instances where TβRII depletion in the articular cartilage caused increased ectopic tissue calcification. Since tamoxifen was used to activate the cartilage-specific knockout of TβRII, and has shown musculoskeletal effects previously, its effect on ectopic tissue calcification must also be explored. (Creamer et al., 1994)

4.5   Effect of Tamoxifen on Ectopic Calcifications

Based on the results in section 3, the presence of tamoxifen coincided with several significant cases of calcified tissue at the medial collateral ligament root. At 4-months, the mice given a corn oil injection, +c and α+c, had significantly fewer instances of ectopic tissue calcification than a subset of the cohorts given a tamoxifen injection. The

4-month corn oil injected wild-type mice (+c) had significantly fewer mice with ectopic

tissue calcification at the root of the MCL than the tamoxifen-injected wild-type (-t).

Similarly, the corn-oil injected *itga1*-null mice (α+c) at both timepoints had significantly

fewer mice with calcified MCL roots than their tamoxifen controls (α-t). Given these

results and the significant results in TβRII knockout mice, which were also injected with

tamoxifen, the effect of tamoxifen in this model should be explored further.

Musculoskeletal effects of tamoxifen were noted in three case studies of patients

undergoing tamoxifen treatment for breast carcinoma. (Creamer et al., 1994) In two of

the cases, the tamoxifen dose was 20mg daily (Not disclosed for the third case).

Compared to the dose in this mouse study (2mg/0.1mL in corn oil vehicle at 14 and 16

days), those doses had greater concentrations at more frequent, regular intervals.

Therefore, comparisons to the results of those studies should be used with caution.

Performing the same analyses in the female mice would provide more insight, not only

because of sample size but also to investigate whether tamoxifen and estrogen have an

impact on calcification in the MCL and other regions.

4.6 Summary of Findings

Table 31: Findings from data results concerning the use of TβRII inhibition as a rescue for OA-like phenotypes in trabecular bone.

Cohort	integrin α1 subunit knockout (α+c)	integrin α1 subunit knockout and TβRII knockout (α+t)
Integrin α1 subunit	**Ubiquitous knockout**	**Ubiquitous knockout**
TβRII Signalling	Normal	**Cartilage specific knockout**
Expectation Based on Hypotheses	• Uncontrolled collagen production in all tissues • Worst case OA-like traits	• 'Rescue' for the *itga1*-null mouse • Decreased OA-like traits in *itga1*-null
Results Relevant to Study Focus	Greater trabecular thickness in medial and lateral femoral condyles at 16 months	No significant difference between the *itga1*-null mice with or without cartilage specific TβRII knockout
Hypothesis	*itga1*-null mice will exhibit OA-like bone behaviour	TβRII inhibition protects *itga1*-null mice from some trabecular bone loss
Does it support hypothesis?	No – results contrary	Unclear – no significant results

Table 32: Findings from results concerning the effect of TβRII knockout in *itga1*-null and wild-type mice.

Cohort	TβRII knockout (+t)	α1 knockout and TβRII knockout (α+t)
Integrin α1 subunit	Normal	**Ubiquitous knockout**
TβRII signalling	**Cartilage specific knockout**	**Cartilage specific knockout**
Expectation based on hypotheses	Depleting TβRII signalling causes OA-like traits in trabecular bone	'Rescue' for the *itga1*-null mouse Does not exhibit OA-like traits
Results relevant to study focus	Increased trabecular separation in the medial femoral condyle of TβRII knockout mice (+t) at 16-months	No significant differences between the *itga1*-null mice with (α+t) or without (α+c)
Hypothesis	Depleting normal levels of TβRII signalling shows increased OA-like phenotypes than the wild type	Double knockout mice have more characteristics of OA in trabecular bone than the wild type
Does it support hypothesis?	Yes	Unclear

4.7 Limitations in Methods

4.7.1 μCT

Trabecular bone quantifications were a major part of the analysis in this project. In mice, trabeculae are small, typically on the scale of ~20 to 60µm, and it is recommended to have a minimum ratio of 2 voxels to object size to get the best results when using µCT. (Bouxsein et al., 2010) To scan efficiently, a resolution of 13.1µm gave a scanning area that could scan 6 hindlimbs simultaneously. According to the guidelines, the resolution is sufficient for the analysis, but, in future studies, it may be ideal to have a higher resolution for greater accuracy in measurements. A higher resolution is especially helpful in the analysis of the tibial epiphysis where the region of trabecular bone between the growth plate and tibial plateau is small.

4.7.2 Trabecular Analysis Algorithm

The trabecular analysis was performed entirely through the proprietary software of Bruker. Preferably for future studies, an analysis program where the methodology of these analyses can be accessed will be used. An open-source program or algorithm provides more transparency in the process of determining these measures and makes it easier for others to reproduce, validate or improve these processes. The open-source imaging analysis Fiji (see section 2.8.1) has plugins that calculate these measures, but there are strict conditions that the image dataset must meet to get accurate results. Improving existing and developing more plugins for the trabecular measures in open-source imaging programs like Fiji is beneficial for future studies.

4.7.3   Effect of Sample Size

The foregoing study has a large number of samples and due to the number of subgroups that need to be analyzed, this limits the sample sizes within each cohort. Since analysis for only two timepoints in only male specimens could be completed, the sample size used in this project is relatively small. Typically, a power analysis is completed before the advancement of the experiment to verify the sample size required to observe significant differences in the analysis. However, since samples from a previous study were used, the analysis was completed first, followed by a power analysis to provide guidelines for future studies on the number of samples required to detect significance (Table 17). Having greater sample numbers per subgroup may provide more clarity to the large interquartile range found in the quantification of calcified tissues, especially at the meniscus (Figure 36). The sample sizes did not appear to hinder the significance of the results in this study as several significant differences were found in the data. Based on the overall post hoc results, significant differences in measures that had p values greater than, but close to, 0.05 did not occur between cohorts that address the main genetic comparisons we looked for in this study. For example, in Table 25, the volume of the medial collateral ligament almost reached statistical significance ($p = 0.06$) between the α+c and +t cohorts, which is not a relevant comparison to the focus of our study.

4.7.4   Binary Checks

Due to complex bone architecture, binary analyses provided a starting point to observe significance. Bone volume quantification for these analyses and of the tibia and femur as

a whole would provide a better representation of significant ectopic calcification. Without a bone volume measurement, the binary result of a sample having an osteophyte at the medial collateral ligament root, for example, may show significance between several cohorts. It does not, however, provide enough information on the severity of this calcification or how the significant cohorts compare to one another. Relative volumes of calcification would provide a better understanding of ectopic calcification and how it relates to each knockout or injection.

4.7.5   Repeatability of Volume Quantifications and Other Measures

When quantifying calcified tissue volumes, the process of identifying the originating soft tissue of each calcification was subjective. If someone else repeated this study, they may have different results. Since all calculations were run by the same person in this study, the results were comparable. However, a methodology that eliminates the guesswork in region identifications would improve the repeatability of methods in this study. As discussed, CTAn was ideal to use under the circumstances of this project due to its built-in functions. However, since the software requires a license, it is not accessible to all who may want to recreate this study. Therefore, in further studies, the repeatability of these methods would be improved by using open-source software and a less subjective method of region selection.

5 Conclusion

Using imaging datasets obtained using micro-computed tomography, several genetic combinations involving knockouts of the ubiquitous integrin α1 subunit and TβRII gene targeted to cartilage in the knee were analyzed. The primary focus of these analyses was to determine whether the effects of these genetic manipulations had similar effects on bone changes associated with OA as they did to the articular cartilage in Dr. A Clark and St. Amant's analysis. The study involved characterizing bone adaptations including trabecular thickness, trabecular separation, bone volume fraction, abnormal calcification of tissues and the formation of osteophytes. The hypothesis that ubiquitous integrin α1 subunit knockout mice (*itga1*-null) have significantly greater trabecular bone loss than the 'wild type' mouse was not supported by the results of this study. The only significant difference in trabecular parameters between these cohorts was a significant increase in trabecular thickness in the medial and lateral femoral condyles of 16-month samples. Additionally, the potentially protective effect of the cartilage-specific TβRII knockout against damage caused by the ubiquitous integrin α1 subunit knockout could not be supported as there were no significant differences in the trabecular parameters between these cohorts. Increased trabecular separation in the medial femoral condyle of TβRII knockout mice supported the hypothesis that inhibition of TβRII in normal cartilage would lead to OA-like phenotypes in bone. The injection of tamoxifen to activate Col2Cre caused some uncertainty of the results as it was present in several significant instances of ectopic calcifications in soft tissues around the knee. However, most instances of significant increase in ectopic tissue calcifications were found in cartilage

specific TβRII depleted mice, with and without the ubiquitous integrin α1 subunit knocked out. This supports findings that showed excess TGFβ in the soft tissues of the knee increases ectopic calcification in soft tissues. Tamoxifen control groups were involved in several of the significant results concerning abnormal changes to the trabecular bone, osteophytes, and collateral ligaments. As such, the effect of tamoxifen as it relates to abnormal calcification should be studied further. Although inconclusive, the results of this study found that the genetic model is viable for further study into bone adaptations and their relationship to the ubiquitous integrin α1 subunit and cartilage specific TβRII knockout.

6 References

Abdi, H. (2010). Holm's Sequential Bonferroni Procedure. *Encyclopedia of Research Design*, 1–8.

Abràmoff, M. D., Magalhães, P. J., & Ram, S. J. (2004). Image processing with imageJ. *Biophotonics International*, *11*(7), 36–41. https://doi.org/10.1201/9781420005615.ax4

Aigner, T., Schmitz, N., & Salter, D. M. (2015). Pathogenesis and pathology of osteoarthritis. *Rheumatology: Sixth Edition*, *2–2*, 1462–1476. https://doi.org/10.1016/B978-0-323-09138-1.00175-3

Amblard, D., Nuzzo, S., Elmoutaouakkil, A., & Vico, L. (2003). *Excised Bone Structures in Mice : Imaging at Micro CT 1*. 921–928.

Anas, E. M. A., Lee, S. Y., & Kamrul Hasan, M. D. (2011). Classification of ring artifacts for their effective removal using type adaptive correction schemes. *Computers in Biology and Medicine*, *41*(6), 390–401. https://doi.org/10.1016/j.compbiomed.2011.03.018

Anderson, M. J., Diko, S., Baehr, L. M., Baar, K., Bodine, S. C., & Christiansen, B. A. (2016). Contribution of mechanical unloading to trabecular bone loss following non-invasive knee injury in mice. *Journal of Orthopaedic Research*, *34*(10), 1680–1687. https://doi.org/10.1002/jor.23178

Bakker, A. C., van de Loo, F. A. J., van Beuningen, H. M., Sime, P., van Lent, P. L. E. M., van der Kraan, P. M., Richards, C. D., & van den Berg, W. B. (2001). Overexpression of active TGF-beta-1 in the murine knee joint: Evidence for synovial-layer-dependent chondro-osteophyte formation. *Osteoarthritis and Cartilage*, *9*(2), 128–136. https://doi.org/10.1053/joca.2000.0368

Blaney Davidson, E. N., Scharstuhl, A., Vitters, E. L., van der Kraan, P. M., & van den Berg, W. B. (2005). Reduced transforming growth factor-beta signaling in cartilage of old mice: role in impaired repair capacity. *Arthritis Research & Therapy*, *7*(6), 14–16. https://doi.org/10.1186/ar1833

Blaney Davidson, E. N., van der Kraan, P. M., & van den Berg, W. B. (2007). TGF-β and osteoarthritis. In *Osteoarthritis and Cartilage* (Vol. 15, Issue 6, pp. 597–604). https://doi.org/10.1016/j.joca.2007.02.005

Blaney Davidson, E. N., Vitters, E. L., Van Der Kraan, P. M., & Van Den Berg, W. B. (2006). Expression of transforming growth factor-β (TGFβ) and the TGFβ signalling molecule SMAD-2P in spontaneous and instability-induced osteoarthritis: Role in cartilage degradation, chondrogenesis and osteophyte formation. *Annals of the Rheumatic Diseases*, *65*(11), 1414–1421. https://doi.org/10.1136/ard.2005.045971

Botter, S. M., van Osch, G. J. V. M., Waarsing, J. H., van der Linden, J. C., Verhaar, J. A. N., Pols, H. A. P., van Leeuwen, J. P. T. M., & Weinans, H. (2008). Cartilage damage pattern in relation to subchondral plate thickness in a collagenase-induced model of osteoarthritis. *Osteoarthritis and Cartilage*, *16*(4), 506–514. https://doi.org/10.1016/j.joca.2007.08.005

Bouxsein, M. L., Boyd, S. K., Christiansen, B. A., Guldberg, R. E., Jepsen, K. J., & Mu,

R. (2010). J BMR Guidelines for Assessment of Bone Microstructure in Rodents Using Micro – Computed Tomography. *Journal of Bone and Mineral Research*, *25*(7), 1468–1486. https://doi.org/10.1002/jbmr.141

Bruker MicroCT. (2015). *Automated trabecular and cortical bone selection Method note MCT-008* (September). Bruker MicroCT.

Bruker MicroCT. (2016). *NRecon User Manual* (July 2016). Bruker MicroCT.

Bruker Skyscan. (2005). *SkyScan 1172 Instruction Manual*. SkyScan N.V.

Chen, D., Shen, J., Zhao, W., Wang, T., Han, L., Hamilton, J. L., & Im, H. J. (2017). Osteoarthritis: Toward a comprehensive understanding of pathological mechanism. *Bone Research*, *5*(August 2016). https://doi.org/10.1038/boneres.2016.44

Chen, M., Lichtler, A. C., Sheu, T. J., Xie, C., Zhang, X., O'Keefe, R. J., & Chen, D. (2007). Generation of a transgenic mouse model with chondrocyte-specific and tamoxifen-inducible expression of Cre recombinase. *Genesis (United States)*, *45*(1), 44–50. https://doi.org/10.1002/dvg.20261

Chen, X., Wang, H., Liao, H. J., Hu, W., Gewin, L., Mernaugh, G., Zhang, S., Zhang, Z. Y., Vega-Montoto, L., Vanacore, R. M., Fässler, R., Zent, R., & Pozzi, A. (2014). Integrin-mediated type II TGF-β receptor tyrosine dephosphorylation controls SMAD-dependent profibrotic signaling. *Journal of Clinical Investigation*, *124*(8), 3295–3310. https://doi.org/10.1172/JCI71668

Christiansen, B. A., Anderson, M. J., Lee, C. A., Williams, J. C., Yik, J. H. N., & Haudenschild, D. R. (2012). Musculoskeletal changes following non-invasive knee injury using a novel mouse model of post-traumatic osteoarthritis. *Osteoarthritis and Cartilage*, *20*(7), 773–782. https://doi.org/10.1016/j.joca.2012.04.014

Christiansen, B. A., Guilak, F., Lockwood, K. A., Olson, S. A., Pitsillides, A. A., Sandell, L. J., Silva, M. J., van der Meulen, M. C. H., & Haudenschild, D. R. (2015). Non-invasive mouse models of post-traumatic osteoarthritis. *Osteoarthritis and Cartilage*, *23*(10), 1627–1638. https://doi.org/10.1016/j.joca.2015.05.009

Clark, A. L., Votta, B. J., Kumar, S., Liedtke, W., & Guilak, F. (2010). Chondroprotective role of the osmotically sensitive ion channel transient receptor potential vanilloid 4: Age- and sex-dependent progression of osteoarthritis in Trpv4-deficient mice. *Arthritis & Rheumatism*, *62*(10), 2973–2983. https://doi.org/10.1002/art.27624

Cohen, J. (1988). *Statistical Power Analysis for the Behavioural Sciences* (2nd ed.). Erlbaum.

Creamer, P., Lim, K., George, E., & Dieppe, P. (1994). Acute inflammatory polyarthritis in association with tamoxifen. *Rheumatology*, *33*(6), 583–585. https://doi.org/10.1093/rheumatology/33.6.583

Doschak, M. ., Wohl, G. R., Hanley, D. A., Bray, R. C., & Zerni. (2004). *Antiresorptive therapy conserves some periarticular bone and Ligament Mechanical Properties After Anterior*. *22*, 942–948.

Doube, M., Klosowski, M. M., Arganda-Carreras, I., Cordelières, F. P., Dougherty, R. P., Jackson, J. S., Schmid, B., Hutchinson, J. R., & Shefelbine, S. J. (2010). BoneJ: Free and extensible bone image analysis in ImageJ. *Bone*, *47*(6), 1076–1079. https://doi.org/10.1016/j.bone.2010.08.023

Ekholm, E., Hankenson, K. D., Uusitalo, H., Hiltunen, A., Gardner, H., Heino, J., & Penttinen, R. (2002). Diminished callus size and cartilage synthesis in α1β1 integrin-deficient mice during bone fracture healing. *American Journal of Pathology*, *160*(5), 1779–1785. https://doi.org/10.1016/S0002-9440(10)61124-8

Fang, H., Huang, L., Welch, I., Norley, C., Holdsworth, D. W., Beier, F., & Cai, D. (2018). Early Changes of Articular Cartilage and Subchondral Bone in The DMM Mouse Model of Osteoarthritis. *Scientific Reports*, *8*(1), 1–9. https://doi.org/10.1038/s41598-018-21184-5

Fässler, R., & Meyer, M. (1995). Consequences of lack of β1 integrin gene expression in mice. *Genes and Development*, *9*(15), 1896–1908. https://doi.org/10.1101/gad.9.15.1896

Fritz, C. O., Morris, P. E., & Richler, J. J. (2012). Effect size estimates: Current use, calculations, and interpretation. *Journal of Experimental Psychology: General*, *141*(1), 2–18. https://doi.org/10.1037/a0024338

Gardner, H. (2014). Integrin α1β1. In *Advances in Experimental Medicine and Biology* (Vol. 819, pp. 21–39). https://doi.org/10.1007/978-94-017-9153-3_2

Gardner, H., Kreidberg, J., Koteliansky, V., & Jaenisch, R. (1996). Deletion of integrin α1 by homologous recombination permits normal murine development but gives rise to a specific deficit in cell adhesion. *Developmental Biology*, *175*(2), 301–313. https://doi.org/10.1006/dbio.1996.0116

Glasson, S. S., Blanchet, T. J., & Morris, E. A. (2007). The surgical destabilization of the medial meniscus (DMM) model of osteoarthritis in the 129/SvEv mouse. *Osteoarthritis and Cartilage*, *15*(9), 1061–1069. https://doi.org/10.1016/j.joca.2007.03.006

Gupta, R. C., Kalidindi, S. R., Doss, R. B., Lall, R., Srivastava, A., & Sinha, A. (2021). Nutraceuticals in arthritis. *Nutraceuticals: Efficacy, Safety and Toxicity*, 193–214. https://doi.org/10.1016/B978-0-12-821038-3.00014-8

Hudson, D. M., Archer, M., Rai, J., Weis, M. A., Fernandes, R. J., & Eyre, D. R. (2021). Age-related type I collagen modifications reveal tissue-defining differences between ligament and tendon. *Matrix Biology Plus*, *12*, 100070. https://doi.org/10.1016/j.mbplus.2021.100070

Jia, H., Ma, X., Wei, Y., Tong, W., Tower, R. J., Chandra, A., Wang, L., Sun, Z., Yang, Z., Badar, F., Zhang, K., Tseng, W. J., Kramer, I., Kneissel, M., Xia, Y., Liu, X. S., Wang, J. H. C., Han, L., Enomoto-Iwamoto, M., & Qin, L. (2018). Loading-Induced Reduction in Sclerostin as a Mechanism of Subchondral Bone Plate Sclerosis in Mouse Knee Joints During Late-Stage Osteoarthritis. *Arthritis and Rheumatology*, *70*(2), 230–241. https://doi.org/10.1002/art.40351

Kamekura, S., Hoshi, K., Shimoaka, T., Chung, U., Chikuda, H., Yamada, T., Uchida, M., Ogata, N., Seichi, A., Nakamura, K., & Kawaguchi, H. (2005). Osteoarthritis development in novel experimental mouse models induced by knee joint instability. *Osteoarthritis and Cartilage*, *13*(7), 632–641. https://doi.org/10.1016/j.joca.2005.03.004

Ketola, J. H., Karhula, S. S., Finnilä, M. A. J., Korhonen, R. K., Herzog, W., Siltanen, S., Nieminen, M. T., & Saarakkala, S. (2018). Iterative and discrete reconstruction in

the evaluation of the rabbit model of osteoarthritis. *Scientific Reports*, *8*(1), 1–10. https://doi.org/10.1038/s41598-018-30334-8

Lai, D., Schwantes-An, T.-H., Corbin, T. J., & White, K. E. (2019). Skeletal Genetics. In *Basic and Applied Bone Biology* (Second Edi). Elsevier Inc. https://doi.org/10.1016/b978-0-12-813259-3.00009-9

Li, Y., Fan, W., Link, F., Wang, S., & Dooley, S. (2022). Transforming growth factor β latency: A mechanism of cytokine storage and signalling regulation in liver homeostasis and disease. *JHEP Reports*, *4*(2), 100397. https://doi.org/10.1016/j.jhepr.2021.100397

Loeser, R. F. (2014). Integrins and chondrocyte-matrix interactions in articular cartilage. In *Matrix Biology* (Vol. 39, pp. 11–16). Matrix Biology. https://doi.org/10.1016/j.matbio.2014.08.007

Loeser, R. F., Goldring, S. R., Scanzello, C. R., & Goldring, M. B. (2012). Osteoarthritis: A Disease of the Joint as an Organ Richard. *Arthritis and Rheumatism*, *64*(6), 1697–1707. https://doi.org/10.1002/art.34453.Osteoarthritis

McEver, R. P., & Luscinskas, F. W. (2017). Cell Adhesion. In *Hematology: Basic Principles and Practice* (Seventh Ed). Elsevier Inc. https://doi.org/10.1016/B978-0-323-35762-3.00012-3

Orhan, K. (2020). Micro-computed Tomography (micro-CT) in Medicine and Engineering. In *Micro-computed Tomography (micro-CT) in Medicine and Engineering*. https://doi.org/10.1007/978-3-030-16641-0

Osteoarthritis in Canada. (2020). Canada, Public Health Agency Of. https://www.canada.ca/en/public-health/services/publications/diseases-conditions/osteoarthritis.html#data

Otsu, & N. (1996). A threshold selection method from gray-level histograms. *IEEE Trans. on Systems, Man and Cybernetics*, *9*(1), 62–66. https://cw.fel.cvut.cz/b201/_media/courses/a6m33bio/otsu.pdf

Parfitt, A. M. (1988). Bone histomorphometry: Standardization of nomenclature, symbols and units (summary of proposed system). *Bone*, *9*(1), 67–69. https://doi.org/10.1016/8756-3282(88)90029-4

Pérez-Ramos, A., & Figueirido, B. (2020). Toward an "Ancient" Virtual World: Improvement Methods on X-ray CT Data Processing and Virtual Reconstruction of Fossil Skulls. *Frontiers in Earth Science*, *8*(September), 1–23. https://doi.org/10.3389/feart.2020.00345

Plotkin, L. I., Aguilar-pérez, A., & Bivi, N. (2019). Local Regulation of Bone Cell Function. In *Basic and Applied Bone Biology* (Second Edi). Elsevier Inc. https://doi.org/10.1016/B978-0-12-813259-3.00004-X

Radin, E. L., Ehrlich, M. G., Chernack, R., Abernethy, P., Paul, I. L., & Rose, R. M. (1978). Effect of repetitive impulsive loading on the knee joints of rabbits. *Clinical Orthopaedics and Related Research*, *131*, 288–293. https://doi.org/10.1097/00003086-197803000-00047

Radin, E. L., & Rose, R. M. (1986). Role of subchondral bone in the initiation and progression of cartilage damage. *Clinical Orthopaedics and Related Research*, *213*, 34–40. https://doi.org/10.1097/00003086-198612000-00005

Roberts, B. C., Thewlis, D., Solomon, L. B., Mercer, G., Reynolds, K. J., & Perilli, E. (2017). Systematic mapping of the subchondral bone 3D microarchitecture in the human tibial plateau: Variations with joint alignment. *Journal of Orthopaedic Research*, *35*(9), 1927–1941. https://doi.org/10.1002/jor.23474

Scharstuhl, A., Glansbeek, H. L., van Beuningen, H. M., Vitters, E. L., van der Kraan, P. M., & van den Berg, W. B. (2002). Inhibition of Endogenous TGF-β During Experimental Osteoarthritis Prevents Osteophyte Formation and Impairs Cartilage Repair. *The Journal of Immunology*, *169*(1), 507–514. https://doi.org/10.4049/jimmunol.169.1.507

Scharstuhl, A., Vitters, E. L., Van Der Kraan, P. M., & Van Den Berg, W. B. (2003). Reduction of Osteophyte Formation and Synovial Thickening by Adenoviral Overexpression of Transforming Growth Factor β/Bone Morphogenetic Protein Inhibitors during Experimental Osteoarthritis. *Arthritis and Rheumatism*, *48*(12), 3442–3451. https://doi.org/10.1002/art.11328

Schrenker, S., Cucchiarini, M., Goebel, L., Oláh, T., Venkatesan, J. K., Schmitt, G., Speicher-Mentges, S., Maihöfer, J., Gao, L., Zurakowski, D., Menger, M. D., Laschke, M. W., & Madry, H. (2022). In vivo rAAV-mediated human TGF-β overexpression reduces perifocal osteoarthritis and improves osteochondral repair in a large animal model at one year. *Osteoarthritis and Cartilage*, *31*, 467–481. https://doi.org/10.1016/j.joca.2022.11.010

Shen, J., Li, J., Wang, B., Jin, H., Wang, M., Zhang, Y., Yang, Y., Im, H. J., O'Keefe, R., & Chen, D. (2013). Deletion of the transforming growth factor β Receptor type II gene in articular chondrocytes leads to a progressive osteoarthritis-like phenotype in mice. *Arthritis and Rheumatism*, *65*(12), 3107–3119. https://doi.org/10.1002/art.38122

Shin, S. Y., Pozzi, A., Boyd, S. K., & Clark, A. L. (2016). Integrin α1β1 protects against signs of post-traumatic osteoarthritis in the female murine knee partially via regulation of epidermal growth factor receptor signalling. *Osteoarthritis and Cartilage*, *24*(10), 1795–1806. https://doi.org/10.1016/j.joca.2016.05.013

St. Amant, J. (2022). *Interplay between integrin alpha 1 beta 1 and transforming growth factor beta receptor II in the development of spontaneous osteoarthritis in the mouse knee*. University of Guelph.

Tarride, J. E., Haq, M., O'Reilly, D. J., Bowen, J. M., Xie, F., Dolovich, L., & Goeree, R. (2012). The excess burden of osteoarthritis in the province of Ontario, Canada. *Arthritis and Rheumatism*, *64*(4), 1153–1161. https://doi.org/10.1002/art.33467

Waarsing, J. H., Day, J. S., & Weinans, H. (2004). An improved segmentation method for in vivo μCT imaging. *Journal of Bone and Mineral Research*, *19*(10), 1640–1650. https://doi.org/10.1359/JBMR.040705

Walton, M. (1979). Patella displacement and osteoarthrosis of the knee joint in mice. *The Journal of Pathology*, *127*(4), 165–172. https://doi.org/10.1002/path.1711270402

Wegner, A. M., Campos, N. R., Robbins, M. A., Haddad, A. F., Cunningham, H. C., Yik, J. H. N., Christiansen, B. A., & Haudenschild, D. R. (2019). Acute Changes in NADPH Oxidase 4 in Early Post-Traumatic Osteoarthritis. *Journal of Orthopaedic Research*, *37*(11), 2429–2436. https://doi.org/10.1002/jor.24417

Wohl, G. R., Shymkiw, R. C., Matyas, J. R., Kloiber, R., & Zernicke, R. F. (2001). Periarticular cancellous bone changes following anterior cruciate ligament injury. *Journal of Applied Physiology*, *91*(1), 336–342. https://doi.org/10.1152/jappl.2001.91.1.336

Yoshioka, N. K., Young, G. M., Khajuria, D. K., Karuppagounder, V., Pinamont, W. J., Fanburg-Smith, J. C., Abraham, T., Elbarbary, R. A., & Kamal, F. (2022). Structural changes in the collagen network of joint tissues in late stages of murine OA. *Scientific Reports*, *12*(1). https://doi.org/10.1038/s41598-022-13062-y

Zemmyo, M., Meharra, E. J., Kühn, K., Creighton-Achermann, L., & Lotz, M. (2003). Accelerated, Aging-Dependent Development of Osteoarthritis in α1 Integrin-Deficient Mice. *Arthritis and Rheumatism*, *48*(10), 2873–2880. https://doi.org/10.1002/art.11246

Zernicke, R. F., Wohl, G. R., Greenwald, R. A., Moak, S. A., Leng, W., & Golub, L. M. (1997). Administration of systemic matrix metalloproteinase inhibitors maintains bone mechanical integrity in adjuvant arthritis. *Journal of Rheumatology*, *24*(7), 1324–1331.

7 Appendix

7.1 Specimen Holder Drawings

3 X KEY FOR LOCATING SLOTS ON LID

6 X Ø7 OD
▽ 22 MM DEPTH
3.5° TAPER
45° CHAMFER AT OPENING

Ø2 CIRCULAR CUTOUT
▽12MM DEPTH

R1 SEMI CIRCLE CUTOUT
▽ 12MM DEPTH

72° TYP

Ø50
Ø28
6
11
7
R2 TYP
48
27
20
12
R1
Ø6

MCMASTER UNIVERSITY

TITLE
SPECIMEN HOLDER BASE

DRAWN
ROSHAN BASHAR
CHECKED
QA
MFG
APPROVED

SIZE
B
DWG NO
HOLDER BASE
REV

SCALE 2:1
SHEET 1 OF 1

ALL DIMENSIONS IN MM

PREVIOUS SLOT INDICATORS
- LID REUSED FROM PREVIOUS DESIGN

3 X LOCATING SLOTS EVERY 90°

5° TAPER

R.5 TYP

Ø35

Ø32.0

Ø26

8

9

15

50

60

45°
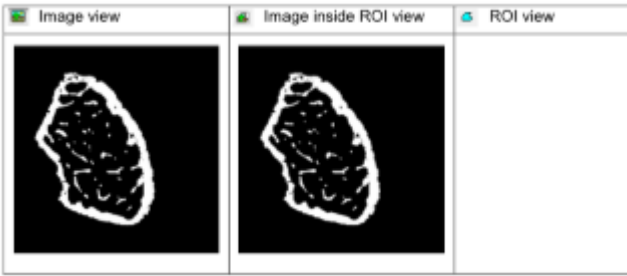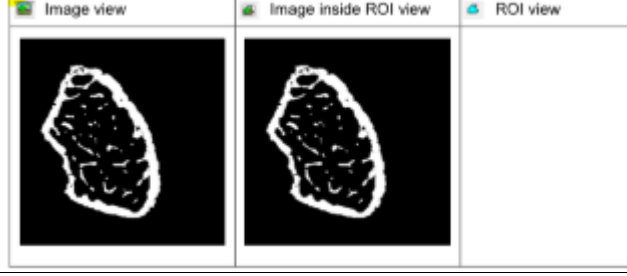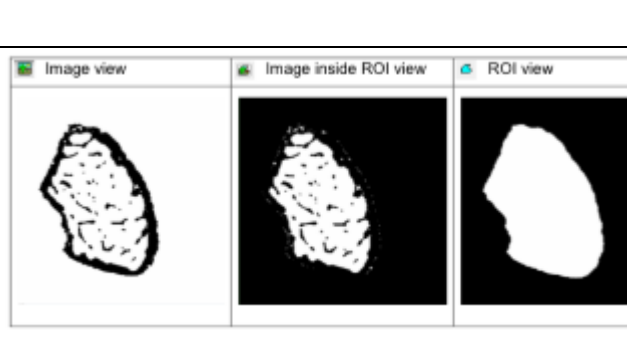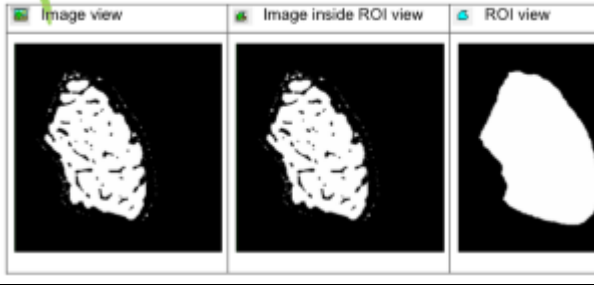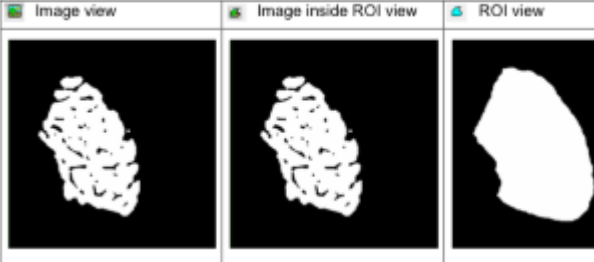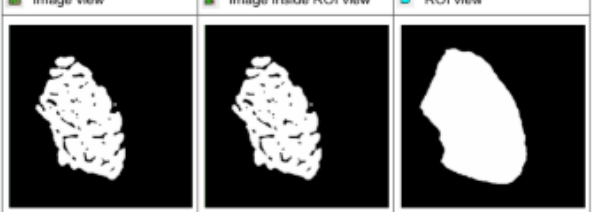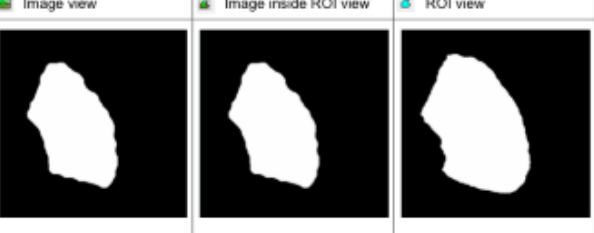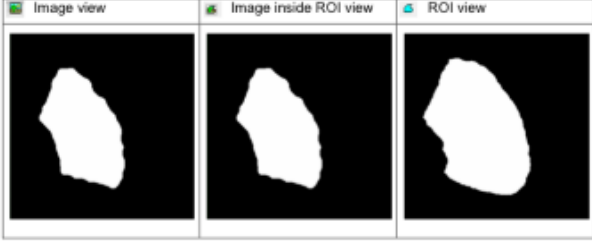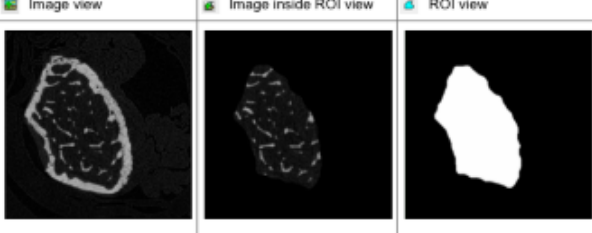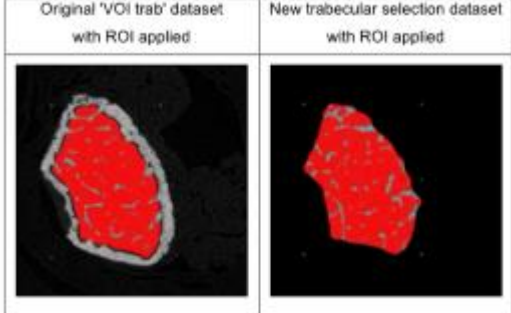
DRAWN	ROSHAN BASHAR
CHECKED	
QA	
MFG	
APPROVED	

MCMASTER UNIVERSITY

TITLE

LID FOR SPECIMEN HOLDER

| SIZE | DWG NO | REV |
| B | SLEEVELID.4.4 | |

SCALE 2:1

SHEET 1 OF 1

7.2 Trabecular Bone Segmentation Method

Adapted from CTAn method note 8 (Bruker MicroCT, 2015)

Step	CTAN Function/Parameters	Purpose of Step	Visual
1	Threshold • Global threshold • Threshold value chosen from previous definition	Segment bone tissue from soft tissue	
2	Despeckle • Sweep • All except the largest object • 3D Space • Apply to image	Removing all other unnecessary parts of bone (ex. Fibula, noise, speckes)	
3	ROI shrink-wrap • Shrink-wrap • 2D space • Stretch over holes enabled (ignores the pores running through the cortical bone) • Diameter: 40	Limits the ROI to the outside borders of the cortical bone	
4	Bitwise operations: • Image = NOT Image	Selection of the bone marrow cavity by inverting the image – bone marrow and outer region now selected	

5	Bitwise operations: • Image = Image AND Region of Interest	Removes the outer region from the ROI and	
6	Morphological operations • 2D Space • Opening • Round • Apply to image • Radius: 2	Removes white speckles at periosteal surface of the bone from previous shrink wrap function	
7	Despeckle • Sweep • All except the largest object • 3D Space • Apply to image	Removes any remaining white speckles	
8	Morphological operations • 2D Space • Closing • Round • Apply to image • Radius: 20	Trabecular bone appears as black speckles or gaps – these are removed by 'closing' the gaps to encapsulate the entire bone marrow cavity region	
9	Morphological operations • 2D Space • Opening • Round • Apply to image • Radius: 10	There may be some pores running through cortical bone – this step removes these pores by 'opening' the selection to smooth the bone marrow cavity selection	

10	Morphological operations • 2D Space • Erosion • Round • Apply to image • Radius: 3	To make sure that the selection does not include any cortical bone – removes a small number of pixels from the perimeter of the selection	
11	Bitwise operations • Region of Interest • COPY • Image	Copy the region of interest from the image to apply to the reloaded dataset with trabecular bone segmented	
12	Reload • Apply to image	Bring back the original dataset and apply the previous region of interest	
13	Threshold	Applies a threshold to segment bone tissue from surrounding soft tissues as before so that new image contains the trabecular bone contained within the bone marrow cavity ROI	
14	Save Bitmaps	Save the new trabecular only, segmented dataset for confirming the selection and running trabecular analyses	

7.3 Data

Trabecular Analysis of 4-Month Male Mice

ID	Cohort	Timepoint	Tibial Epiphysis Medial			Tibial Epiphysis Lateral			Femoral Condyles Medial			Femoral Condyles Lateral		
			Trabecular Thickness (mm)	Trabecular Separation (mm)	Bone Volume Fraction (%)	Trabecular Thickness (mm)	Trabecular Separation (mm)	Bone Volume Fraction (%)	Trabecular Thickness (mm)	Trabecular Separation (mm)	Bone Volume Fraction (%)	Trabecular Thickness (mm)	Trabecular Separation (mm)	Bone Volume Fraction (%)
3TC41-1-6	+c	4	0.093	0.127	51.6	0.077	0.120	50.7	0.081	0.132	47.7	0.075	0.162	37.3
3TC38-1-4	+c	4	0.069	0.068	57.7	0.074	0.086	59.1	0.087	0.146	44.1	0.083	0.155	40.5
3TC39-1-5	+c	4	0.085	0.092	60.1	0.081	0.134	46.3	0.086	0.155	44.4	0.076	0.170	33.4
3TC35-1-8	+c	4	0.083	0.131	49.2	0.070	0.111	48.2	0.078	0.150	43.2	0.073	0.173	35.5
3TC30-2-4	+c	4	0.089	0.095	56.8	0.087	0.079	62.1	0.086	0.149	46.3	0.083	0.152	41.3
3TC32-2-3	+t	4	0.096	0.117	52.9	0.080	0.127	45.7	0.079	0.148	43.3	0.076	0.174	33.8
3TC30-2-3	+t	4	0.085	0.103	52.2	0.076	0.161	39.8	0.085	0.175	36.9	0.070	0.179	28.0
3TC38-1-5	+t	4	0.095	0.107	55.2	0.086	0.131	50.3	0.081	0.166	36.8	0.075	0.216	27.7
3TC30-2-1	+t	4	0.088	0.135	52.9	0.085	0.124	53.1	0.086	0.165	42.0	0.079	0.173	37.1
3TC30-2-2	+t	4	0.098	0.122	55.5	0.085	0.129	48.3	0.081	0.163	41.7	0.076	0.177	38.0
3TC39-1-6	-t	4	0.094	0.112	58.7	0.085	0.120	53.7	0.091	0.129	52.4	0.090	0.158	46.9
3TC37-1-6	-t	4	0.099	0.099	61.4	0.093	0.094	60.5	0.085	0.164	40.0	0.083	0.152	34.1
3TC38-1-6	-t	4	0.110	0.118	53.3	0.084	0.098	59.3	0.081	0.158	39.3	0.084	0.169	37.7
3TC41-1-5	-t	4	0.085	0.096	60.0	0.081	0.132	48.9	0.087	0.154	41.5	0.076	0.172	32.5
3TC32-2-5	-t	4	0.082	0.105	55.7	0.071	0.121	45.5	0.084	0.166	41.1	0.072	0.186	32.4
3αTC17-4-5	α+c	4	0.083	0.130	47.7	0.080	0.119	46.2	0.086	0.146	41.8	0.070	0.169	30.9
3αTC17-4-3	α+c	4	0.081	0.125	49.7	0.081	0.139	42.9	0.076	0.158	36.2	0.074	0.172	34.8
3αTC23-1-4	α+c	4	0.087	0.110	56.0	0.085	0.087	59.1	0.079	0.143	45.5	0.075	0.154	37.2
3αTC21-1-5	α+c	4	0.089	0.117	57.8	0.083	0.116	51.6	0.086	0.150	46.1	0.084	0.158	43.4
3αTC23-1-5	α+c	4	0.067	0.057	68.8	0.082	0.075	67.3	0.083	0.144	47.0	0.082	0.156	40.8
3αTC17-4-8	α+c	4	0.100	0.108	63.8	0.086	0.096	63.1	0.091	0.180	40.6	0.093	0.138	47.0
3αTC17-4-4	α+c	4	0.097	0.120	58.8	0.092	0.123	51.4	0.090	0.142	46.5	0.091	0.162	46.4
3αTC21-1-4	α+t	4	0.070	0.113	44.3	0.081	0.124	44.7	0.081	0.185	35.0	0.079	0.159	35.4
3αTC25-1-7	α+t	4	0.080	0.122	47.8	0.072	0.153	39.4	0.086	0.189	36.9	0.087	0.169	37.1
3αTC25-1-5	α+t	4	0.099	0.111	59.6	0.078	0.144	42.1	0.086	0.145	46.0	0.084	0.161	38.4
3αTC6-3-5	α+t	4	0.083	0.104	57.1	0.077	0.123	49.7	0.086	0.158	40.9	0.071	0.202	31.1
3αTC25-1-4	α+t	4	0.099	0.107	58.9	0.086	0.136	46.9	0.082	0.154	41.8	0.090	0.137	45.7
3αTC9-4-4	α-t	4	0.088	0.122	46.7	0.083	0.112	46.7	0.085	0.158	40.6	0.082	0.178	34.6
3αTC18-3-2	α-t	4	0.098	0.115	57.8	0.093	0.124	51.2	0.097	0.137	50.7	0.085	0.170	40.2
3αTC25-1-6	α-t	4	0.097	0.098	66.3	0.080	0.111	50.8	0.090	0.166	41.9	0.083	0.186	34.4
3atc20-1-3	α-t	4	0.094	0.114	58.6	0.086	0.116	53.1	0.084	0.134	46.7	0.087	0.149	41.9
3atc20-1-4	α-t	4	0.082	0.142	51.8	0.065	0.147	33.1	0.088	0.149	40.8	0.072	0.170	30.1

Trabecular Analysis of 16-Month Male Mice

ID	Cohort	Timepoint	Tibial Epiphysis Medial Trabecular Thickness (mm)	Tibial Epiphysis Medial Trabecular Separation (mm)	Tibial Epiphysis Medial Bone Volume Fraction (%)	Tibial Epiphysis Lateral Trabecular Thickness (mm)	Tibial Epiphysis Lateral Trabecular Separation (mm)	Tibial Epiphysis Lateral Bone Volume Fraction (%)	Femoral Condyles Medial Trabecular Thickness (mm)	Femoral Condyles Medial Trabecular Separation (mm)	Femoral Condyles Medial Bone Volume Fraction (%)	Femoral Condyles Lateral Trabecular Thickness (mm)	Femoral Condyles Lateral Trabecular Separation (mm)	Femoral Condyles Lateral Bone Volume Fraction (%)
3TC16-1-9	+c	16	0.089	0.157	43.1	0.097	0.128	49.0	0.083	0.152	40.2	0.078	0.175	34.7
3TC17-1-6	+c	16	0.109	0.127	55.1	0.079	0.145	37.6	0.092	0.149	46.6	0.082	0.171	35.1
3TC33-1-1	+c	16	0.104	0.141	50.1	0.084	0.114	51.2	0.080	0.153	40.6	0.072	0.173	32.8
3TC16-1-7	+c	16	0.089	0.147	47.2	0.078	0.174	41.2	0.083	0.152	43.7	0.074	0.171	33.0
3TC16-1-8	+c	16	0.087	0.105	54.1	0.085	0.114	54.2	0.081	0.139	48.4	0.078	0.146	42.8
3TC16-1-6	+c	16	0.084	0.134	47.0	0.076	0.119	45.5	0.076	0.147	40.7	0.075	0.172	35.3
3TC17-1-8	+c	16	0.089	0.133	46.0	0.083	0.125	46.2	0.082	0.142	44.2	0.075	0.171	34.4
3TC24-1-4	+c	16	0.097	0.135	51.3	0.081	0.114	44.5	0.078	0.168	37.4	0.073	0.165	31.6
3TC29-1-3	+t	16	0.103	0.128	49.0	0.086	0.133	43.9	0.094	0.195	32.9	0.090	0.185	32.6
3TC32-1-9	+t	16	0.113	0.143	50.4	0.082	0.158	42.5	0.083	0.224	27.5	0.085	0.255	22.7
3TC28-1-2	+t	16	0.094	0.146	45.7	0.076	0.147	39.9	0.086	0.167	42.9	0.073	0.183	33.9
3TC24-1-5	+t	16	0.093	0.135	48.9	0.079	0.155	42.5	0.086	0.188	37.1	0.084	0.170	35.1
3TC35-1-3	+t	16	0.079	0.129	51.7	0.075	0.150	38.1	0.083	0.170	35.7	0.079	0.181	29.2
3TC17-1-7	-t	16	0.098	0.132	50.4	0.088	0.123	47.6	0.081	0.185	35.4	0.076	0.176	32.4
3TC28-1-4	-t	16	0.107	0.123	58.9	0.101	0.167	53.0	0.116	0.116	65.9	0.105	0.133	55.1
3TC32-1-8	-t	16	0.098	0.130	48.5	0.081	0.158	41.3	0.083	0.179	37.6	0.078	0.188	33.4
3TC28-1-5	-t	16	0.110	0.121	56.8	0.084	0.116	52.8	0.095	0.154	46.2	0.086	0.168	38.9
3TC29-1-6	-t	16	0.112	0.126	58.3	0.083	0.160	43.0	0.094	0.157	46.3	0.080	0.185	31.7
3TC33-1-2	-t	16	0.085	0.132	44.2	0.080	0.178	37.7	0.093	0.199	39.2	0.083	0.200	32.6
3TC16-1-5	-t	16	0.092	0.151	45.1	0.072	0.153	37.8	0.076	0.182	36.3	0.076	0.162	35.5
3αTC13-2-3	α+c	16	0.096	0.142	49.1	0.081	0.155	39.1	0.092	0.158	46.5	0.089	0.171	40.4
3αTC18-1-6	α+c	16	0.097	0.153	48.7	0.092	0.205	39.6	0.104	0.155	51.9	0.087	0.168	42.0
3αTC18-2-3	α+c	16	0.085	0.139	44.8	0.077	0.142	40.9	0.092	0.149	42.1	0.080	0.176	33.1
3αTC18-2-2	α+c	16	0.095	0.134	49.4	0.098	0.149	51.6	0.089	0.167	46.3	0.094	0.159	44.2
3αTC13-2-2	α+c	16	0.092	0.173	44.1	0.079	0.152	40.9	0.105	0.166	41.8	0.089	0.180	36.1
3αTC6-2-7	α+t	16	0.097	0.134	49.0	0.077	0.171	36.4	0.096	0.223	34.6	0.080	0.213	28.4
3αTC16-1-5	α+t	16	0.083	0.139	44.7	0.082	0.147	42.0	0.086	0.159	42.6	0.083	0.183	36.4
3αTC3-2-6	α+t	16	0.088	0.168	46.0	0.078	0.143	45.0	0.083	0.202	31.2	0.078	0.189	31.5
3αTC1-4-5	α+t	16	0.102	0.152	50.6	0.085	0.159	41.4	0.102	0.143	47.2	0.086	0.194	36.5
3αTC3-2-8	α+t	16	0.089	0.158	47.1	0.079	0.161	43.7	0.084	0.189	37.0	0.082	0.177	35.9
3αTC16-1-4	α+t	16	0.094	0.143	50.7	0.077	0.182	41.0	0.085	0.178	41.9	0.077	0.182	41.0
3αTC17-1-6	α+t	16	0.111	0.160	49.0	0.066	0.117	41.1	0.090	0.208	34.4	0.078	0.201	30.4
3αTC1-4-6	α-t	16	0.091	0.123	45.5	0.069	0.152	34.7	0.085	0.220	29.4	0.073	0.250	22.8
3αTC1-4-7	α-t	16	0.078	0.158	39.5	0.069	0.125	41.5	0.074	0.135	30.5	0.084	0.192	35.7
3αTC17-1-7	α-t	16	0.091	0.125	50.0	0.081	0.198	37.3	0.085	0.163	39.1	0.081	0.195	32.2
3αTC13-2-4	α-t	16	0.105	0.134	52.9	0.094	0.167	45.5	0.101	0.198	33.5	0.098	0.196	38.6
3αTC6-2-6	α-t	16	0.101	0.146	50.0	0.095	0.177	44.9	0.102	0.199	33.0	0.097	0.194	37.7
3αTC18-2-4	α-t	16	0.084	0.070	67.7	0.081	0.111	49.0	0.090	0.164	43.7	0.078	0.177	35.6
3αTC12-1-5	α-t	16	0.093	0.161	45.7	0.075	0.179	36.9	0.082	0.185	39.3	0.078	0.204	31.5

Volume and Binary Analysis of 4-Month Male Mice

				Collateral Ligaments		Meniscus		Binary Analysis (0 - No, 1 - Yes)				
								Root of MCL		Patella		
ID	Cohort	Timepoint	Volume of Patella	Medial	Lateral	Medial	Lateral	Calcified Tissue	Osteophytosis	Osteophytosis	Dislocation from patellofemoral groove	Calcified tissue in the quadriceps
				Volume of calcified tissue (mm³)								
3TC41-1-6	+c	4	0.745	0.000	0.000	0.057	0.074	0	0	1	0	1
3TC38-1-4	+c	4	1.021	0.002	0.000	0.054	0.087	1	1	0	0	1
3TC39-1-5	+c	4	0.920	0.000	0.000	0.050	0.090	1	0	1	0	1
3TC35-1-8	+c	4	0.682	0.000	0.000	0.068	0.085	0	0	1	0	0
3TC30-2-4	+c	4	0.680	0.000	0.000	0.056	0.093	0	0	1	0	0
3TC32-2-3	+t	4	0.721	0.205	0.000	0.050	0.085	1	1	1	0	0
3TC30-2-3	+t	4	0.799	0.001	0.000	0.055	0.082	0	0	1	0	0
3TC38-1-5	+t	4	0.703	0.000	0.000	0.038	0.079	1	0	1	0	0
3TC30-2-1	+t	4	0.711	0.087	0.000	0.050	0.085	1	1	0	0	0
3TC30-2-2	+t	4	0.772	0.040	0.000	0.046	0.072	1	1	0	0	0
3TC39-1-6	-t	4	0.985	0.000	0.000	0.039	0.069	1	0	0	0	1
3TC37-1-6	-t	4	0.780	0.000	0.000	0.061	0.104	1	0	1	0	0
3TC38-1-6	-t	4	0.724	0.000	0.000	0.072	0.092	1	0	1	0	0
3TC41-1-5	-t	4	0.753	0.000	0.000	0.050	0.103	1	0	1	0	0
3TC32-2-5	-t	4	0.704	0.000	0.000	0.050	0.087	1	0	0	1	0
3αTC17-4-5	α+c	4	0.795	0.000	0.000	0.048	0.077	0	0	0	0	0
3αTC17-4-3	α+c	4	0.742	0.000	0.000	0.061	0.084	0	0	0	1	0
3αTC23-1-4	α+c	4	0.715	0.000	0.007	0.081	0.082	0	0	0	0	1
3αTC21-1-5	α+c	4	0.669	0.000	0.000	0.053	0.067	0	0	0	0	0
3αTC23-1-5	α+c	4	0.772	0.000	0.000	0.061	0.088	0	0	0	0	0
3αTC17-4-8	α+c	4	0.963	0.000	0.000	0.069	0.096	0	0	1	1	0
3αTC17-4-4	α+c	4	0.758	0.000	0.000	0.055	0.076	0	0	0	0	1
3αTC21-1-4	α+t	4	0.597	0.087	0.000	0.047	0.067	1	1	0	0	0
3αTC25-1-7	α+t	4	0.684	0.022	0.000	0.061	0.076	1	1	0	0	0
3αTC25-1-5	α+t	4	0.564	0.072	0.000	0.053	0.068	1	0	0	0	0
3αTC6-3-5	α+t	4	0.640	0.102	0.000	0.050	0.052	1	1	0	0	0
3αTC25-1-4	α+t	4	0.727	0.000	0.000	0.062	0.082	1	1	0	0	0
3αTC9-4-4	α-t	4	0.738	0.000	0.000	0.046	0.083	1	0	0	0	0
3αTC18-3-2	α-t	4	0.680	0.000	0.000	0.045	0.082	1	0	0	0	0
3αTC25-1-6	α-t	4	0.726	0.001	0.001	0.052	0.065	1	0	0	0	0
3atc20-1-3	α-t	4	0.674	0.000	0.000	0.044	0.081	1	0	0	0	0
3atc20-1-4	α-t	4	0.776	0.000	0.000	0.038	0.073	1	0	0	1	0

Volume and Binary Analysis of 16-Month Male Mice

| ID | Cohort | Timepoint | Volume of Patella | Collateral Ligament — Volume of calcified tissue (mm3) | | Meniscus | | Binary Analysis (0 - No, 1 - Yes) | | | | |
				Medial	Lateral	Medial	Lateral	Root of MCL Calcified Tissue	Root of MCL Osteophytosis	Patella Osteophytosis	Dislocation from patellofemoral groove	Calcified tissue in the quadriceps
3TC16-1-9	+c	16	0.969	0.029	0.024	0.015	0.104	0	0	1	0	1
3TC17-1-6	+c	16	1.426	0.092	0.000	0.198	0.184	0	0	1	1	0
3TC33-1-1	+c	16	1.040	0.072	0.010	0.113	0.100	0	0	1	0	0
3TC16-1-7	+c	16	0.921	0.043	0.000	0.084	0.129	1	1	1	0	0
3TC16-1-8	+c	16	1.271	0.240	0.004	0.227	0.255	1	1	1	1	0
3TC16-1-6	+c	16	0.873	0.000	0.000	0.079	0.113	1	0	0	0	0
3TC17-1-8	+c	16	1.275	0.014	0.000	0.091	0.130	0	0	1	1	0
3TC24-1-4	+c	16	1.175	0.058	0.039	0.124	0.143	0	0	1	0	0
3TC29-1-3	+t	16	1.322	0.122	0.000	0.114	0.218	1	0	1	0	0
3TC32-1-9	+t	16	0.946	0.304	0.039	0.085	0.143	1	0	1	0	0
3TC28-1-2	+t	16	1.047	0.015	0.004	0.099	0.132	1	0	1	1	0
3TC24-1-5	+t	16	1.021	0.065	0.035	0.096	0.132	1	1	1	0	0
3TC35-1-3	+t	16	0.769	0.000	0.000	0.065	0.083	1	0	1	0	0
3TC17-1-7	-t	16	1.113	0.005	0.000	0.080	0.122	0	0	1	0	0
3TC28-1-4	-t	16	1.318	0.027	0.000	0.206	0.135	1	0	1	0	0
3TC32-1-8	-t	16	0.810	0.206	0.013	0.103	0.133	1	0	1	1	0
3TC28-1-5	-t	16	0.864	0.071	0.000	0.090	0.103	1	1	1	0	0
3TC29-1-6	-t	16	1.207	0.545	0.000	0.171	0.156	1	1	1	0	1
3TC33-1-2	-t	16	1.359	0.167	0.023	0.147	0.164	1	1	1	0	0
3TC16-1-5	-t	16	0.944	0.107	0.026	0.073	0.137	1	1	1	0	0
3αTC13-2-3	α+c	16	0.980	0.030	0.000	0.339	0.224	0	0	1	0	0
3αTC18-1-6	α+c	16	0.894	0.017	0.006	0.152	0.124	0	0	1	0	0
3αTC18-2-3	α+c	16	0.684	0.003	0.003	0.083	0.094	1	1	1	0	0
3αTC18-2-2	α+c	16	0.787	0.000	0.000	0.066	0.115	0	0	1	0	0
3αTC13-2-2	α+c	16	1.132	0.064	0.022	0.615	0.441	1	0	1	0	0
3αTC6-2-7	α+t	16	0.744	0.005	0.017	0.119	0.105	1	1	1	0	0
3αTC16-1-5	α+t	16	0.829	0.082	0.004	0.093	0.092	1	1	1	1	0
3αTC3-2-6	α+t	16	1.797	0.041	0.033	2.703	0.437	1	1	1	1	0
3αTC1-4-5	α+t	16	1.091	0.017	0.000	0.121	0.125	1	1	1	0	0
3αTC3-2-8	α+t	16	0.884	0.078	0.002	0.439	0.115	1	0	1	0	0
3αTC16-1-4	α+t	16	0.926	0.090	0.000	0.072	0.103	1	0	1	0	1
3αTC17-1-6	α+t	16	1.160	0.185	0.042	0.767	0.350	1	1	1	0	0
3αTC1-4-6	α-t	16	1.414	0.096	0.000	0.255	0.169	1	0	1	1	1
3αTC1-4-7	α-t	16	1.496	0.249	0.036	0.628	0.643	1	0	1	1	0
3αTC17-1-7	α-t	16	1.113	0.099	0.000	0.120	0.120	1	1	1	0	1
3αTC13-2-4	α-t	16	0.998	0.024	0.000	0.101	0.147	1	0	1	1	0
3αTC6-2-6	α-t	16	0.996	0.023	0.000	0.099	0.155	1	0	0	1	0
3αTC18-2-4	α-t	16	0.782	0.004	0.000	0.067	0.106	1	0	1	0	0
3αTC12-1-5	α-t	16	0.997	0.141	0.005	0.276	0.199	1	0	1	0	0

7.4   Computer specifications

Used to run all software for reconstructions, image manipulation and analysis.

Desktop computer, Custom Build.

Windows 10 Education

64GB Memory

8TB HDD

Intel(R) Core (TM) i7-10700 CPU @ 2.90GHz   2.90 GHz

Dedicated Graphics: NVIDIA Quadro P2000